USAAVRADCOM-TR-80-D-7

AD A088325

INVESTIGATION OF PERFORMANCE, NOISE, AND DETECTABILITY CHARACTERISTICS OF REMOTELY PILOTED VEHICLE (RPV) PROPELLERS

D. S. JanakiRam
RASA Division
Systems Research Laboratories, Inc.
1055 J. Clyde Morris Boulevard
Newport News, Virginia 23602

June 1980

Final Report

AUG 21 1980

A

80 8 21 0

APPLIED TECHNOLOGY LABORATORY POSITION STATEMENT

Reconnaissance and target detection RPVs that use piston engine driven propellers are highly susceptible to ground detection due to propulsion system noise. This report examines the noise and detectability aspects of designing propellers for RPVs using piston engines in the 25 horsepower category. Results of this work, although preliminary, cover design variables considered essential to selecting best choice minimum detection propeller configurations. Future R&D in this area is desired to develop performance/noise data from small-scale propellers to a level that compares with that of large-scale propellers.

Bill W. Scruggs, Jr., of the Aeronautical Systems Division served as project engineer for this effort.

REPORT DOCUMENTATION PAGE	READ INSTRUCTIONS BEFORE COMPLETING FORM

1. REPORT NUMBER	2. GOVT ACCESSION NO.	3. RECIPIENT'S CATALOG NUMBER
USAAVRADCOM TR-80-D-7	AD-A088325	

4. TITLE *(and Subtitle)*	5. TYPE OF REPORT & PERIOD COVERED
INVESTIGATION OF PERFORMANCE, NOISE, AND DETECTABILITY CHARACTERISTICS OF REMOTELY PILOTED VEHICLE (RPV) PROPELLERS.	Final Report.
	6. PERFORMING ORG. REPORT NUMBER
	RASA/SRL-14-79-05

7. AUTHOR(s)	8. CONTRACT OR GRANT NUMBER(s)
D. S. JanakiRam	DAAJ02-77-C-0029

9. PERFORMING ORGANIZATION NAME AND ADDRESS	10. PROGRAM ELEMENT, PROJECT, TASK AREA & WORK UNIT NUMBERS
RASA Division Systems Research Laboratories, Inc. 1055 J. Clyde Morris Boulevard Newport News, Virginia 23602	62209A 1L62114AH7300 001 EK

11. CONTROLLING OFFICE NAME AND ADDRESS	12. REPORT DATE
Applied Technology Laboratory, US Army Research and Technology Laboratories (AVRADCOM), Fort Eustis, Virginia 23604	June 1980
	13. NUMBER OF PAGES
	167

14. MONITORING AGENCY NAME & ADDRESS *(if different from Controlling Office)*	15. SECURITY CLASS. *(of this report)*
	UNCLASSIFIED
	15a. DECLASSIFICATION/DOWNGRADING SCHEDULE

16. DISTRIBUTION STATEMENT *(of this Report)*

Approved for public release; distribution unlimited.

17. DISTRIBUTION STATEMENT *(of the abstract entered in Block 20, if different from Report)*

18. SUPPLEMENTARY NOTES

19. KEY WORDS *(Continue on reverse side if necessary and identify by block number)*

Detectability
Noise
Propeller
RPV

20. ABSTRACT *(Continue on reverse side if necessary and identify by block number)*

Several small-scale propeller configurations applicable to a conceptual Remotely Piloted Vehicle (RPV) aircraft were designed, fabricated, and tested to determine their performance, acoustic, and detectability characteristics. The tests were conducted in static and simulated forward flight conditions in a wind tunnel. Propellers tested included tractor, pusher, and ducted configurations. The acoustic data obtained was used to determine the slant

DD ₁ FORM 1473 EDITION OF 1 NOV 65 IS OBSOLETE

range and altitude of no detection of each propeller configuration.
The data was analyzed to determine the effects of blade number,
blade design (activity factor and twist), diameter, tip speed,
thrust, and forward velocity on the acoustic and detectability
characteristics of the propeller configurations tested.   The per-
formance data did not show any conclusive trends except that the
ducted and pusher propeller configurations tested were less
efficient than their open and tractor counterparts respectively.

It is concluded that the acoustic and detectability characteristics
of small-scale RPV propellers are, in general, significantly differ-
ent from those of the large-scale propellers.   It was found that
the forward velocity has a significant effect on the acoustic char-
acteristics as well as the detection distances (slant range and
altitude of no detection) of most of the RPV propeller configura-
tions tested.   An increase in forward velocity resulted in a signi-
ficant drop in the SPLs at higher harmonics (beyond 4th or 5th) of
the blade passage frequency in the forward direction as well as in
and about the plane of the propeller.   In fact, for most of the
propeller configurations tested, an increase of forward velocity
from 15 ft/sec (4.6 m/sec) to 50 ft/sec (15.24 m/sec) resulted in a
drop of about 10 to 20 dB in the higher harmonic SPLs.   However, it
was found that most of the RPV propellers tested would be detected
at one of the first few harmonics of their blade passage frequency
(mostly first or second harmonic).   The effect of forward velocity
on the detection distances of RPV propellers seems to depend on
such parameters as blade number, blade planform (activity factor),
and diameter.   The variation of slant range with forward velocity
is, in general, different from that of the altitude of no detec-
tion, though they may be similar over a small range of forward ve-
locities.   Of the propellers tested at the design values of tip
speed and thrust, three-bladed propellers were generally less de-
tectable than either the two- or four-bladed propellers for most of
the forward velocities considered.   Generally, such blade param-
eters as activity factor, twist, and radius did not have a strong
effect on the acoustic and detectability characteristics of RPV
propellers.   However, as expected, tip speed and thrust had a very
strong effect on the acoustic and detectability characteristics of
RPV propellers.   Ducted and pusher propeller configurations were in
general found to be more detectable than their open and tractor
counterparts, respectively.   Most of the propellers tested showed a
strong directivity in their acoustic radiation patterns, though the
directivity pattern of a given propeller was not significantly
affected by the forward velocity.

PREFACE

TABLE OF CONTENTS

LIST OF ILLUSTRATIONS

LIST OF TABLES

INTRODUCTION

Many lightweight aircraft and a few present-day RPVs use propellers as their means of propulsion. It has been established that on a propeller-driven aircraft, the propeller is a primary source of noise. The noise radiated by a propeller is of considerable importance both from the civil viewpoint as regards annoyance and from the military viewpoint as regards detectability.

The primary objective of this investigation is to develop noise and detectability trending data of small-scale propellers. The results are aimed at establishing criteria for design of small, low noise propellers (minimum detection) applicable to a conceptual RPV aircraft.

The distance at which an aerial vehicle can be aurally detected depends primarily on the frequency and sound pressure levels of the noise generated by the vehicle, the effects of atmosphere on noise propagation, the altitude at which the vehicle is operating, the ambient noise level at the point of detection, and the response characteristics of the observer. In order to minimize the detection distance, it is imperative that one look for means of reducing the noise level of the source, which in the case of muffled piston engine RPVs is the propeller. The propellers used in mini-RPVs are smaller [1 to 2 feet (.3048 to .6096 m) in diameter] than those used in the conventional aircraft. Extensive research has been done in the past to quiet propellers, but most of this work was aimed at quieting large-scale propellers [diameter of 6 feet (2 m) or greater].

Generally, the propeller noise is divided into three sources: loading noise, thickness noise, and vortex noise. The first two sources collectively called rotational noise result in a series of harmonic tones with frequencies which are multiples of blade passage frequency. The vortex noise can be attributed to the effects of viscosity such as boundary layer turbulence, separation, vortex shedding, and airfoil encounters with turbulent wake. Unlike rotational noise, vortex noise is regarded as having random characteristics with wide-band spectral content.

The loading noise is due to the steady aerodynamic loads (thrust and torque) acting on the blade elements of the propeller. The pioneering analytical work in this area was done

by Gutin (Ref. 1), who obtained analytically the sound pressure levels and the directivity patterns associated with the thrust and torque loads of a propeller in static condition. Refined analyses (Refs. 2, 3, and 4) to obtain a better correlation between the predictions and experimental observations as well as to remove some of the limitations inherent in Gutin's theory were developed over the years by several scientists. As a result, the modern methods can predict the loading noise at the lower end of the spectrum reasonably well.

Displacement of the fluid caused by the finite thickness of the propeller blades also results in harmonic noise (Ref. 5). Calculations have shown that at conventional propeller tip speeds, thickness noise is generally small compared to that arising from thrust and torque. At higher tip speeds, however, it may exceed the loading noise in the higher harmonics.

The first theory of vortex noise was developed by Yudin (Ref. 6) and was based on the flow around rotating rods. Early prediction methods were mostly empirical and had to depend on experiments to obtain the empirical constants, as the underlying mechanisms of broad-band noise were not thoroughly understood. More recently, a few broad-band noise prediction

[1] Gutin, L., On the Sound Field of a Rotating Propeller, NACA TM 1195, 1948.

[2] Hubbard, Harvey H., and Regier, Arthur A., Free-Space Oscillating Pressures Near the Tips of Rotating Propellers, NACA TR 996, 1950.

[3] Garrick, I.E., and Watkins, C.E., A Theoretical Study of the Effect of Forward Speed on the Free-Space Sound-Pressure Field Around Propellers, Report 1198, NACA, 1954.

[4] Ollerhead, J.B., and Lowson, M.V., Problems of Helicopter Noise Estimation and Reduction, Paper No. 69-195, AIAA, Feb. 17-19, 1969.

[5] Arnoldi, R.A., Near-Field Computations of Propeller Blade Thickness Noise, Report R-0896-2, UAC Research Department, East Hartford, CT, Aug. 1956.

[6] Yudin, E.Y., On the Vortex Sound from Rotating Rods, RM 1136, NACA, 1947.

methods (Refs. 7 and 8) have been developed which seem to satis-
factorily predict measured results.

At moderate tip speeds, that is, slightly below the onset of
compressibility effects, both vortex noise and rotational noise
due to thickness are lower than the rotational noise due to
thrust and torque. However, at low tip speeds, vortex noise
becomes important.

After identifying the sources of propeller noise, scientists
(Refs. 9 and 10) over the years have tried to design "quiet
propellers" without adversely affecting their performance. It
was established that the most powerful single factor affecting
the noise level of a propeller is its tip speed. As the tip
speed is reduced, overall noise levels are reduced and there
is a trend toward the reduction of the levels of the high
frequency spectral components. Reducing tip speed requires
that the diameter be increased to recover the aerodynamic ef-
ficiency, which results in an increase in the propeller weight.
Reducing the tip speed also requires that the rpm be decreased,
thus necessitating a greater gear ratio with the consequent
increase in the weight of the gearbox. At a given tip speed
such factors as blade loading and blade geometry can be sig-
nificant as far as noise reduction is concerned. An increase
in the number of blades for a given power is generally bene-
ficial in reducing noise. Reducing blade loading or increas-
ing blade area will also generally result in a reduction of
propeller noise.

[7] Barry, Frank W., and Magliozzi, Bernard, Noise Detectability
Prediction Method for Low Tip Speed Propellers, AFAPL-TR-71-
37, Wright-Patterson AFB, Ohio, June 1971.

[8] Brown, David, and Ollerhead, J.B., Propeller Noise at Low
Tip Speeds, AFAPL-TR-71-55, Wright-Patterson AFB, Ohio,
Sep. 1971.

[9] Regier, A.A., and Hubbard, Harvey H., Factors Affecting the
Design of Quiet Propellers, NACA RM No. L7405, Sep. 1947.

[10] Magliozzi, B., V/STOL Rotary Propulsion Systems Noise Pre-
diction and Reduction, Vol. 1, Report No. FAA-RD-76-49-1,
US Dept of Transportation, Washington, D.C., May 1976.

A parametric investigation which was conducted (Ref. 11) to
relate the far-field noise to the propeller design parameters
showed that relatively low noise characteristics were obtained
for a propeller with a lightly loaded tip region, thin air-
foil sections, a fairly high activity factor, tapered planform,
and low-to-medium camber. Those conclusions were made on the
basis of static tests and thus may not necessarily be wholly
valid for propellers in flight. A trend study (Ref. 7) using
noise detectability methods also showed that for minimum de-
tectability, propellers should operate at the lowest possible
tip speed, have a wide blade chord, have a larger diameter
than that required for performance, and have three to five
blades; four blades is the apparent optimum, as more blades
increased detectability of broad-band noise and fewer blades
increased detectability of harmonic noise. While the tip
speed should be a minimum consistent with achieving the re-
quired thrust, a trade-off study to consider the increased
horsepower required at low tip speeds may be needed to select
the optimum tip speed.

Until recently, the majority of the research work conducted
on propeller noise has been based on static test data, as
the methodologies available for the prediction of propeller
noise characteristics were scarce. Test data taken during
a flyover (Ref. 12) shows that the tone and broad-band noise
is significantly lower in flyover than at the static condi-
tion, which may be due to the relief of blade loading in for-
ward flight and to different inflow conditions. It has also
been suggested that the lower noise levels in forward flight
may be due to a drop in fluctuating loads in that regime due
to the rapid transport of the wake downstream. In order to
understand noise sources and to develop prediction methodol-
ogies which correctly reflect the influence of forward flight
on propeller noise, definitive forward flight testing will
be required. However, until such in-flight test data becomes
available, the best course of action for noise reduction

---

[11] Magliozzi, B., and Ganger, T.G., Advanced V/STOL Propeller
Technology -- Far-Field Noise Investigation, AFFDL-TR-71-88,
Vol. XIII, Wright-Patterson AFB, OH., March 1972.

[12] Magliozzi, B., The Influence of Forward Flight on Propeller
Noise, NASA CR-145105, Feb. 1977.

appears to be to design quiet propellers based on the guide-
lines developed to date and aerodynamic performance methodol-
ogy in static thrust conditions.

While the reduction in the noise level of the propeller auto-
matically aids the detectability problem, some other approaches
have also been tried to reduce the noise level and hence the
aural detectability of the propeller-driven aircraft.

One such approach is to add a shroud to the propeller. Al-
though most of the previous discussion also applies to
shrouded propellers, the addition of a shroud introduces addi-
tional potential for noise reduction. A shroud as a propeller
silencer and thrust augmentor at takeoff was proposed before
World War II, but research in this area was not forthcoming
until after the war. It was reasoned that a large part of
the thrust of a shrouded propeller is the result of suction
at the leading edge of the shroud and that this suction should
give thrust with little noise, at least during takeoff.
Harvey Hubbard (Ref. 13) was one of the first scientists to
explore the noise characteristics of shrouded propellers.
He found that as in the case with unshrouded propellers, an
increase in the number of blades and a reduction in tip speed
tend to reduce the sound pressures. He also concluded that,
in general, if the shrouded propeller satisfies the require-
ment of a good aerodynamic design, good sound characteristics
will also be obtained. For example, if the flow over the
shroud breaks down ahead of the propeller plane, the noise
could be considerably higher than that of a conventional free
propeller due to the interaction of the rotating propeller
blades with the irregular flow over the shroud.

External aerodynamic diffusion using a highly divergent shroud
with proper boundary layer control as a means of reducing the
noise output of a propeller was investigated by Longhouse
(Ref. 14). External aerodynamic diffusion provides an exten-
sion of the use of propeller thrust relief as a means of dis-
crete frequency noise reduction. He found that external

---

[13] Hubbard, Harvey H., Sound Measurements for Five Shrouded
Propellers at Static Conditions, NACA TN No. 2024, Apr 1950.

[14] Longhouse, Richard E., Application of External Aerodynamic
Diffusion to Reduce Shrouded Propeller Noise, Acoustical
Society of America: Fall Meeting, Miami, Florida, Nov 28-
Dec 1, 1972.

aerodynamic diffusion is an effective agent against steady lift and rotor-stator potential interaction noise. While the shrouded propeller with its aerodynamic advantages is found to be an attractive approach for noise reduction, a detailed investigation of the effects of such parameters as the tip clearance, shroud chord length, and propeller location in the shroud on the noise output of the shrouded propeller must be made. It is also noted that the shroud is not effective at high forward speeds due to large drag, and as such may not contribute to a significant noise reduction and may even increase the noise output unless proper acoustic linings are used. Based purely on analytical considerations, it has been estimated that, compared to an unshrouded propeller of equal takeoff performance, there may be a potential for as much as a 20 dB noise reduction (Ref. 15) with a shrouded propeller operating in the static thrust condition. It was also shown (Ref. 15) that other concepts like variable camber propeller may help reduce the noise as well as increase the cruise efficiency.

While most of the noise reduction studies to date have been confined to large-scale propellers used in general aviation aircraft, it was the aim of this study to examine means of achieving noise reduction for small-scale propellers [1 to 2 feet (.3048 to .6096 m) in diameter] that will be used in RPVs. The first step in undertaking such a task would be to extend the ideas used for large-scale propellers to the small-scale propellers. However, scale effects could be important in such a case. The parameters that highlight the scale effects are tip Mach number and Reynolds number. If the tip Mach number is in the range where compressibility effects do not play a major role, its effect should be very small. However, the smaller Reynolds number associated with the small-scale propellers could have a definite effect. The propeller blade section characteristics (C_D and $C_{L_{max}}$) are strongly influenced by the Reynolds number. The airfoil data at low Reynolds numbers (3 to 6×10^5) is very scarce. Only recently have appropriate corrections for the drag coefficient

---

[15] Rosen, George, and Rohrbach, Carl, The Quiet Propeller -- A New Potential, Hamilton Standard, AIAA Paper No. 69-1038.

16

at low Reynolds number been proposed (Ref. 16). These corrections may be helpful in designing low-noise, small-scale propellers.

Hoehne and Luce (Ref. 17) have investigated the noise characteristics of small-scale propellers that might be used on RPVs. Based on the available experimental data and an extension of the ideas expounded by Trillo (Ref. 18), they devised an empirical prediction method correlating the noise characteristics with the propeller performance data available from NACA tests of large-scale propellers. Scale effects were ignored in this method. It was found that a decrease in noise could be obtained by operating at larger blade angles, lower rpm, and smaller diameter, but at a penalty in propulsive efficiency. Shimovetz and Smith (Ref. 19) examined the noise reduction of propeller-driven RPVs in which aural detectability of the engines was one of the most important criteria. They concentrated on the engine exhaust noise and arrived at the best possible muffler designs. It was concluded that when the engine exhaust noise was muffled, the predominant noise source was the propeller.

The noise characteristics of small propellers with and without forward flight simulation were examined by Grosche and

---

[16] Borst, Henry V., et al., Aerodynamic Design and Analysis of Propellers for Mini-Remotely Piloted Air Vehicles, Vol. I Open Propellers, USAAMRDL TR-77-45..., Applied Technology Lab., US Army Research and Technology Labs. (AVRADCOM), Fort Eustis, VA, Jan. 1978, AD A050593.

[17] Hoehne, Vernon O., and Luce, Ross G., A Research Program to Define the Relationship Between Small-Scale Propeller Performance and Noise, Final Report, Battelle Memorial Institute, Columbus, OH, Mar. 1969.

[18] Trillo, R.L., An Empirical Study of Hovercraft Propeller Noise, Hovercraft and Hydrofoil, Dec.-Jan. 1965, pp. 12-34.

[19] Shimovetz, R.M., and Smith, D.L., Mini RPV Engine Noise Reduction, AFFDL-TR-76-28, Wright-Patterson AFB, OH, Mar. 1976.

Stiewitt (Ref. 20). The purpose of the tests was to explore the noise-generating mechanisms of small-scale propellers in forward flight. Based on the noise measurements, they have shown that low forward velocities of less than 60 ft/sec (20 m/sec) reduced the rotational noise and high frequency broadband noise of the propeller by up to 20 dB as compared to static tests. It was also found that the high frequency part of the propeller noise spectrum depends markedly on the angle of attack of the blades for forward velocities greater than 60 ft/sec (20 m/sec), while laminar vortex shedding noise dominated the sound radiation for moderate angles of attack (about 3° to 5°). At higher angles of attack (8°), the laminar vortex shedding sound disappeared. Strong broad-band noise was again generated, probably due to turbulent boundary layer and flow separation, as the angle of attack was further increased.

This report presents the results of a systematic investigation of the noise characteristics and aural detectability of small-scale RPV propellers. Based on the effects of various parameters on noise developed for full-scale propellers, several propeller configurations with changes in the diameter, blade number, blade planform shape, twist distribution, and airfoil section were designed and fabricated. Ducted propeller configurations and tandem propeller configurations with small axial spacing and different blade phase relationships were also designed. Various propeller configurations were tested in the static operating condition and at different forward flight velocities simulated in a wind tunnel. The acoustic data obtained was reduced to determine the aural detection distances, and the propeller configurations with the least aural detectability were then determined. In the following sections, the details of the design, the experimental tests, the data analysis, and the results are presented.

---

[20] Grosche, F.R., and Stiewitt, H., Investigation of Rotor Noise Source Mechanisms with Forward Speed Simulation, Presented at AIAA 4th Aeroacoustics Conference, Atlanta, Georgia, Oct. 1977.

DESIGN OF TEST EQUIPMENT

All propeller configurations were designed to develop 4 thrust
horsepower (thp) at a cruise speed of 75 knots (38.58 m/sec)
at 4000 feet (1220 m) altitude and 95°F (35°C). Although
the number of blades for the propeller configurations varied
between two and six, a blade number of four was used for the
basic designs. Two propellers of diameters 20 inches (.508 m)
and 26 inches (.6604 m) were designed to provide optimum per-
formance. These propellers were used to provide a comparative
basis with the low-noise configurations. Two axisymmetric
ducts, one for the large diameter propeller and the other for
the small diameter propeller were designed such that the duct
propeller combination also developed 4 thp at the cruise speed.

DESIGN OF OPTIMUM PERFORMANCE PROPELLERS

The design of the optimum performance propellers was based on
the principles formulated by Betz (Ref. 21). According to
Betz, a propeller with a given thrust or power has the mini-
mum loss of energy and the highest efficiency if the trailing
vortex sheets, after an initial limited deformation, move
axially downstream as rigid screw surfaces. It can be shown
that the ultimate wake vortex system for an optimum propel-
ler having the highest possible efficiency for a given diam-
eter, number of blades, advance ratio, and power input is
one having that particular distribution of blade bound vortex
strength which results in the ultimate wake vortex sheets
having constant pitch. This implies that all sectional ele-
ments of the optimum propeller blade will be operating at the
same propulsive efficiency. Theodorsen extended these ideas
and formulated a design procedure for optimum performance
propellers (Ref. 22). This procedure was used in the design
of the two optimum performance propellers. For a given num-
ber of blades, diameter, rotational speed, and power input,
a blade geometry (chord and twist distribution) which results
in the highest efficiency was obtained.

---

[21] Betz, A., Screw Propellers with Minimum Energy Loss, Tech-
nical Translation 736, National Research Council of Canada,
Ottawa, Ontario, Canada, 1958. Original work was published
in 1919.

[22] Theodorsen, T., Theory of Propellers, McGraw-Hill Book Com-
pany, Inc., New York, New York, 1948.

The propeller rotational speeds were chosen consistent with the given engine power curves (see Fig. 1); that is, the engine will develop the required power at the chosen rotational speeds. A rotational speed of 4500 rpm was chosen for the large diameter propeller [26 inches (.6604 m)]. Since it was decided that both the large and the small diameter propellers should have the same tip speed, 510 fps (155.5 m/sec), the small diameter propeller had a design rpm of 5850. The basic tip speed was kept constant to remove tip speed as a variable from the other test parameters.

The procedure utilized (Ref. 22) to design the propellers is based on the wake edge helix angle, which is fixed by the apparent wake velocity parameter $\overline{w}$ (w/^{V}F), where w is the apparent wake velocity of a contracting wake and ^{V}F is the forward velocity of the propeller. For a given power input, a design value of the apparent wake velocity parameter $\overline{w}$ is first obtained using the procedure outlined in Reference 22. Knowing $\overline{w}$, the nondimensional bound vortex strengths as well as the angles of inclination of the resultant velocity vector at various blade radial stations were determined. For the design analysis, each blade was divided into eleven nondimensional radial stations ranging from x = .25 to x = .95 where x is the local nondimensional radius. The spanwise distribution of airfoil chord was chosen to be linear and consistent with the normal propeller designs. For the chosen chord distribution, the lift coefficient distribution at the different radial stations was determined using the expressions given in Reference 22. A NACA 230 series airfoil section was chosen for the blades, since the section characteristics for various thickness ratios (Ref. 23) and suitable formulae to extrapolate these for low Reynolds numbers (2 to 3x10^5) associated with the present propeller design were available (Ref. 24). Knowing the airfoil section and assuming its thickness ratio at each radial station, the airfoil characteristics at the low Reynolds numbers of these sections were determined. Using the expressions given in Reference 22 and the airfoil characteristics, the blade angle distribution along the blade was determined. The profile losses of the

[23] Jacobs, Eastman N., and Abbott, Ira H., Airfoil Section Data Obtained in the NACA Variable Density Tunnel as Affected by Support Interference and Other Corrections, NACA Report No. 669, 1939.

[24] Jacobs, Eastman N., and Albert, Sherman, Airfoil Section Characteristics as Affected by Variations of the Reynolds Number, NACA Report No. 586, 1937.
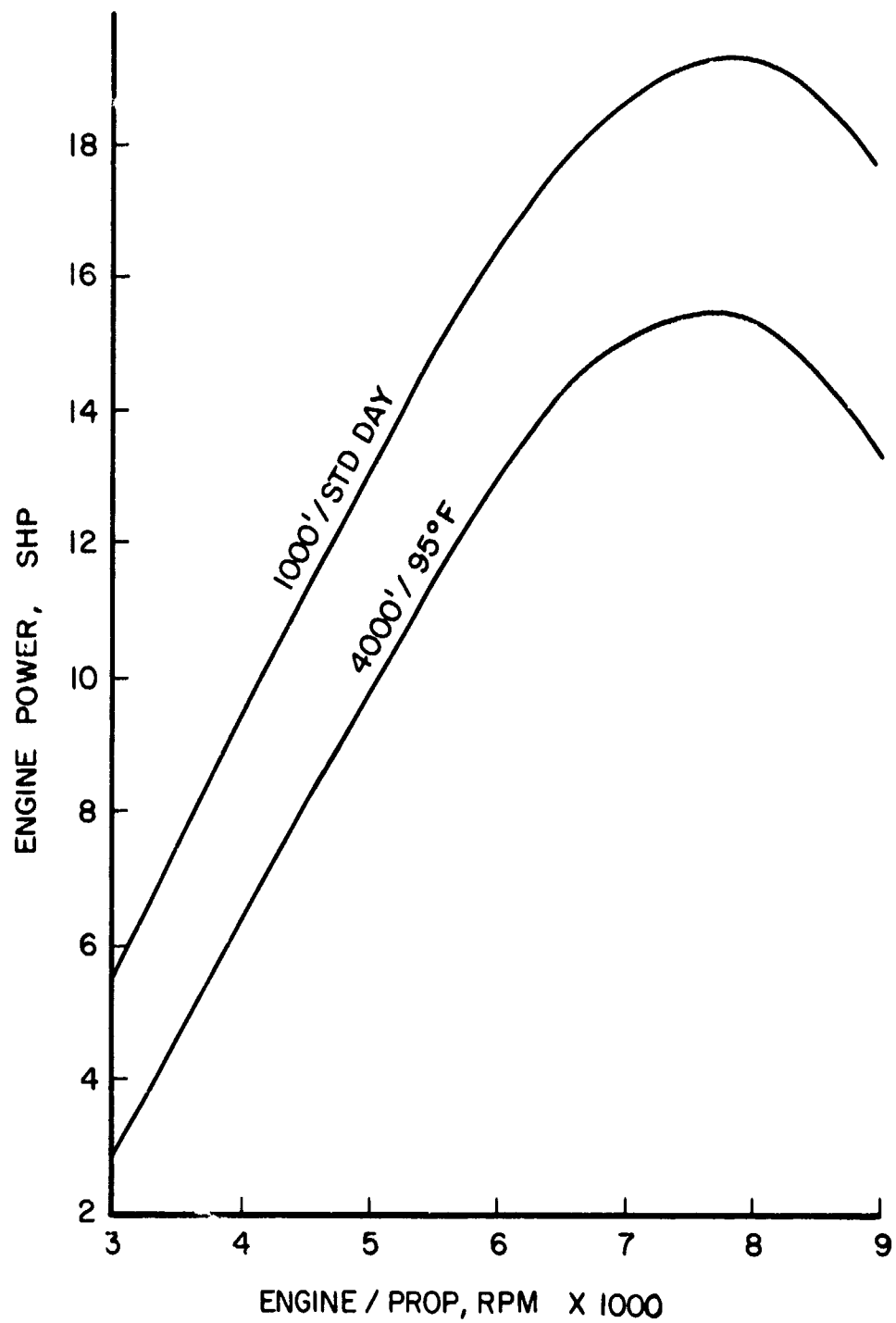
Figure 1. Modified Engine Curves for RPV Vehicles.

blades were then computed and incorporated into the determination of net thrust and total power absorbed. The above design procedure was iterated until an optimum blade geometry that resulted in the desired thrust was obtained.

The blade design characteristics were determined at eleven different radial stations. These are presented in tabular form for each of the two propellers in Table 1. These are also presented graphically in Figure 2. It is to be noted that the spanwise distribution of airfoil thickness ratio is the same for both the small and large diameter propellers. To help fabricate these propeller blades, the surface coordinates of the various airfoil sections along the blade were determined using the available NACA 230 airfoil section data. Since the blades had square tips, the design characteristics were suitably extrapolated to the tip. The blades have rounded shank sections inboard of x (r/R) = 0.25, and a smooth transition was made between the round blade shank section and the airfoil section at x = 0.25. The shank section was centered at the 50% chord line, as was the planform taper.

DESIGN OF AXISYMMETRIC DUCT

The axisymmetric ducts used in combination with the optimum performance and low-noise propellers were designed using the numerical computation method developed by Kaskel, et al. (Ref. 25). This design method is based on the three-dimensional theory of ducted propellers developed by the same authors. Using this theory, a computation method was developed wherein for a given propeller, defined by the radial distribution of circulation, propeller thrust coefficient, diameter, number of blades, and duct geometry, the duct thrust coefficient was determined. An optimum circulation distribution with a tip correction was used for the propeller. The axisymmetric ducts were designed such that the duct-propeller combination developed about 4 thp at the design cruise speed of 75 knots (38.58 m/sec). The duct designs for both diameters were based on the characteristics of the four-bladed optimum performance propellers. A typical duct-propeller layout is shown in Figure 3. The important duct-propeller design parameters are the duct airfoil

---

[25] Kaskel, A.L., Ordway, D.E., Hough, G.R., and Ritter, A., A Detailed Numerical Evaluation of Shroud Performance for Finite-Bladed Ducted Propellers, Therm, Inc., TAR TR-639, December 1963.

TABLE 1

CHARACTERISTICS OF PERFORMANCE BLADES

NACA 230 Series
Airfoil Sections Used

NONDIMEN-SIONAL RADIUS, X(=r/R)	THICK-NESS RATIO, t/c	LARGE DIAMETER, D=26" (.6604 m) (BD2 DESIGN)		SMALL DIAMETER, D=20" (.5048 m) (BD1 DESIGN)	
		C/D*	BLADE ANGLE, β (deg)	C/D*	BLADE ANGLE, β (deg)
0.25	0.180	0.1039	49.72	0.140	53.404
0.30	0.150	0.0995	44.87	0.135	48.764
0.40	0.120	0.0910	37.09	0.125	40.987
0.50	0.100	0.0820	31.59	0.115	35.334
0.55	0.090	0.0777	29.51	0.110	33.178
0.60	0.083	0.0730	27.63	0.105	31.152
0.70	0.068	0.0640	24.36	0.095	27.489
0.75	0.060	0.0600	23.00	0.090	25.914
0.80	0.054	0.0560	21.65	0.085	24.412
0.90	0.044	0.0475	19.03	0.075	21.266
0.95	0.040	0.0430	17.50	0.070	19.305
1.00	0.040	0.0390	16.00	0.065	17.500

C/D* = Local Chord Length/Diameter of the Propeller Blade
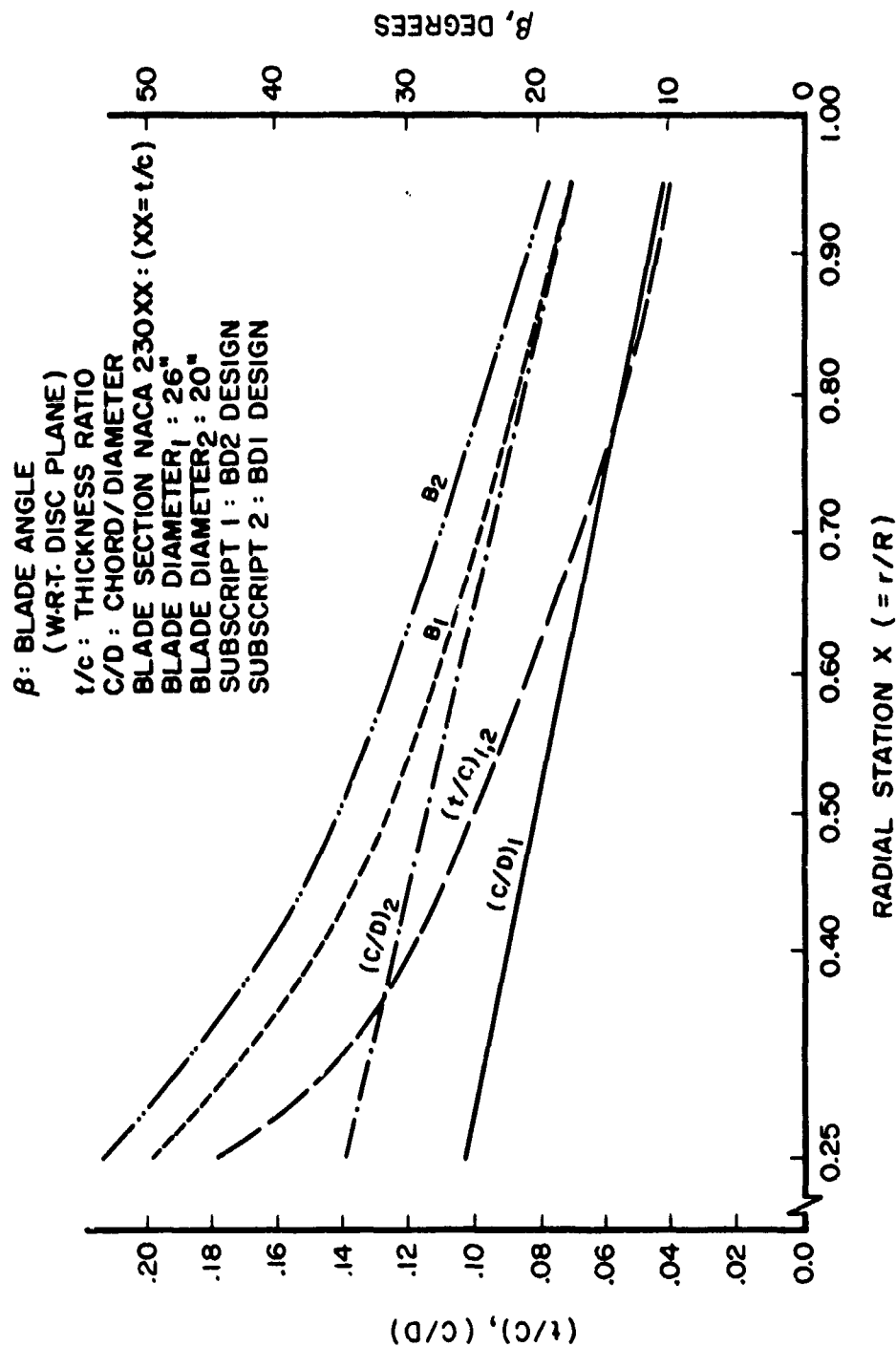
Figure 2. Blade Characteristics of Performance Propellers.

β: BLADE ANGLE
(W.R.T. DISC PLANE)
t/c: THICKNESS RATIO
C/D: CHORD/DIAMETER
BLADE SECTION NACA 230XX: (XX=t/c)
BLADE DIAMETER$_1$: 26"
BLADE DIAMETER$_2$: 20"
SUBSCRIPT 1: BD2 DESIGN
SUBSCRIPT 2: BD1 DESIGN

β, DEGREES

RADIAL STATION X (=r/R)

(t/c), (C/D)

B_2
B_1
$(t/c)_{1,2}$
$(C/D)_2$
$(C/D)_1$

R_C: RADIUS TO THE DUCT CHORD SURFACE

R_P: PROPELLER RADIUS

R_i: RADIUS OF THE INNER DUCT SURFACE AT THE PROPELLER PLANE

C': CHORD LENGTH OF THE DUCT

X_P: DISTANCE FROM THE L·E OF THE DUCT TO THE PROPELLER PLANE

Figure 3. Duct-Propeller Layout.

section, the chord length of the duct, the blade tip clearance, and the location of the propeller plane from the leading edge of the duct section. A thickness ratio of 12% was chosen in order to accommodate the acoustic lining put on the interior surface of the ducts. The duct was designed such that its section chord line is parallel to the thrust axis of the propeller and its camber surface is concave upward (see Fig. 3). The blade tip clearance is given by $(R_i - R_p)$, where R_i is the radius of the inner duct surface in the plane of the propeller and R_p is the radius of the propeller. The plane of the propeller was chosen to be at the midchord of the duct section. All the duct geometric parameters were based on current practice and chosen such that the numerical design method used was able to handle them. These geometric parameters for both the large and small ducts are given in Table 2.

For a given propeller thrust coefficient and the chosen duct and propeller geometry, the duct thrust coefficient was determined using the design method outlined in Reference 25. Several values were chosen for the thrust of the propeller, and for each thrust value the thrust developed by the duct was determined. The particular propeller thrust value which gave a total thrust (propeller + duct thrust) of about 18 pounds (80 newtons) at 75 knots (38.58 m/sec) was chosen and the corresponding duct design was selected. According to the design, the duct for the smaller propeller developed about 18% of the total thrust at the design cruise conditions. The larger duct developed about 15% of the total thrust.

DESIGN OF PROPELLER CONFIGURATIONS FOR NOISE INVESTIGATION

The acoustic propeller configurations were designed such that the parameters that affect the noise output of propeller configurations could be investigated. Since the survivability is one of the most important considerations of propeller-driven RPV vehicles, the slant range detectability was chosen to be the determining criterion in the design of the basic quiet propeller; i.e., the propeller configuration with the least slant range distance at the given operating conditions was considered the low-noise propeller configuration. The operating conditions for these designs were such that the propeller developed 4 thp at a cruise speed of 75 knots (38.58 m/sec) and an altitude of 1000 feet (304.8 m). Two four-bladed

26

TABLE 2

CHARACTERISTICS OF SHROUDS OR DUCTS

Propeller Designation	Small Diameter	Large Diameter
Radius of the Propeller, R_p, Inches (Meters)	10(.254)	13(.330)
Radius of the Inner Shroud Surface in the Plane of the Propeller, R_i, Inches (Meters)	10.10(.257)	13.13(.334)
Radius of the Shroud Chord Surface, R_c, Inches (Meters)	10.783(.274)	14.010(.356)
Location of the Propeller Plane-Distance Measured from the LE or Shroud, X_p, Inches (Meters)	5.319(.135)	6.915(.76)
Chord Length of the Shroud Section, C', Inches (Meters)	10.638(.270)	13.829(.351)
Shroud Airfoil Section	NACA 23012	NACA 23012

low-noise propeller configurations were designed. One configuration had a diameter of 26 inches (.6604 m) and the other had a diameter of 20 inches (.508 m). Both propeller configurations were designed for the same tip speed as that used in the design of optimum performance propellers.

The design was facilitated by the use of three prediction programs: the performance program developed by RASA personnel, the noise prediction program (Ref. 26), and the aural detectability program (Ref. 27). These three programs are briefly described below.

The prediction program used to estimate the performance of the propeller uses a relatively simple yet reasonably accurate expression for the determination of induced velocities at the propeller disk (Ref. 28). Airfoil characteristics appropriate to the low Reynolds numbers of these propellers (Ref. 24) were used in this program. For each propeller configuration (that is for a given blade planform, twist distribution, rotational speed, and number of blades), the program predicts the total velocity, its direction relative to the propeller disk, and the aerodynamic angle of attack at various radial stations along each propeller blade. The program then varies the collective pitch of the propeller blades in an iterative procedure until the required thrust of 18 pounds (80 newtons) corresponding to 4 thp at the design cruise speed of 75 knots (38.58 m/sec) is reached.

The output of the performance program is used as part of the input to the rotor acoustic prediction program (Ref. 26). This acoustic program predicts the rotational and vortex noise signatures of the propeller at any specified observer location. The blades are divided into several (up to 20)

[26] Johnson, H.K., Development of an Improved Design Tool for Predicting and Simulating Helicopter Rotor Noise, RASA Report 74-02, USAAMRDL TR-74-37, Eustis Directorate, US Army Air Mobility R&D Laboratory, Ft Eustis, VA, June 1974, AD 785579.

[27] Abrahamson, Louis A., Correlation of Actual and Analytical Helicopter Aural Detection Criteria, USAAMRDL TR-74-102A, Eustis Directorate, US Army Air Mobility R&D Laboratory, Ft Eustis, VA, Jan 1975, ADB002067L.

[28] Gessow, Alfred, and Meyers, Garry C. Jr., Aerodynamics of the Helicopter, Frederick Ungar Pub. Co., 1967, pp. 68.

radial sections at which the various blade and aerodynamic parameters are represented. The output of the program is the noise pressure-time history at a finite number of observer locations in the fixed system. The pressure-time history is transformed into a narrow-band spectrum by means of a fast Fourier transform.

The aural detectability program (Ref. 27) uses as input a noise spectrum obtained at a microphone location toward which the propeller is approaching in a given flight profile. The narrow-band sound pressure levels obtained for a given microphone location in the noise prediction program were used as input to the detectability program. The program computes the slant range detection distance for each frequency band for a given ambient noise spectrum using a detectability criterion developed by Ollerhead (Ref. 29). An empirical model for atmospheric attenuation of sound in the lower atmosphere over long distances was also used. The minimum slant range detection was used as the criterion for determining the best four-bladed noise propeller configuration.

In tne case of large-scale propellers, a parametric investigation (Ref. 11) showed that relatively low-noise characteristics were obtained for a propeller with a lightly loaded tip region, thin airfoil sections, a fairly high activity factor, tapered plai rm, and low-to-medium camber. A trend study (Ref. 7) using noise detectability methods also showed that in the case of large-scale propellers, for minimum detectability, propellers should operate at the lowest possible tip speed, have a wide blade chord, and have three to five blades with four blades being the apparent optimum. Both of the above trend studies were based on the use of empirical relations based on static conditions. In the absence of any information regarding low-noise characteristics of small-scale propellers in forward flight, the results of these studies were used as guidelines to arrive at the quiet RPV propeller designs.

For eacn propeller diameter, eight different configurations based on variations of planform (the activity factor and taper) and twist distribution were analyzed to determine the configuration that had the smallest slant range detection

[29] Ollerhead, J.B., Helicopter Aural Detectability, USAAMRDL TR-71-33, Eustis Directorate, US Army Air Mobility R&D Laboratory, Ft Eustis, VA, July 1971, AD730788.

distance. Each of the configurations studied had the same airfoil section (NACA 230XX) and the same thickness distribution as the optimum performance propellers.

Four different planforms characterized by varying activity factor and taper ratio and two different twist distributions characterized by different amounts of total twist were selected to form eight different propeller configurations for the small as well as the large diameter propeller. The planform shapes and the amounts of twist used were based on the results obtained for large-scale propellers in Reference 7. Linear chord and linear twist distributions were chosen to facilitate easy fabrication. The four planform shapes considered were designated by P1, P2, P3, and P4, where P1 refers to rectangular blades with A·F = 160.6; P2 refers to blades with a taper ratio of 2:1 with A·F = 160.6; P3 refers to blades with a taper ratio of 3:1 and with A·F = 160.6; and P4 refers to blades with a taper ratio of 2:1 and with A·F = 193. Note that A·F refers to the activity factor of the planform and is given by

$$A \cdot F = \frac{100\ 000}{16} \int_{r/R\ =\ .15}^{1} (C/D)\,(r/R)^3 d\,(r/R)$$

where C/D is the chord diameter ratio at a radial station r. The two twist distributions were designated by T1 and T2 where T1 has a total twist of 30°, i.e., $\phi_{r/R=.25} - \phi_{r/R=.95} = 30°$, and T2 has a total twist of about 25°. Note that ϕ is the blade angle at any radius r. Each propeller configuration was then designated by an identifier. For example, P4,T2,SD refers to a propeller configuration with P4 planform and T2 twist and SD refers to the small diameter propeller. Similarly, P4,T2,LD refers to the large diameter propeller with planform P4 and twist distribution T2.

For each propeller configuration, the performance program predicted the aerodynamic angle of attack, total velocity, and its direction at various blade sections. Each propeller configuration developed about 18 pounds (80 newtons) of thrust at the design operating conditions. The output of the program was then used as input to the acoustic prediction program to generate the noise spectra at three microphone locations on the ground corresponding to the directions 30°, 20°, and 10° from the thrust axis of the propeller. Note that the propeller is at an altitude of 1000 feet (304.8 m).

30

These noise spectra were then used to generate the slant range spectra using the slant range prediction program. The moderate ambient noise (Fig. 4), a representative model of battlefield noise (Ref. 30), was used in the computation of slant range detection distances. By using the noise spectra at three different angular locations of the microphone with respect to the propeller thrust axis, the effect of the directivity pattern on the slant ranges was taken into account.

Based on these computations, the configuration P4,T2,SD was selected as the optimum noise configuration for the smaller propeller. This configuration, with an A·F of 193 and a taper ratio of 2:1 and a total twist of 23°, had the least slant range detection distance. Similarly, for the larger propeller, the configuration P4,T2,LD also had the smallest slant range detection distance. These results seem to follow the trends obtained for large-scale propellers (Ref. 7).

The blade characteristics of the two optimum noise configurations were determined at eleven spanwise stations and are given in Table 3. In addition to these two low-noise configurations, another low-noise propeller of smaller size [diameter 20 inches (.5080 m)] with P4 planform and T2 twist distribution but with a different airfoil section was also designed. The NACA 65 series airfoil section chosen for this blade design has a design lift coefficient of 0.4 compared to a value of 0.3 used in the other designs. The thickness distribution along the blade, however, is the same as that of the low-noise configuration. This blade design was primarily used to investigate the effect of airfoil section on the noise characteristics of the blade.

In all, five different blades were designed. Two of them were designed to optimize performance and the rest were designed to have the least slant range detection distance under the design operating conditions. The salient features of these blade designs are presented in Table 4. Several sets of these blades were then fabricated. The details of the fabrication of the propeller blades and the other test equipment are given in the following section of this report.

---

[30] The Boeing Company, Vertol Div, Analysis of the Effects of Aural-Detection Range on Helicopter Operations, USAAMRDL TR-73-80, Eustis Directorate, US Army Air Mobility R&D Laboratory, Ft Eustis, VA., Mar 1974, CONF.
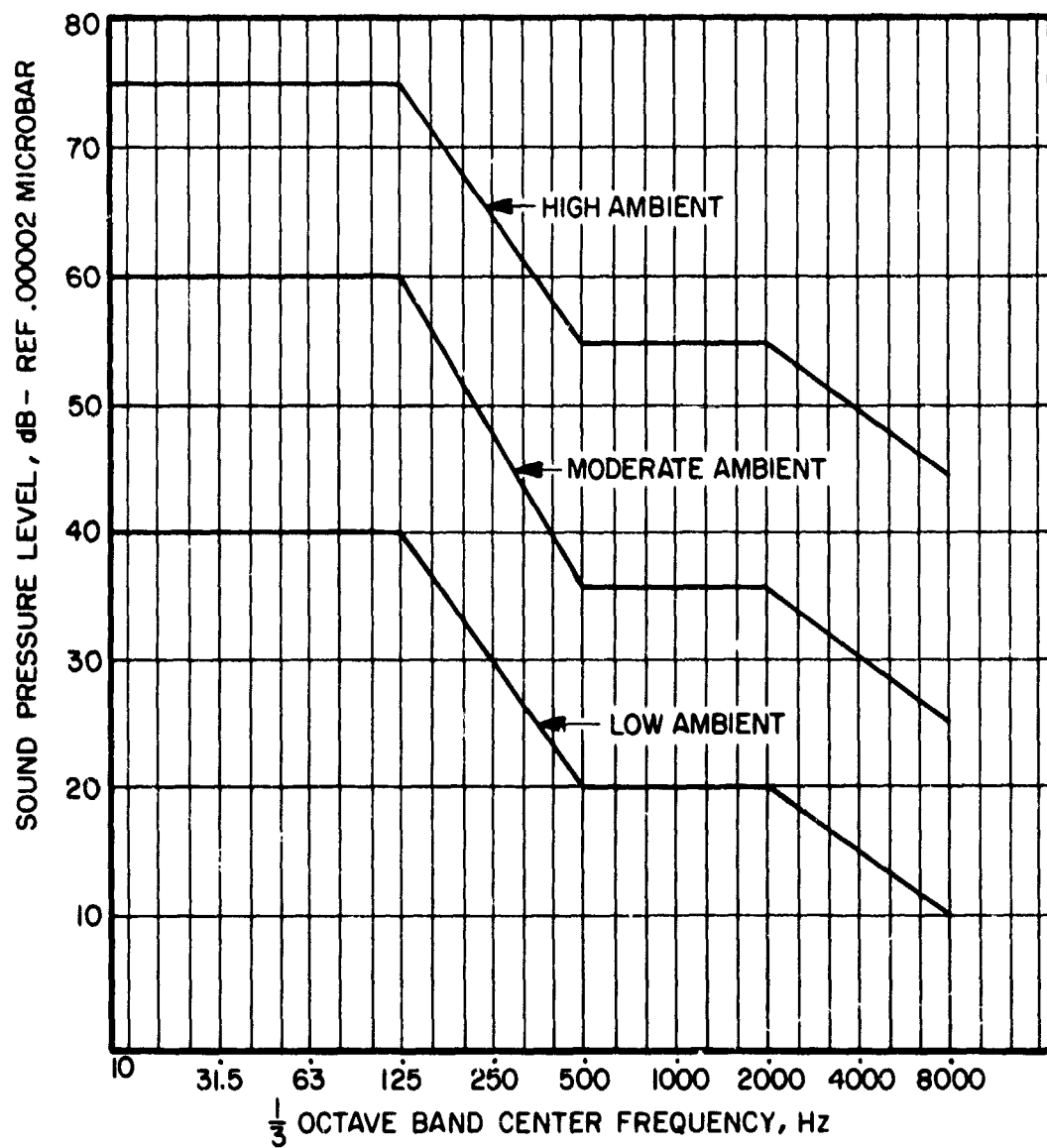
Figure 4.   Ambient Noise Levels.

32

TABLE 3

CHARACTERISTICS OF ACOUSTIC BLADES

NACA 230 Series
Airfoil Section Used

NONDIMEN-SIONAL RADIUS, X(=r/R)	THICK-NESS RATIO, t/c	LARGE DIAMETER, D=26" (.6604m) (BD4 DESIGN)		SMALL DIAMETER, D=20" (.5048m) (BD3 DESIGN)	
		*C/D	BLADE ANGLE, β (deg)	*C/D	BLADE ANGLE, β (deg)
0.25	0.180	0.1882	36.80	0.1882	38.76
0.30	0.150	0.1824	35.16	0.1824	37.12
0.40	0.120	0.1706	31.87	0.1706	33.83
0.50	0.100	0.1588	28.58	0.1588	30.54
0.55	0.090	0.1529	26.93	0.1529	28.89
0.60	0.083	0.1471	25.29	0.1471	27.25
0.70	0.068	0.1353	22.00	0.1353	23.96
0.75	0.060	0.1294	20.35	0.1294	22.31
0.80	0.054	0.1235	18.71	0.1235	20.67
0.90	0.044	0.1118	15.42	0.1118	17.38
0.95	0.040	0.1059	13.77	0.1059	15.73
1.00	0.040	0.1000	12.13	0.1000	14.09

*C/D = Local Chord Length/Diameter of the Propeller Blade

TABLE 4

CHARACTERISTICS OF DIFFERENT BLADE DESIGNS

Blade Design Designation	Size of the Blade Diameter in Inches (Meters)	Airfoil Section Used	Taper Ratio $\dfrac{C_r/R=.15}{C_r/R=1.0}$	Activity Factor	Amount of Twist in Degrees	Remarks
BD1	20 (.5048)	NACA 230XX	2.3	133	36	Optimum Performance Design Linear Chord Distribution
BD2	26 (.6604)	NACA 230XX	2.9	88	34	Optimum Performance Design Linear Chord Distribution
BD3	20 (.5048)	NACA 230XX	2	193	25	Low Noise Design Linear Chord and Twist Distributions
BD4	26 (.6604)	NACA 230XX	2	193	25	Low Noise Design Linear Chord and Twist Distributions
BD5	20 (.5048)	NACA 65-4XX	2	193	25	Low Noise Design Same as BD3 Except for a Different Airfoil Section

FABRICATION OF TEST STAND, PROPELLERS, AND DUCTS

The design and fabrication of the test equipment that was used to obtain the test data are discussed in the following sections. The various pieces of equipment, which included the propeller test stand and blade hubs as well as the various blade sets and ducts, will be discussed separately.

PROPELLER TEST STAND

To provide propeller rotational power and to measure propeller performance, a test stand was designed and fabricated. This test stand incorporates such features as an electric drive motor, an interconnecting shaft between the motor and propeller hub, a support structure allowing both static and simulated forward flight, and a means to measure propeller thrust and torque. These features are outlined below.

The support structure for the propeller test stand consists of a horizontal mounting plate having physical dimensions and interface holes allowing the test stand to be mounted in both the static thrust test cell and the subsonic wind tunnel at the University of Maryland. This mounting plate is connected to the test stand nacelle by a faired strut consisting of two 4 inch (0.1 m) diameter aluminum tubes approximately 48 inches (1.2 m) long having a 0.63 inch (.016 m) stretch formed skin between the tubes. These tubes provide both support for the test stand and conduit routing for the motor power leads, motor cooling water lines, and the various electrically shielded instrumentation wires associated with the equipment mounted within the test stand nacelle. The strut assembly terminates in a horizontally mounted 10 inch (.254 m) diameter tube which functions as a stationary mounting for the remainder of the test stand nacelle. The support strut assembly is located as far as physically possible from the propeller plane to minimize acoustical reflections from the strut surface. Figure 5 shows the strut assembly and its location with respect to the test stand nacelle.

The test stand nacelle was designed and fabricated such that several features are incorporated. The nacelle forms a stationary base which carries an internal free-floating reaction frame which allows unrestricted motion in the direction of propeller thrust. The basic nacelle consists of a 10 inch (.254 m) diameter tube having a series of bulkheads which
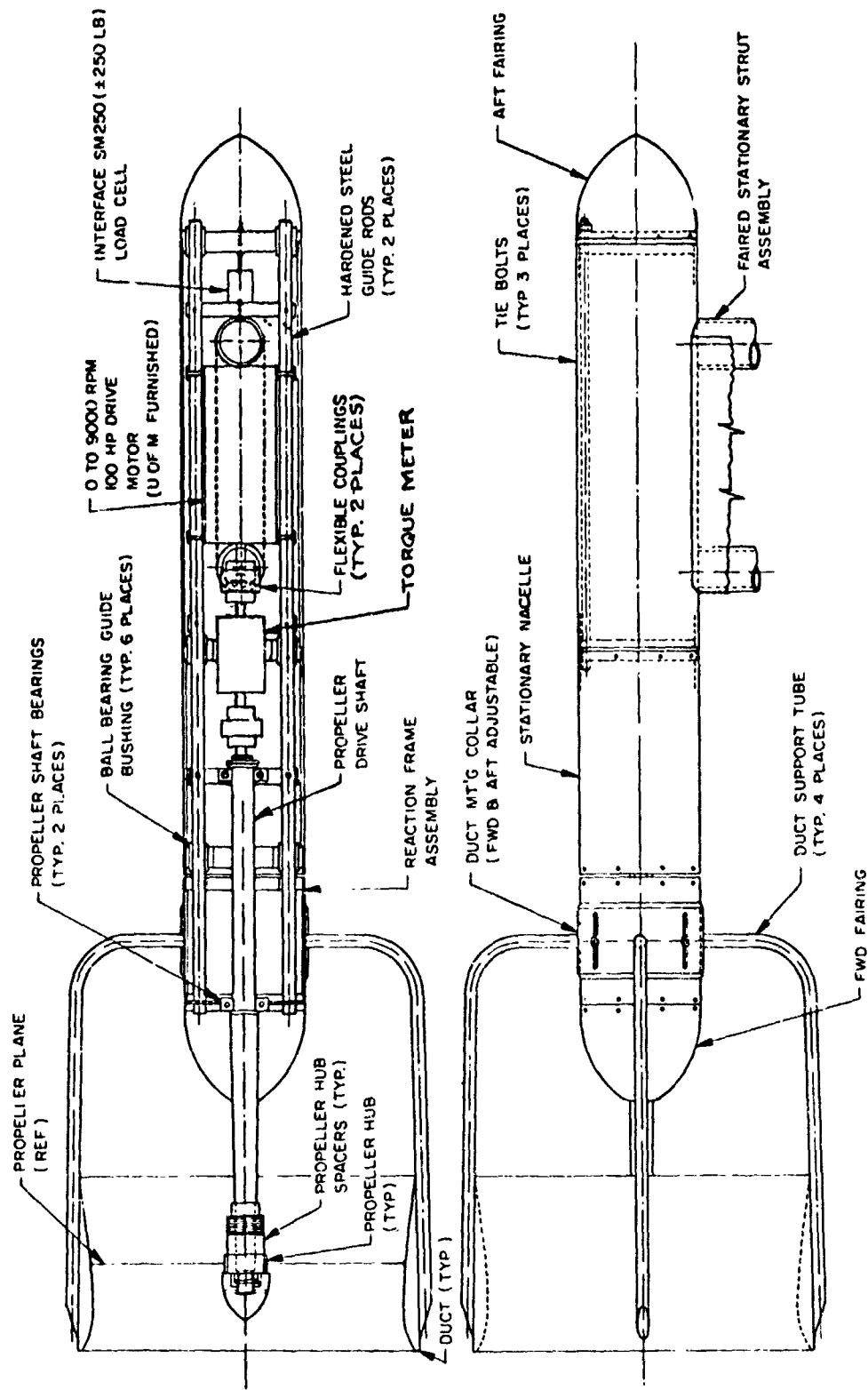
Figure 5. RPV Propeller Test Stand Assembly.

INTERFACE SM250 (±250 LB) LOAD CELL

HARDENED STEEL GUIDE RODS (TYP. 2 PLACES)

0 TO 9000 RPM 100 HP DRIVE MOTOR (U OF M FURNISHED)

FLEXIBLE COUPLINGS (TYP. 2 PLACES)

TORQUE METER

PROPELLER SHAFT BEARINGS (TYP. 2 PLACES)

BALL BEARING GUIDE BUSHING (TYP. 6 PLACES)

PROPELLER DRIVE SHAFT

REACTION FRAME ASSEMBLY

DUCT MT'G COLLAR (FWD & AFT ADJUSTABLE)

PROPELLER PLANE (REF)

PROPELLER HUB SPACERS (TYP.)

PROPELLER HUB (TYP)

DUCT (TYP)

AFT FAIRING

FAIRED STATIONARY STRUT ASSEMBLY

TIE BOLTS (TYP 3 PLACES)

STATIONARY NACELLE

DUCT SUPPORT TUBE (TYP. 4 PLACES)

FWD FAIRING

carry the reaction frame assembly and provide the thrust load cell connection between the reaction frame and the stationary structure.

The reaction frame assembly forms the active part of the test stand. This assembly, when viewed from the propeller disk plane aft, incorporates a splined drive shaft, a set of shaft bearings, a flexible coupling, and the electrical drive motor. All components of this drive system are supported by bulkheads which are spaced on two 1 inch (.0254 m) diameter hardened guide rods. The construction of the reaction frame assembly is analogous to that of a ladder in which the guide rods are the side rails and the various bulkheads appear as the rungs. The complete reaction frame assembly is suspended within the stationary test stand nacelle by passing the hardened guide rods through three ball bearing guide bushings per side. All bulkheads of the reaction frame are physically pinned to the guide rods such that the dimensional relationship from one to the other is maintained, thus allowing drive shaft bearing preload and the proper shaft end clearance to be established between the drive motor shaft and the propeller shaft.

The forward section of the reaction frame incorporates a short length of 10 inch (.254 m) diameter tube (same diameter as the stationary nacelle) on which the propeller duct supports are mounted (the duct support is described later in this report). The forward end of this tube is provided with a spun aluminum ogive fairing through which the drive shaft passes.

As shown in Figure 5, the drive motor is an integral part of the reaction frame assembly. This drive motor (provided by the University of Maryland) is of a polyphase squirrel-cage construction having an output of 0 to 9,000 rpm and a 100 hp maximum capacity. The drive motor is controlled using the University of Maryland model control system which is a variable frequency constant voltage per Hz system. This system allows any given motor rpm to be set and closely controlled. Rotational power provided by this motor is transmitted to the propeller drive shaft using a flexible coupling which is pressure packed with an elastomer to preclude any acoustical noise generation by the coupling.

The propeller ducts are mounted on the forward tubular section of the reaction frame using an adjustable collar (adjustable forward and aft along the axis of rotation such that

37

proper propeller tip to duct clearance may be achieved) and four 1 inch (.0254 m) diameter support tubes. This mounting arrangement is shown in Figure 5.

Thrust movement of a propeller is achieved using a universal (tension and compression) load cell attached on the center-line of thrust between the horizontally free-moving reaction frame and the stationary nacelle structure. Thus, the total thrust of an open propeller or propeller and duct configuration is transmitted to the reaction frame through the preloaded propeller shaft bearings and is translated by the precision ($\pm$ .03% full scale) Interface Model No. SM250 [$\pm$ 250 pounds ($\pm$ 1112.5 newtons)] load cell into an electrical signal which is read out on a Doric Model 420 Digital Transducer Indicator directly in pounds at the data acquisition station. For a latter series of wind tunnel tests, a torque meter was installed between the drive shaft and drive motor through a pair of flexible couplings (see Fig. 5). The torque meter [LEBOW 1104H-2K, range 2000 in-lbs (226 newton-meters)] was used to measure the torque absorbed by the drive shaft. The electrical signal from the torque meter was read out on a Doric Model 420 Digital Transducer Indicator directly in inch-pounds at the data acquisition station.

The aft end of the stationary nacelle is closed by using an additional spun aluminum ogive cone similar to the forward fairing of the reaction frame.

Figure 6 shows a photograph of the propeller test stand assembly.

PROPELLER BLADES/DUCTS

The different blade designs used in the tests, as well as their characteristics, are given in Table 4. Several blades were fabricated so that propeller configurations with at least six blades of each design could be tested. The blades were fabricated from a thermosetting plastic (40% glass fiber reinforced with 6/6 nylon) using an injection molding process. The injection molding process was found to be more advantageous than the other traditional handcrafting methods. The primary advantages were the dimensional repeatability and the low per-unit cost. Through the use of a single molding cavity in which all propeller blades for a given design are manufactured, blade to blade variations are reduced to a minimum. Also, the process being automated sharply reduces the per-unit cost when the initial tooling expense is amortized over

38
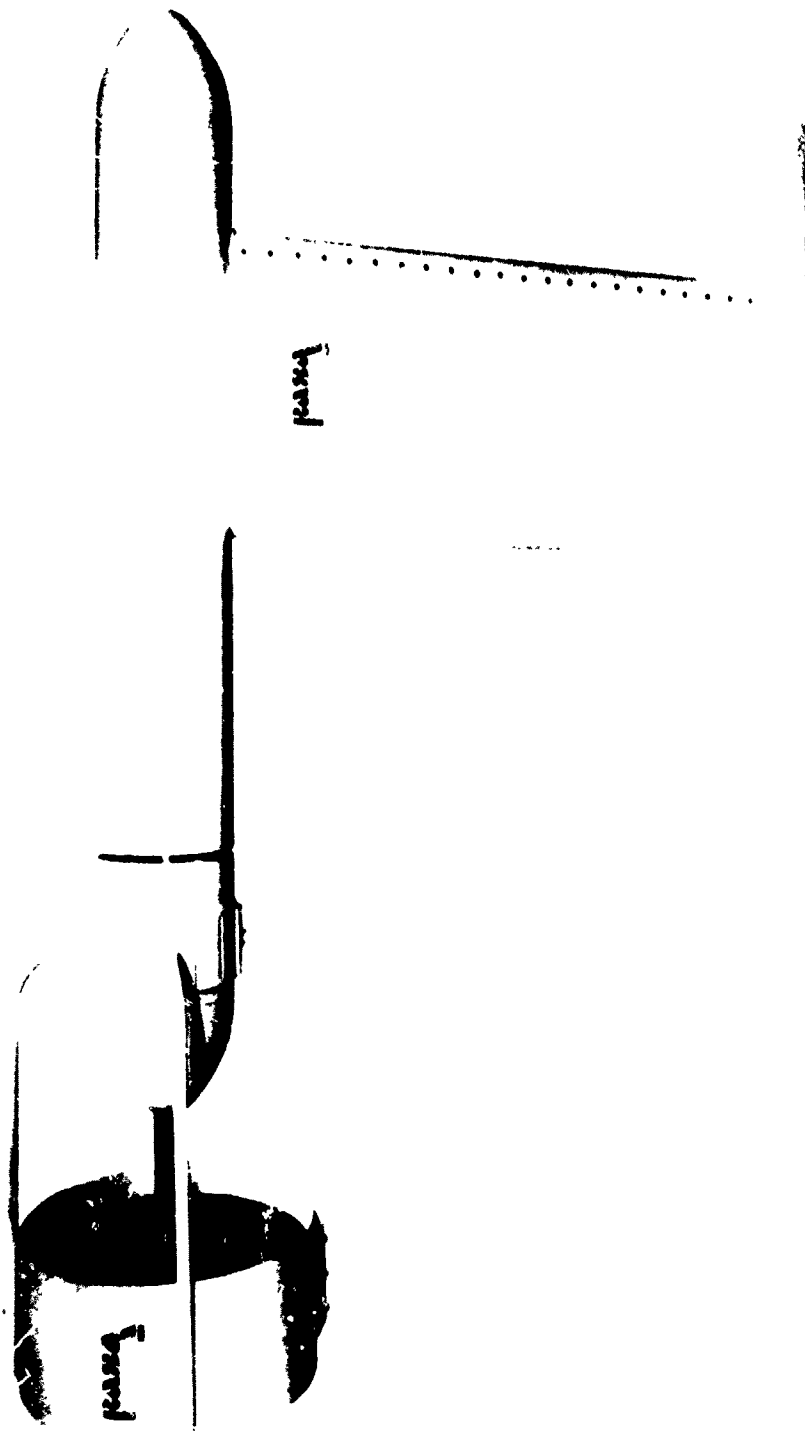
Figure 6.   Propeller Test Stand With Duct.

a production run. The different basic blade designs that were fabricated using this process are shown in Figure 7.

The design characteristics of the two ducts that were fabricated were given in Table 2. The two ducts were fabricated from laminated mahogany shells. These shells were turned on a lathe as per the specifications. The inner surfaces of the two ducts were lined (except very near the leading and trailing edges) with sound-absorbing material. The sound-absorbing material, a composite material of polyurethane foam backed by a barium sulphide loaded PVC, was contoured into the inner surface to form the design aerodynamic surface. A photograph of the duct is shown in Figure 8. For a latter series of wind tunnel tests, the foam in the ducts was replaced by a fiberglass hardskin.

HUBS

To test propeller configurations with different numbers of blades (two, three, four, and six) and to facilitate testing of spaced/phased propeller configurations, five hubs were designed and fabricated. These hubs were machined from stainless steel. The hub configurations, the number of blades they house, and their shapes are listed below.

Hub No.	No. of Blades	Shape
1	2, 3, 6	Hexagon
2	2, 4	Square
3	3	Hexagon
4	4	Square
5	3	Triangular

Hub numbers 4 and 5 were specifically built for blades with design BD4 (see Table 4). The other three hubs can accommodate any of the other blade designs (large as well as small diameter blades). Each individual hub has an internal straight spline matched to the external spline of the propeller drive shaft. Through the use of shaft spacers and two blade hubs, a phased/spaced propeller configuration can be obtained. The pitch angles of the blades are changed manually by a system of mating location holes in the hub socket and blade shank and a location pin. Through a careful selection of these numbers of holes, 1/2° increments of blade pitch are provided.
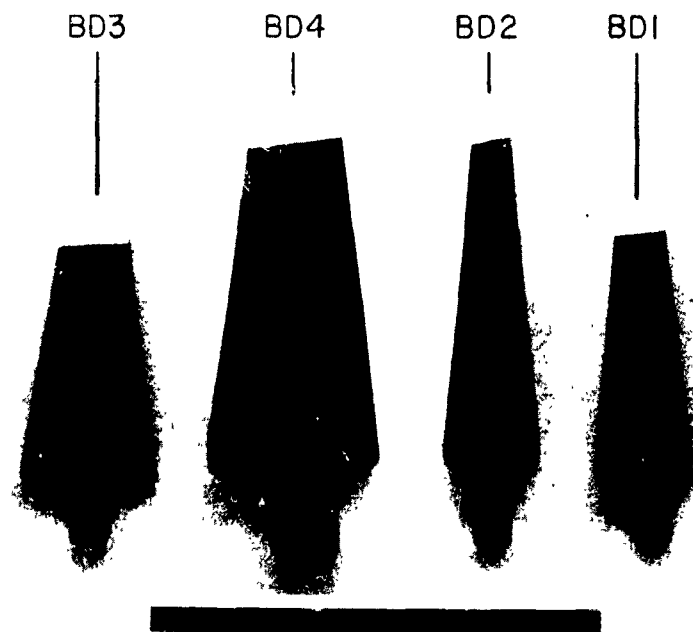
Figure 7.   Blade Designs That Were Fabricated.
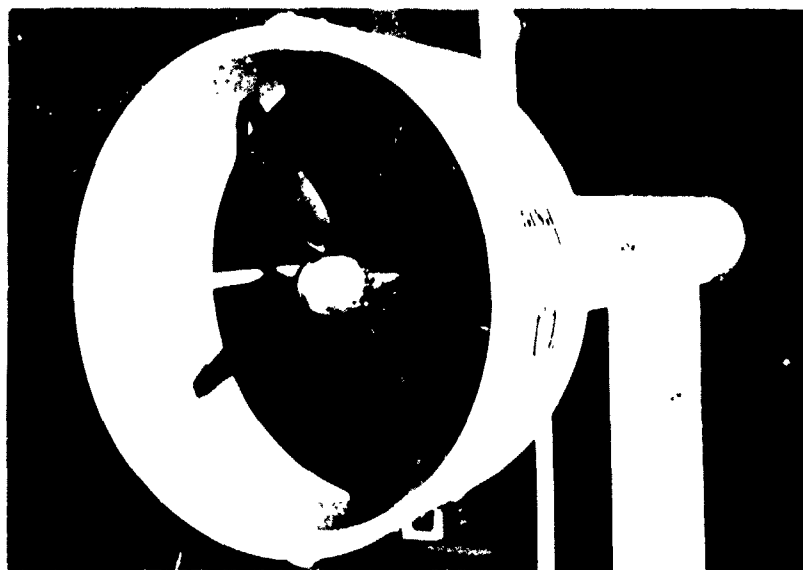
Figure 8.   Propeller-Duct Assembly in the Test Stand.

The test equipment that was fabricated has the capability of testing the following:

(1) Various propellers and propeller duct configurations.

(2) Propeller and propeller duct configurations of different diameters.

(3) Ducts alone to measure their thrust-drag characteristics.

(4) Propellers and propeller duct configurations in both the tractor and pusher modes.

(5) Propellers with blades having various pitch angle settings over a wide range of rpms.

(6) Propellers with two, three, four, and six blades in a coplanar configuration.

(7) Two multi-bladed propellers with axial separation (spaced propellers).

(8) Two multi-bladed propellers with axial separation and with variable blade-to-blade phasing.

With slight modifications, the test equipment could be utilized to test mini-RPVs having wing spans up to 7 feet (2.1336 m) in either a tractor or pusher configuration at various angles of attack, while measuring six components of vehicle forces and moments.

PERFORMANCE AND NOISE TESTS

The aim of these tests was to obtain sufficient performance and acoustic data of various propeller configurations in the static and forward flight conditions to determine propeller configurations that resulted in low detectability characteristics. In the first phase of the tests all the propeller configurations were tested statically in a semianechoic test chamber. Tne acoustic and performance data obtained during the static tests was utilized in the slant range prediction program to predict the detection distances. Based on the results obtained from this analysis, the propeller configurations having the lower detection distances were selected and tested at the design operating conditions in forward flight. The details of the test setup, instrumentation test procedures, and various propeller configurations tested in both static and dynamic modes (wind tunnel) will be discussed in the next few sections.

STATIC TESTS

A large number of propeller configurations utilizing the blade designs given in Table 4 with varying blade number, rotational speed, and blade physical arrangement (spacing and phasing) were tested statically in a semianechoic chamber.

Test Setup/Instrumentation

A schematic of the static test setup is given in Figure 9. The propeller test stand was mounted in a semianechoic test cell at the University of Maryland. The anechoic test chamber was lined with acoustic foam and was contoured such that it could fit in the test section of the University of Maryland wind tunnel. The primary difference between the chamber inside and outside of the wind tunnel is that there were anechoic walls ahead of and behind the test section in the outside chamber (see Fig. 9), while both ends of the chamber were open to the free stream in the wind tunnel. The absorption characteristics of the acoustic foam are such that it absorbed 52% of the noise at 200 Hz, 84% at 500 Hz, and 97% above 1000 Hz. Since the lowest blade passage frequency of the propeller tested was of the order of 150 Hz [26 inch (.6604 m) diameter two-bladed rotor], it was believed that the anechoic characteristics of this chamber were more than adequate for the tests conducted.
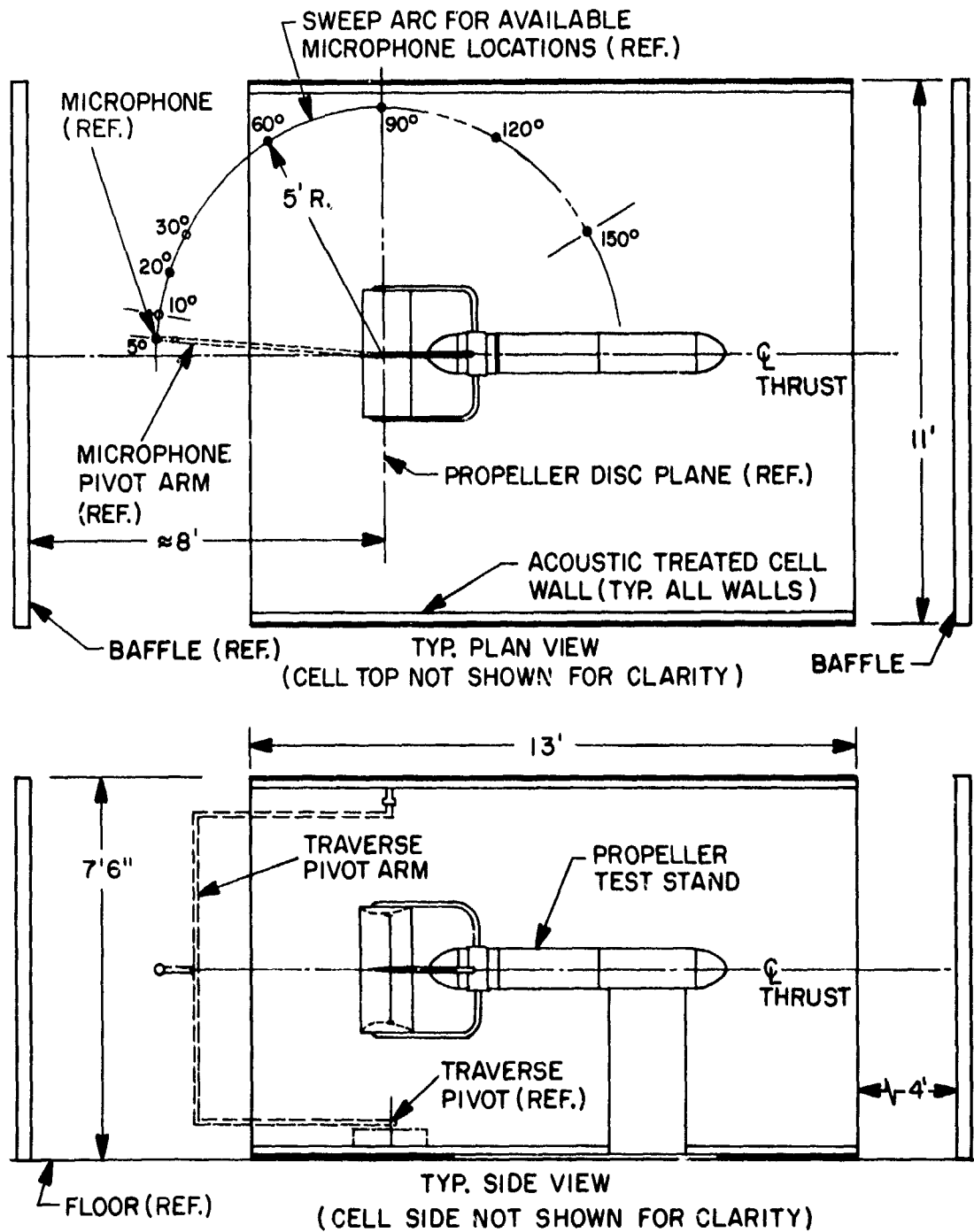
Figure 9. Static Test Arrangement - RPV Propeller Test.

44

Noise measurements were made on a semicircle having a
5 foot (1.524 m) radius with its center at the center of the
propeller hub. It was believed that this distance, which is
about 2½ diameters away from the center of the hub, was far
enough for the microphones to be in the far field of propel-
ler noise environment. The microphone was placed on a suit-
able mechanical linkage (see Fig. 9). This linkage was moved
by a remotely controlled motor such that the microphone
traced a semicircle [5 foot (1.524 m) radius] in a horizontal
plane containing the thrust axis. The noise measurements
were generally taken for at least seven angular locations of
the microphone ($\theta = 10°, 20°, 30°, 60°, 90°, 120°$ and $150°$,
where θ is the angle from the forward thrust axis of the
propeller) on this semicircle so that a representative di-
rectivity pattern of the noise of each propeller configu-
ration could be obtained. The microphone signals after
signal conditioning were recorded on an FM tape recorder.
In addition, on-line spectral analysis of the data was also
accomplished.

The instrumentation used during the tests can be broadly
classified into two categories: that associated with per-
formance measurements and that associated with acoustic
measurements. The instrumentation associated with per-
formance measurements consists of a thrust load cell, the
motor frequency controller, and the necessary instruments
to measure the input power to the motor. The real time
thrust was measured by using a load cell mounted between
the propeller drive reaction frame and the stationary sup-
port structure. The load cell output was digitally displayed
(in pounds) on a Digital Transducer Indicator. The rpm
readout was provided by a digital frequency counter integral
with the frequency controller of the drive motor. In this
series of static tests, due to the absence of a torque meter
in the propeller test stand, the input power to the drive
motor was measured. It is believed that in the range of rpms
used in the tests, the motor is about 80% efficient; there-
fore, the propeller shaft horsepower was taken as 80% of the
motor input power. The drive motor instrumentation was cali-
brated prior to the test by means of an independent line motor
and the load cell was calibrated by loading the system with a
set of calibrated weights.

The acoustic instrumentation consisted of a microphone, an
amplifier, an FM tape recorder, an oscilloscope, a narrow-
band spectrum analyzer, and a 1/3 octave band analyzer. The
propeller noise signal from the B&K4133 microphone, after

45

amplification and signal conditioning, was recorded on an FM tape recorder and paralleled to a narrow-band spectrum analyzer. The FM recorder had seven channels and a separate voice track. Using a tape speed of 60 ips (1.524 m/sec), the pressure-time history was recorded for a length of time greater than that required to develop a frequency spectrum on the narrow-band spectrum analyzer or the 1/3 octave band analyzer. The pressure-time histories input to and output from the FM recorder were fed to an oscilloscope in order to maintain the signal and to obtain a permanent record of the pressure-time history through the use of a scope camera.

The pressure-time history signal was also fed to a narrow-band spectrum analyzer (EMR Schlumberger 1510) and the frequency spectrum displayed on an integral oscilloscope was photographed. The recorded pressure-time history from the microphone was played back through a B&K 1/3 octave band analyzer to develop the 1/3 octave band spectrum. A schematic of the instrumentation is shown in Figure 10 and a photograph of the instrumentation setup is shown in Figure 11.

Prior to testing the propellers in the acoustic chamber, background noise levels were recorded for the system with the motor rotating at the various operating speeds without the propeller. The background noise data recorded at θ = 120° has been reduced to frequency spectra. Figure 12 shows the narrow-band spectra of the background noise for two different motor rotational speeds, with and without the duct mounted on the test stand. The spectra corresponding to microphone location of θ = 120° were shown because the background noise levels at this azimuthal location were found to be the highest. This is because rotational noise of the motor is highest just behind it. As shown in Figure 12, there were some small peaks at frequencies corresponding to the motor rotational speed and its integer multiples. However, as will be seen later, the background noise with the motor running is at least 10 to 15 dB less than the propeller noise at the blade passage frequencies. Therefore, the background noise was not a significant factor in the static tests.

Test Procedure/Data Acquisition

The test procedure consisted of obtaining performance and acoustic data at the designated operating conditions for the various propeller configurations operating in the tractor mode. To understand the manner in which the test was conducted, a three-bladed propeller configuration with the BD3 blade design (see Table 4) will be discussed.

46
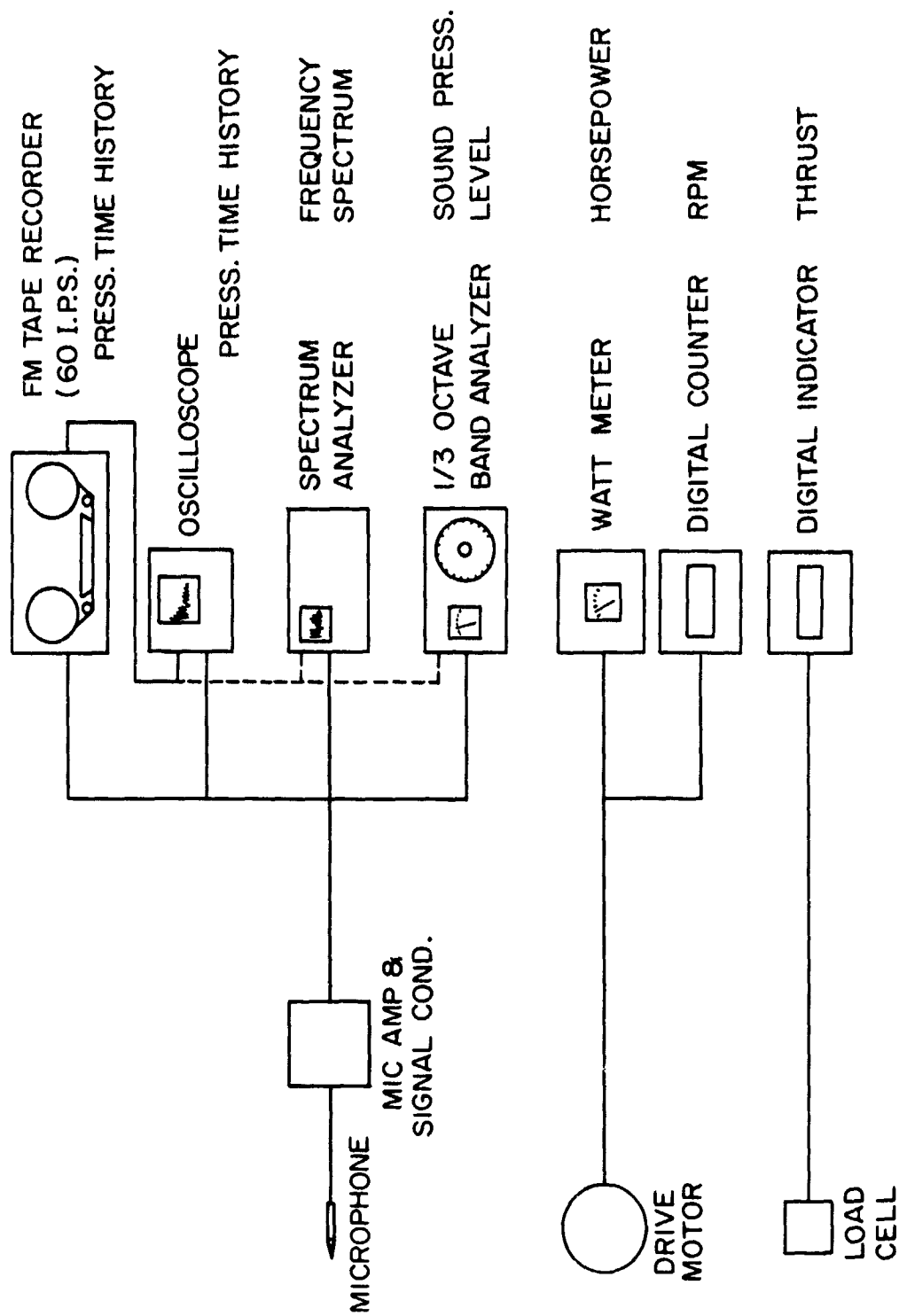
Figure 10. Schematic of Instrumentation.
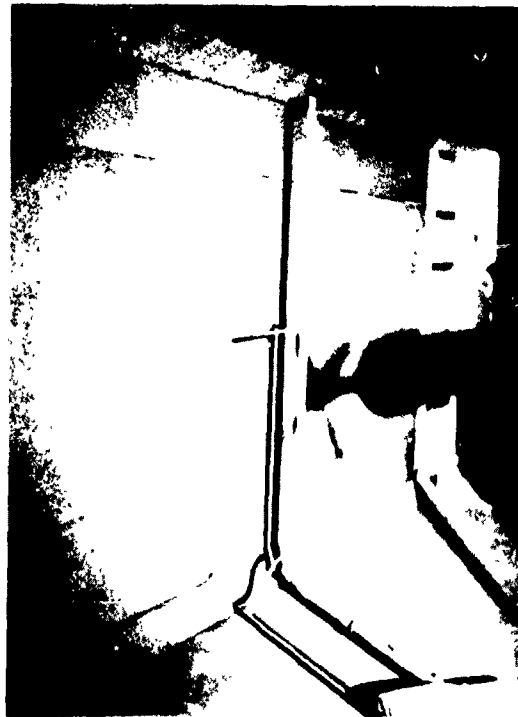
TRAVERSE MECHANISM   TEST STAND
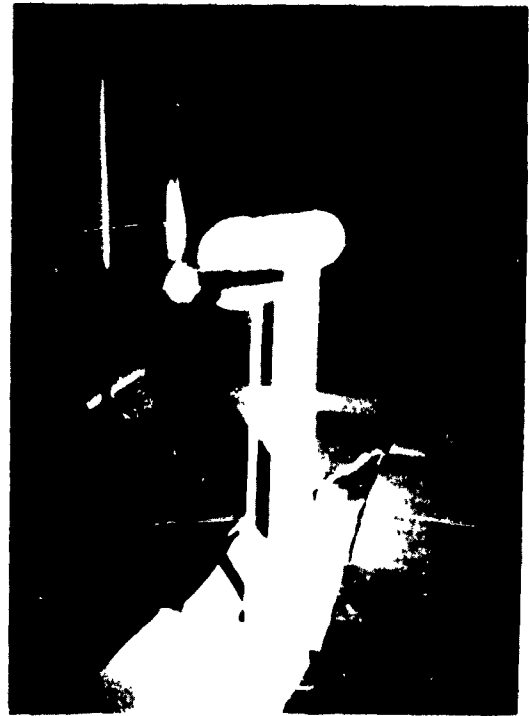
(a) TEST SETUP

(b) INSTRUMENTATION

Figure 11.   Test Setup and Instrumentation for Static Tests.
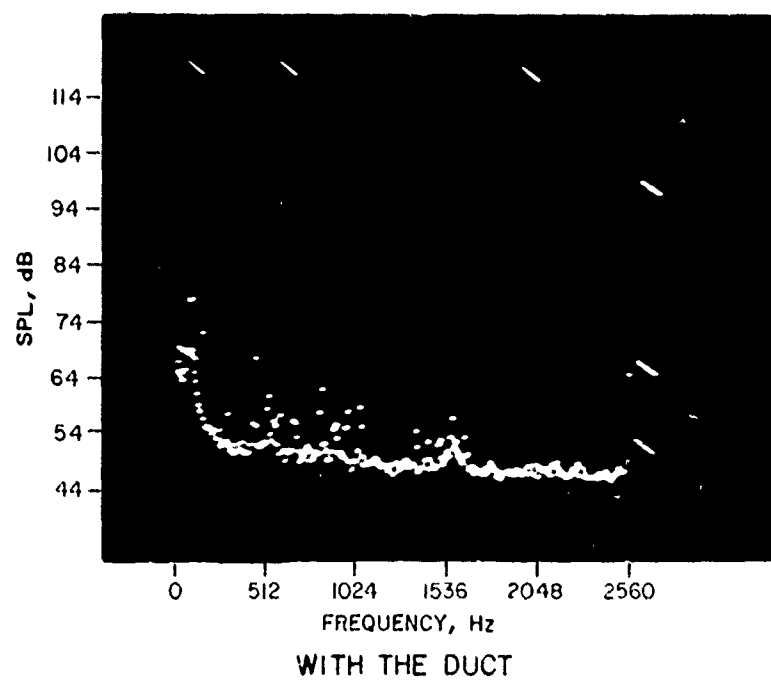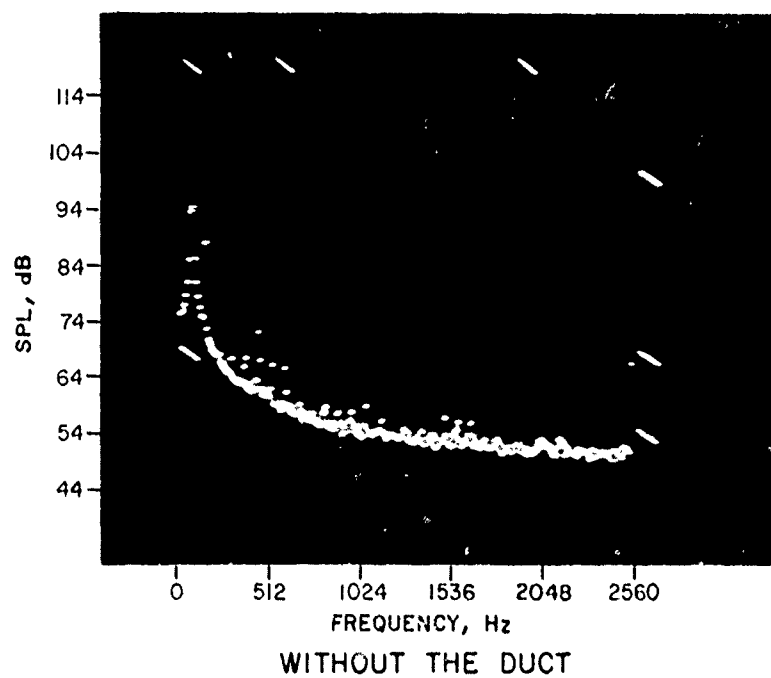
a. Drive Motor Running at 4500 RPM.

Figure 12. Background Noise Spectra - Static Tests.

WITHOUT THE DUCT

WITH THE DUCT
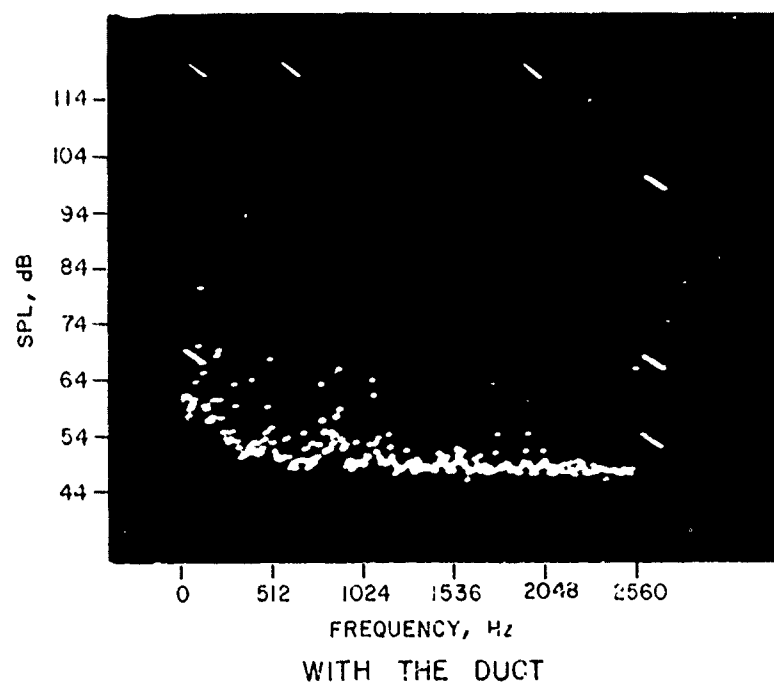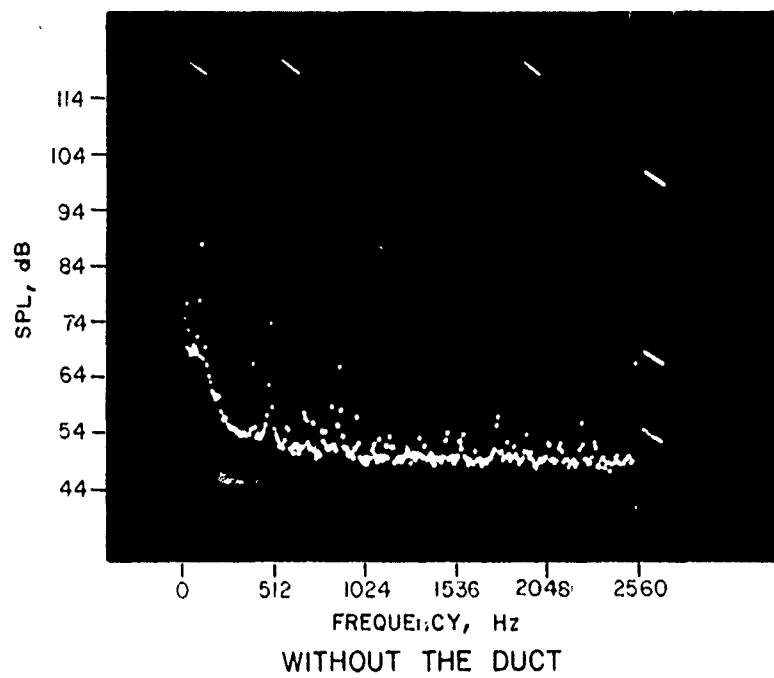
b. Drive Motor Running at 5850 RPM.

Figure 12. Continued.

50

The three-bladed propeller was mounted on the test stand with its blades set at a given collective pitch angle ($\phi_{.75R}$). The propeller was then rotated at different speeds and the thrust and power readings were recorded. A series of thrust vs. rpm curves (see Fig.13) corresponding to different collective pitch angle settings were generated in this manner. This procedure was repeated until the blade thrust and rotational speed were such that acoustic and performance data could be taken at the following five designated operating conditions:

  (1) Design value of thrust at design rpm,

  (2) Design thrust at a speed approximately 20% lower than the design rpm,

  (3) Design thrust at a speed approximately 20% higher than the design rpm,

  (4) A value of thrust approximately 80% of the design value of thrust at the design rpm, and

  (5) A value of thrust approximately 120% of the design value of thrust at the design rpm.

For the three-bladed (BD3) propeller considered here, the design speed is 5850 rpm. For all the propeller configurations tested, the design value of thrust is 18 pounds (80 newtons). The operating conditions given above were designated as (1), (2), (3), (4) and (5) in Figure 13. As shown in Figure 13, corresponding to each different blade angle ($\phi_{.75R}$), a different thrust vs. rpm curve was obtained. When one of these curves passed through one or more designated operating conditions, the acoustic and performance data were recorded. For example, for $\phi_{.75R}$ = 13.8°, the thrust vs. rpm curve passed through the design point (1) at a thrust value of 18.2 pounds (81 newtons) at the design speed of 5850 rpm. At these operating conditions the acoustic data was taken at seven microphone azimuthal locations on a semicircle of 5 foot (1.524 m) radius whose center is at the hub. The microphone locations generally utilized during the test were at θ = 10°, 20°, 30°, 60°, 90°, 120°, and 150°, where θ is the angle from the thrust axis to the microphone location. The acoustic signal was recorded on an FM tape recorder and was also paralleled to a narrow-band spectrum analyzer which was utilized to obtain an on-line spectrum which was then photographed.

51

3 BLADED -BD3- PROPELLER
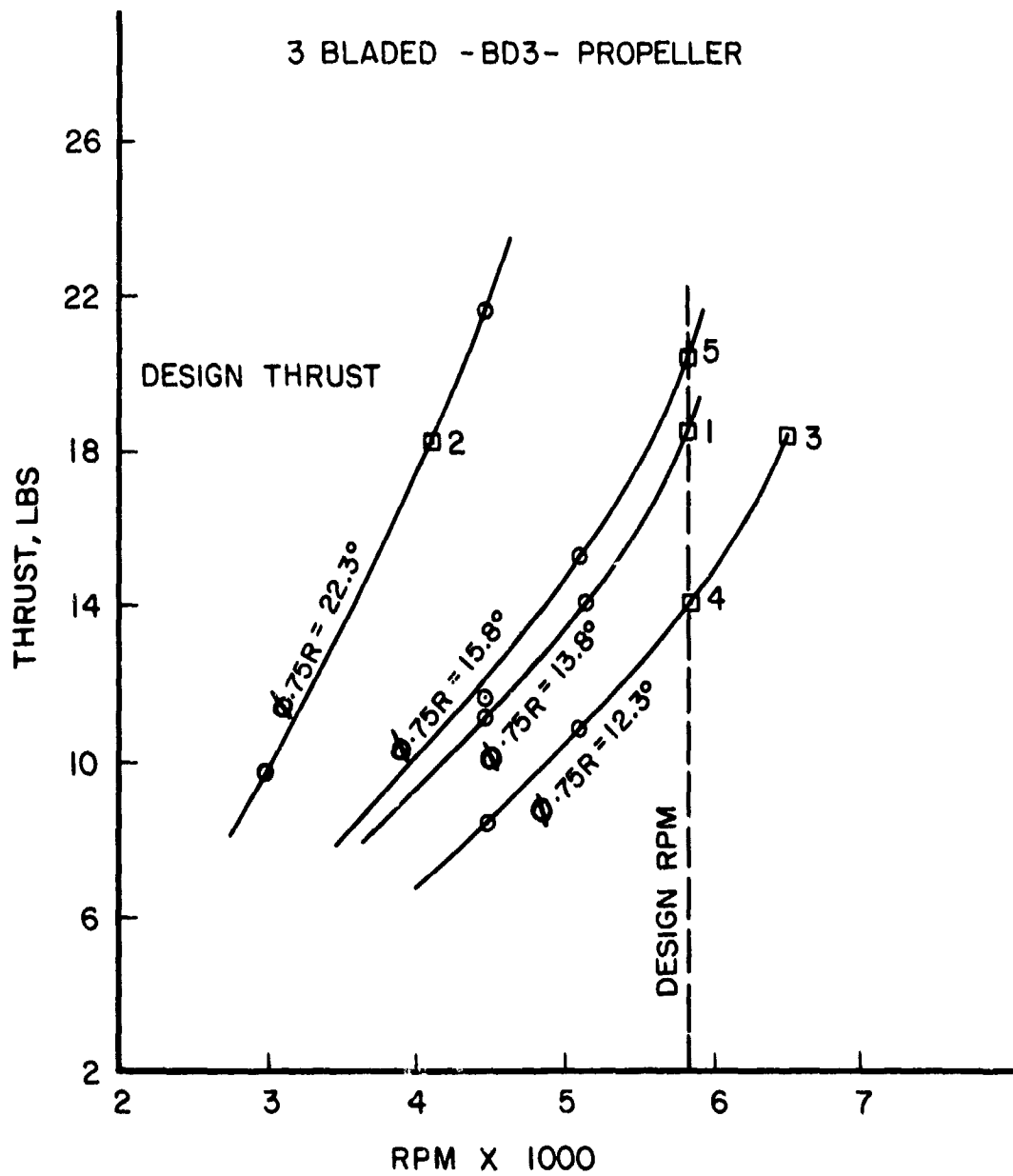
Figure 13. Static Tests - Performance Curves.

Most of the narrow-band spectral data was taken at a band-
width of 10 Hz and over a frequency range of 0-2.56 kHz.
The analog signal was also paralleled to an oscilloscope on
which the pressure-time history was photographed.

Configurations Tested

All the propeller configurations that were tested statically
can be broadly classified into three categories:

   (1)   Conventional free propellers
   (2)   Ducted propellers
   (3)   Unconventional propellers

The first category includes all the unducted coplanar propel-
ler configurations tested. These configurations differ from
each other in blade number (two, three, four and six) and
blade design (BD1, BD2, BD3, BD4 and BD5). As shown in
Table 4 the different blade designs are characterized by
changes in diameter, activity factor, airfoil section, taper
ratio, and twist distribution. All the free propellers were
run at the same design tip speed. The smaller size propel-
lers [diameter of 20 inches (.5048 m)] characterized by the
blade designs BD1, BD3, and BD5 had a design rotational speed
of 5850 rpm while the larger size propellers [diameter of
26 inches (.6604 m)] characterized by the blade designs BD2
and BD4 had a design rotational speed of 4500 rpm. For most
of the free propeller configurations, the performance and
acoustic data were taken at the designated operating condi-
tions (1), (2), (3), (4), and (5) (Fig.13) as described in
the previous section. However, operating conditions were
not exactly the same for all these free propeller configura-
tions. For example, operating condition (2) means running
the propeller at a speed lower than the design tip speed at
the design thrust condition of 18 pounds (80 newtons). This
speed may vary slightly between the various propeller config-
urations tested. However, for all of these propeller config-
urations, the design operating condition (1) implies that the
propellers were run at approximately the same design tip speed
and design thrust condition. All the free propeller configu-
rations tested in the static condition were listed in Table 5,
and each propeller configuration was designated by a configu-
ration ID. The configuration was also represented by its
blade number and its blade design. For example, 2 BLD, BD3
refers to the propeller configuration with two blades and with
the blade design given by BD3. As can be seen from Table 5,

53

TABLE 5

CONVENTIONAL FREE PROPELLER CONFIGURATIONS

TESTED IN THE STATIC CONDITION

CONF. ID	CONFIGURATION DESIGNATION	OPERATING CONDITIONS AT WHICH THE DATA WAS TAKEN
1	2 BLD, BD1	1, 2, 3, 4, 5
3	2 BLD, BD3	1, 2, 3, 4, 5
5	2 BLD, BD5	1, 2, 3, 4, 5
7	2 BLD, BD2	1, 3, 4, 5
9	2 BLD, BD4	1
11	4 BLD, BD1	1, 2, 3, 4, 5
13	4 BLD, BD3	1, 2, 3, 4, 5
21	4 BLD, BD2	2, 2', 3', 5, 5'
23	4 BLD, BD4	1
31	6 BLD, BD3	1, 2, 3, 4, 5
39	3 BLD, BD3	1, 2, 3, 4, 5

some of these configurations were not tested at all the designated operating conditions due to the presence of the resonance of the system at those rotational speeds. In the case of 4 BLD, BD2, resonances were encountered at the operating conditions (1), (3), and (4). Therefore, this propeller was tested at the operating condition (2'), (3'), and (5') where (2') refers to testing at about 80% of the design thrust value, but at a speed lower than design rpm. (3') refers to testing at the design thrust value of 18 pounds (80 newtons) at a speed lower than design rpm and (5') refers to testing at about 120% of the design thrust value at a speed lower than the design rpm.

The second category includes all the ducted propeller configurations tested in the static condition. Unlike the free propellers, all the ducted propeller configurations were tested at only one operating condition. This operating condition

refers to testing at the design tip speed and at a thrust value of about 20 pounds (89 newtons), slightly higher than the design value of 18 pounds (80 newtons). The design rotational speeds of the ducted propeller configurations were the same as those of the corresponding free propellers (5850 rpm for small propellers and 4500 rpm for large propellers). All the ducted propeller configurations tested in the static condition are given in Table 6.

TABLE 6

DUCTED PROPELLER CONFIGURATIONS

TESTED IN THE STATIC CONDITION

CONFIGURATION ID	CONFIGURATION DESIGNATION
2	2 BLD, BD1
4	2 BLD, BD3
6	2 BLD, BD5
8	2 BLD, BD2
12	4 BLD, BD1
14	4 BLD, BD3
22	4 BLD, BD2
32	6 BLD, BD3

The third category includes all the unconventional propellers tested in the static condition. These propellers are also referred to as spaced/phased propellers in this report. These are essentially tandem propeller configurations with a very small axial separation between the two propeller planes. A schematic of a typical spaced/phased propeller configuration is shown in Figure 14. A spaced/phased propeller configuration is characterized by two variables, ΔZ and $\Delta \psi$, where ΔZ refers to the axial separation between the two propeller planes and $\Delta \psi$ refers to the angle by which each blade in the front propeller plane leads the following one in the back propeller plane. Only multi-bladed propellers with a blade number greater
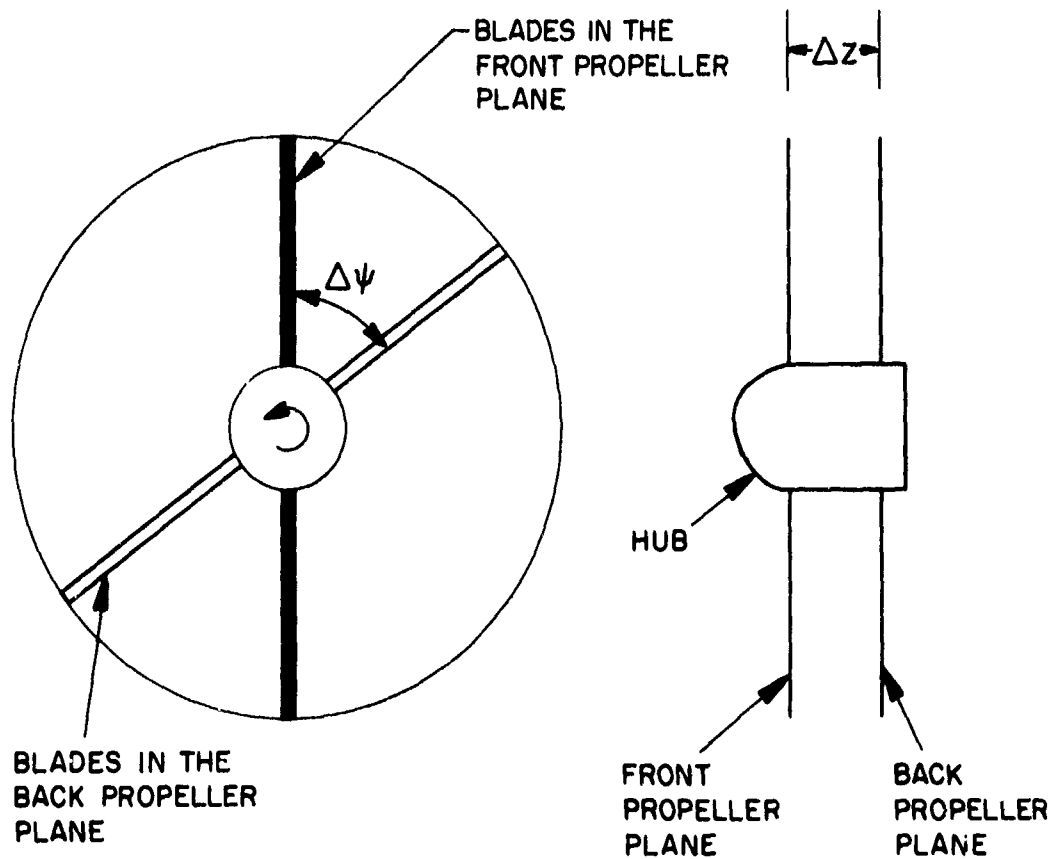
ΔZ = AXIAL SPACING

$\Delta \psi$ = AZIMUTHAL PHASING

Figure 14. Schematic of a Spaced/Phased Propeller Configuration.

than or equal to 4 can be tested in this configuration. All
the phased/spaced propellers tested in the static condition
were given in Table 7. These configurations differ from each
other in their blade number and phasing ($\Delta\psi$) between the
blades. It was shown in Reference 31 that in the case of
rotors, a spacing (ΔZ) of one chord length (at the 3/4 radius
of the blade) is optimum from both the performance and noise
points of view. Therefore, all these propeller configurations
were tested at the same axial spacing of one chord length (at
3/4 radius of the blade). All the spaced/phased propeller
configurations were tested at the design operating condition
(1) which corresponds to the design thrust value [18 pounds
(80 newtons)] at the design tip speed [510 fps (155.5 m/sec)].
Table 7 lists all the spaced/phased propeller configurations
that were tested along with the values of spacing (ΔZ) and
phasing ($\Delta\psi$) for each configuration.

TABLE 7

SPACED/PHASED PROPELLER CONFIGURATIONS

TESTED IN THE STATIC CONDITION

CONF. ID	CONFIGURATION DESIGNATION	AXIAL SPACING ΔZ IN INCHES (METERS)	AZIMUTHAL PHASING $\Delta\psi$ IN DEGREES
15	4 BLD, BD3	2.6 (.066)	90
17	4 BLD, BD3	2.6 (.066)	40
19	4 BLD, BD3	2.6 (.066)	140
33	6 BLD, BD3	2.6 (.066)	60
35	6 BLD, BD3	2.6 (.066)	30
37	6 BLD, BD3	2.6 (.066)	90

[31] Gangwani, S.T., The Effect of Main Rotor Blade Phasing and
Spacing on Performance, Blade Loads and Acoustics, RASA
Report 3169-14, NASA CR-2737, 1976.

WIND TUNNEL TESTS

Based on a preliminary analysis of static performance and acoustic data, a few propeller configurations were selected to be tested in simulated forward flight conditions in the University of Maryland wind tunnel. The test section of the tunnel was lined with acoustic foam to reduce the acoustic signal reflections off the walls. All of the propeller configurations were designed for a forward flight cruise speed of 75 knots [127 ft/sec (38.6 m/sec)]. During initial wind tunnel tests, however, it was found that the tunnel background noise at 127 ft/sec (38.6 m/sec) was very high, at least in the lower frequency range (0-1000 Hz). At the lower blade passage frequencies of some of the propeller configurations, for example, the sound pressure levels of the propellers were found to be lower than the tunnel background noise. Therefore, it was decided to test the propellers at tunnel speeds of 91 ft/sec [27.74 m/sec (56 knots)], which is the loitering speed of the mini-RPVs. It was found that at a tunnel speed of 91 ft/sec (27.74 m/sec) the sound pressure levels of most of the propeller configurations tested were at least 5 to 10 dB above the tunnel background noise in the frequency range of interest. In some cases, however, the sound pressure levels were only marginally above the tunnel background noise. Despite the fact that the propellers tested under these conditions were operating at off-design conditions, it is believed that the results of these tests determined the effect of forward flight on the noise characteristics of the propellers under constant thrust conditions. For some propeller configurations, tests were also conducted at 50 ft/sec (15.24 m/sec) to evaluate the change in the propeller noise as a function of forward velocity. The wind tunnel tests included testing of some propeller configurations in the tractor as well as the pusher modes. The propeller configurations tested in the pusher mode were also tested with a wing operating at zero angle of attack upstream of the propeller disk to determine the effect of upstream turbulence on the noise characteristics of the propeller.

After completing these wind tunnel tests, as part of an extension to the original contract, an additional series of wind tunnel tests were conducted. The purpose of these tests was to obtain additional forward flight data to supplement

that already obtained. These tests included only tractor
propeller configurations. These propeller configurations
were tested at three different wind tunnel speeds [50 ft/sec
(15.24 m/sec), 70 ft/sec (21.34 m/sec), and 91 ft/sec
(27.74 m/sec)] at the design thrust value of 18 pounds
(80 newtons) and the design tip speed of 510 ft/sec
(155.5 m/sec). The propeller configurations were also tested
statically with the tunnel switched off. However, the static
conditions could not be realized in the tunnel due to the
additional inflow generated by the wake velocity in the closed
circuit wind tunnel. At the design thrust value, this veloc-
ity is measured to be about 15 ft/sec (4.6 m/sec). Therefore,
for the purpose of data evaluation, these static tests were
considered to be simulated forward flight tests at low tunnel
velocities. In addition to the above, a few selected propel-
ler configurations were also tested at two more tip speeds
[340 ft/sec (103.6 m/sec), 576 ft/sec (175.6 m/sec)] and two
more thrust values of approximately 27 pounds (120 newtons)
and 36 pounds (160 newtons).

Test Setup/Instrumentation

The remotely piloted vehicle (RPV) propeller test stand used
in the static tests was mounted on the six-component balance
system located in the floor of the test section of the Uni-
versity of Maryland wind tunnel. A schematic of the test
setup in the wind tunnel test section is shown in Figure 15.
The use of the same acoustic test cell for both the static
and forward flight tests allowed accurate comparisons of the
static and wind tunnel data. As in the static tests, the
microphone was mounted on a pivot arm of the mechanical
linkage system, which was driven by a remotely controlled
motor located on the drive table at the foot of the linkage.
The pivot arm was designed such that the microphone always
pointed upstream regardless of its angular location with re-
spect to the propeller hub. The microphone was equipped
with a wind screen bullet cone to minimize the effect of the
airstream on the acoustic data.

The instrumentation used to obtain the performance and acous-
tic data was exactly the same as that used in static tests.
A schematic of the instrumentation used was given in Figure 11.
The power and rpm data were also measured in the same manner
as in the static tests. The acoustic data was obtained at
designated microphone locations in the azimuth around the
propeller hub.

59

SWEEP ARC FOR AVAILABLE
MICROPHONE LOCATIONS (REF.)

MICROPHONE
(REF.)

#4
60°
#3
30°
#2
20°
#1
10°
#0

5°MIN.

FLOW

#5
90°

#6
120°

145°

#7
150°

5'R

6 COMPONENT
BALANCE &
TURNTABLE
(REF.)

THRUST
& TUNNEL ₵

PROPELLER DISC
PLANE (REF.)

ACOUSTIC TREATED
CELL WALL (TYP. ALL WALLS)

11'

TYP. PLAN VIEW
(TUNNEL TOP NOT SHOWN FOR CLARITY)

13'

FLOW

PROPELLER
TEST STAND

THRUST
& TUNNEL ₵

MICROPHONE
PIVOT ARM
(REF.)

MICROPHONE
PIVOT (REF.)

TYP. SIDE VIEW
(TUNNEL SIDE NOT SHOWN FOR CLARITY)

Figure 15.   Dynamic Test Arrangement - RPV Propeller Test.

The test setup for the propellers operating in the pusher
mode was obtained by turning the turntable on which the pro-
peller test stand was mounted through 180°. The mechanical
linkage used for sweeping the microphone was suitably adjusted
such that the microphone again faced upstream as it described
a semicircle of 5-foot radius (1.524 m) about the center of
the hub. Figure 16a shows the test setup in the pusher mode
for a ducted configuration. Figure 16b shows the test setup
in the pusher mode but with an upstream nonlifting wing
mounted on the nacelle of the test stand.

In the additional wind tunnel tests, the acoustic data was
also recorded at a far microphone located about 30 feet
(9.15 m) upstream of the propeller plane. The far micro-
phone was moved up and down a vertical stand, in a vertical
plane containing the thrust axis of the propeller. The acous-
tic data was recorded at three different angular locations
(θ = 5°, 10°, and 15°, where θ is the angle from the thrust
axis in the vertical plane). The purpose of this far micro-
phone data was to help obtain a more accurate directivity
pattern near the thrust axis. Due to the axial symmetry of
the propeller, the acoustic data obtained at a microphone at
an angular location θ from the thrust axis of the propeller
would be the same whether the angle is measured in the ver-
tical plane or the horizontal plane containing the thrust
axis of the propeller.

Test Procedure/Data Acquisition

As was done in the static tests, the selected propeller con-
figurations were mounted on the test stand and the perform-
ance and acoustic data were taken simultaneously at the
designated operating conditions. Unlike in the static tests,
a few propeller configurations were tested in both the trac-
tor and pusher modes of operation. In the pusher mode, the
propeller configurations were also tested with an upstream
nonlifting wing.

Before the propellers were mounted on the test stand, the
tunnel was brought up to the selected test speed and the
system tare thrust reading on the load cell was taken. In
addition, acoustic data was taken at eight microphone loca-
tions, θ = 5°, 10°, 20°, 30°, 60°, 90°, 120° and 150°, to
measure the background noise spectra at the selected locations.
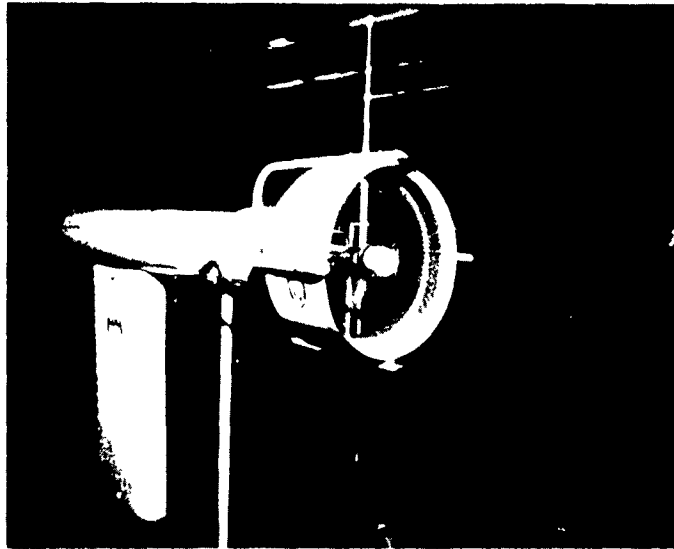
(a) WITHOUT AN UPSTREAM WING
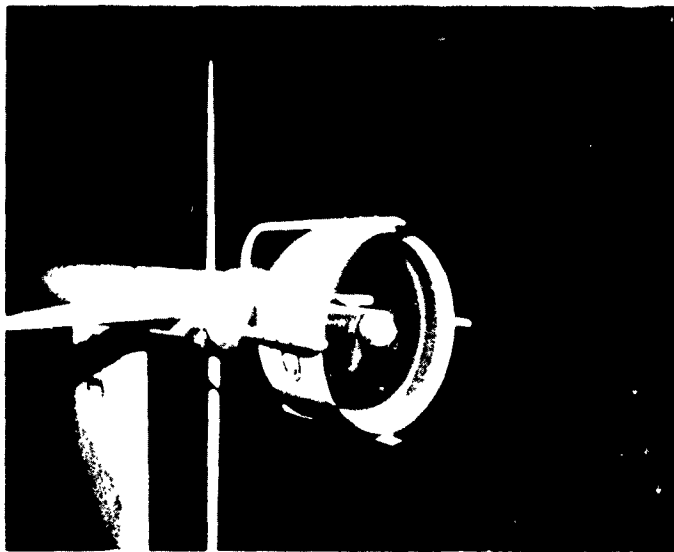
(b) WITH AN UPSTREAM WING

Figure 16.   Test Setup in the Pusher Mode.

After establishing the initial load cell tares and background noise, the given propeller configuration was mounted on the test stand with its blades set at a given collective pitch angle. The tunnel was then brought to the selected speed and the propeller was rotated at various speeds to develop a thrust vs. rpm curve. A series of thrust vs. rpm curves were developed in this manner for various collective pitch angles to determine the blade pitch angle at which the selected operating conditions (thrust and tip speed) were obtained. A set of acoustic and performance data was then taken at these operating conditions. The acoustic data was recorded on an FM tape recorder, and as was done during the static tests, the acoustic signal was also paralleled to a narrow-band spectrum analyzer, and its output as displayed on an oscilloscope was photographed. Most of the narrow-band spectral data was taken at a bandwidth of 10 Hz and over a frequency range of 0-2.56 kHz. This procedure was repeated for all the propeller configurations whether they were tested in the tractor or pusher mode.

The test procedure used in the additional wind tunnel tests is essentially the same as that described above. However, in these tests the torque absorbed by each propeller configuration was also recorded. Also, the acoustic data was recorded at three far microphone locations in addition to the near microphone locations. The near microphone locations used in these tests were θ = 10°, 15°, 20°, 30°, 60°, 90° and 120°. The far microphone data was obtained at angular locations of 5°, 10°, and 15°. The acoustic data from the microphone was fed to an on-line narrow-band spectrum analyzer and a 1/3 octave band analyzer. The data was also recorded on an FM tape recorder. The spectral data from the analyzers was recorded on a magnetic tape of an on-line data computer system. This data was later used to generate the spectral plots on a digital plotter.

Configurations Tested

All the propeller configurations tested in static condition were evaluated in terms of their performance and acoustic characteristics to select the best low-noise propeller configurations for the wind tunnel tests. The evaluation also included such practical aspects as the weight consideration and the need to develop suitable trending data for design considerations. For example, an evaluation of the static tests showed that the ducted propeller configurations were

very noisy. Nevertheless, to develop a suitable trending data, a few propeller configurations were tested with ducts.

The propeller configurations in the earlier series of wind tunnel tests were tested in the tractor mode and/or the pusher mode. Most of these propeller configurations were tested at a tunnel speed of 91 ft/sec (27.74 m/sec). However, a couple of configurations were also tested at a speed of 50 ft/sec (15.24 m/sec) to obtain the effect of changing flight speed on the noise characteristics of the propeller configurations. Propeller configuration 4 BLD, BD4 was also tested with its thrust axis at a small angle of attack (3.8°) to the free stream to determine the effect (if any) of the RPV course angle of attack on the noise characteristics. All the propeller configurations tested in the tractor mode are listed in Table 8, which also gives the tunnel speeds at which the tests were made. Table 9 gives the configurations tested in the pusher mode. These configurations were also tested with an upstream nonlifting wing. All the pusher configurations were tested at a tunnel speed of 91 ft/sec (27.74 m/sec).

The additional wind tunnel tests were more extensive in that they included a larger number of propeller configurations and more parametric variations. Such parameters as tip speed, thrust, and tunnel velocity were varied. Table 10 gives the propeller configurations and the operating conditions at which they were tested. All propeller configurations were tested only in the tractor mode. It can easily be seen from Table 10 that a few propeller configurations were tested at the same conditions as those used in the earlier series of wind tunnel tests. Parametric variations such as tip speed and thrust were made only in propeller configurations with BD3 blades. This is because a preliminary analysis of the earlier series of wind tunnel tests showed that propellers with BD3 blades are generally less noisy. As shown in Table 10, a three-bladed BD3 propeller was also tested with a duct. Unlike the earlier series of wind tunnel tests, the duct used in these tests had a fiberglass hard skin interior.

TABLE 8

PROPELLER CONFIGURATIONS TESTED IN THE TRACTOR MODE

CONFIGURATION ID	CONFIGURATION DESIGNATION	TUNNEL SPEED FOR THE CONFIGURATION (FT/SEC)
1 - 91	2 BLD, BD1	91
3 - 91	2 BLD, BD3	91
7 - 91	2 BLD, BD2	91
9 - 91	2 BLD, BD4	91
11 - 91	4 BLD, BD1	91
15 - 91	4 BLD, BD3 Spaced	91
21 - 91	4 BLD, BD2	91
23 - 91	4 BLD, BD4	91
39 - 91	3 BLD, BD3	91
4 - 91	2 BLD, BD3, Ducted	91
8 - 91	2 BLD, BD2, Ducted	91
12 - 91	4 BLD, BD1, Ducted	91
1 - 50	2 BLD, BD1	50
11 - 50	4 BLD, BD1	50
23 - 50	4 BLD, BD4	50
*23 - 50	4 BLD, BD4	50

* Tested with thrust axis at an angle of attack of 3.8°

TABLE 9

PROPELLER CONFIGURATIONS TESTED IN
THE PUSHER MODE

WITHOUT AN UPSTREAM WING		WITH AN UPSTREAM WING	
CONF. ID	CONFIGURATION DESIGNATION	CONF. ID	CONFIGURATION DESIGNATION
7P	2 BLD, BD2	7PW	2 BLD, BD2
8P	2 BLD, BD2, Shrouded	8PW	2 BLD, BD2, Shrouded
11P	4 BLD, BD1	11PW	4 BLD, BD1
12P	4 BLD, BD1, Shrouded	12PW	4 BLD, BD1, Shrouded

P: Pusher Configuration

PW: Pusher Configuration with an Upstream Wing

TABLE 10
PROPELLER CONFIGURATIONS TESTED IN ADDITIONAL FORWARD FLIGHT TESTS

PROP. CONFIG.	FREE TRACTOR PROPELLER										DUCTED PROPELLER TRACTOR	
	DESIGN TIP SPEED (510 Ft/Sec) TUNNEL VELOCITY (Ft/Sec)				LOWER TIP SPEED (340 Ft/Sec) TUNNEL VELOCITY (Ft/Sec)			HIGHER TIP SPEED (576 Ft/Sec) TUNNEL VELOCITY (Ft/Sec)			DESIGN TIP SPEED (510 Ft/Sec) TUNNEL VELOCITY (Ft/Sec)	
	15	50	70	91	12	30	50	18	70	91	15	55
2BLD, BD1	X	X	X									
3BLD, BD1	X	X	X	X								
4BLD, BD1	X		X									
2BLD, BD2	X	X	X	X								
3BLD, BD2	X	X	X	X								
4BLD, BD2		X	X	X								
2BLD, BD3	X	X	X		X	X	X	X	X(75)			
3BLD, BD3	□	□	□	□							□	
3BLD, BD3	△	△	△	△				△	△	△(88)		X
3BLD, BD3	X	X	X	X	X	X	X	X	X	X		
4BLD, BD3	X	X	X	X	X	X	X(55)		X(80)			
2BLD, BD4	X	X	X	X		X						
3BLD, BD4	X	X	X	X	X	X	X(55)					
4BLD, BD4	X	X	X									

X – Data Point at Design Thrust (18 lbs)
△ – Data Point at Intermediate Thrust (≈27 lbs)
□ – Data Point at High Thrust (≈36 lbs)
A Bracketed Value Beside the Data Point Symbol Indicates the Tunnel Velocity (in Ft/Sec)

67

ANALYSIS OF TEST DATA

All of the test data obtained for different propeller configurations during both the static and wind tunnel tests can be broadly classified as performance data and acoustic data. This data was reduced and analyzed not only to compare the noise characteristics of different propeller configurations but also to develop appropriate trend curves. In this section, the methods used to reduce the measured data are discussed.

PERFORMANCE DATA REDUCTION

The performance data obtained for different propeller configurations consisted of the thrust and power at the designated operating conditions. A significant performance variable is the efficiency of the propeller. In the static mode, the efficiency of each propeller configuration was obtained by computing the value of figure of merit which is defined as

$$\text{Figure of Merit, FM} = \frac{T^{3/2}}{P\,(2\rho\pi R^2)^{1/2}}$$

where T is the thrust ... pounds (newtons), P is the input shaft power in ft-lb/sec (newton-m/sec), ρ is the density of air, and R is the radius of the propeller in feet (m). In the earlier series of tests, due to the absence of a torque meter, the shaft input power could not be measured directly. The input power values to the drive motor were recorded. A motor efficiency of about 80% was assumed in computing the shaft horsepower. In the latter series of tests, the torque, Q, absorbed by the shaft was directly measured in in-lb. The input shaft power can then be obtained as

$$P = .008266\,QN$$

where N is the rpm of the propeller. The drive motor was also calibrated using the torque meter and it was found that in the rpm range of interest and under the prevailing load conditions, the motor has an efficiency of about 80%. In the case of wind tunnel tests, the propulsive efficiency of each propeller configuration is defined as

$$\eta = TV_F/550P$$

where V_F is the tunnel speed, T is the thrust, and P is the shaft horsepower. The performance data reduction thus consisted of computing the efficiencies of the different propeller configurations for the various operating conditions.

ACOUSTIC DATA REDUCTION

The acoustic data (pressure-time history) of each propeller configuration was obtained at seven designated azimuthal positions on a semicircle of 5 ft (1.524 m) radius from the center of the hub. This acoustic data was subsequently analyzed to obtain narrow-band and 1/3 octave band spectra. Most of the narrow-band spectra were obtained for a bandwidth of 10 Hz over a frequency range of 0-2500 Hz. The analysis of the narrow-band spectra was limited to making comparisons for the various propeller configurations. The narrow-band spectral data was also used to obtain the sound pressure levels at various harmonics of blade passage frequencies. These harmonics were then used to obtain the directivity pattern of each propeller configuration. The 1/3 octave band data consists of sound pressure levels (in dB) at various 1/3 octave band center frequencies in the range of 10 Hz to 31.1 kHz.

Two different types of aural detection ranges were computed for each propeller configuration. The first one was the altitude of no detection and is defined as the altitude above which an aircraft can fly without being aurally detected on the ground. The second one is the slant range detection distance and is defined as the greatest distance in the direction of flight from the aircraft at a given altitude to a point on the ground at which it is aurally detected. It can be easily seen that the directivity pattern of the aircraft noise plays an important role in these detection distances. For example, the sound pressure levels in the forward quadrant are very important from the slant range point of view, while the SPLs in and about the propeller plane are more important from the point of view of altitude of no detection. As is shown later, the altitude of no detection can also be considered as a slant range detection distance perpendicular to the flight path of the aircraft.

Determination of the Altitude of No Detection

The altitude of no detection of a propeller-driven aircraft depends on the SPLs in and around the plane of the propeller, the atmospheric losses, and the ambient noise on the ground. The determination of the detection level L_D for a given ambient noise used in these calculations was developed by Fidell, et al. (Ref. 32). According to Fidell, et al., the detection performance of human beings is evaluated using the concepts based on the psychophysical theory of signal detectability (TSD). The important physical quantity that establishes the criteria in this theory is signal to noise ratio. The TSD method is simpler since it requires no distinction to be made on the basis of the tonal content of the aircraft noise signatures. This method provides better fit to the data than other available methods. It permits prediction of auditory performance at various levels of detection rates (50% correct detection, 70% correct detection, etc.) and a specified false alarm rates. The TSD method, due to its versatility, was used here to establish the altitude of no detection.

The essence of this method for predicting the detectability of light aircraft noise in different noise backgrounds is that human auditory performance is based on the signal to noise ratio in the single 1/3 octave band to which human sensitivity is the highest. A 50% detection rate and 1% false alarm rate were selected. A graph (Fig. 17) obtained from Reference 32 was used to obtain the detection level, L_D (in dB), for a given ambient noise. Sloping grid lines (Fig. 17) are used for plotting the specified background noise in 1/3 octave band levels. When the background noise is plotted on this grid, it is used (in conjunction with the pure tone threshold) to produce the 1/3 octave band detection levels (L_D). After plotting the background noise on this graph, detection levels (L_D) were then read directly from the horizontal grid lines. Thus, the detection levels were obtained for the specified ambient noise spectra (given in Fig. 4).

---

[32] Fidell, Sanford, Pearsons, Karl S., and Bennett, Ricarda L., Predicting Aural Detectability of Aircraft in Noise Backgrounds, AFFDL-TR-72-17, Wright-Patterson AFB, OH, July 1972.
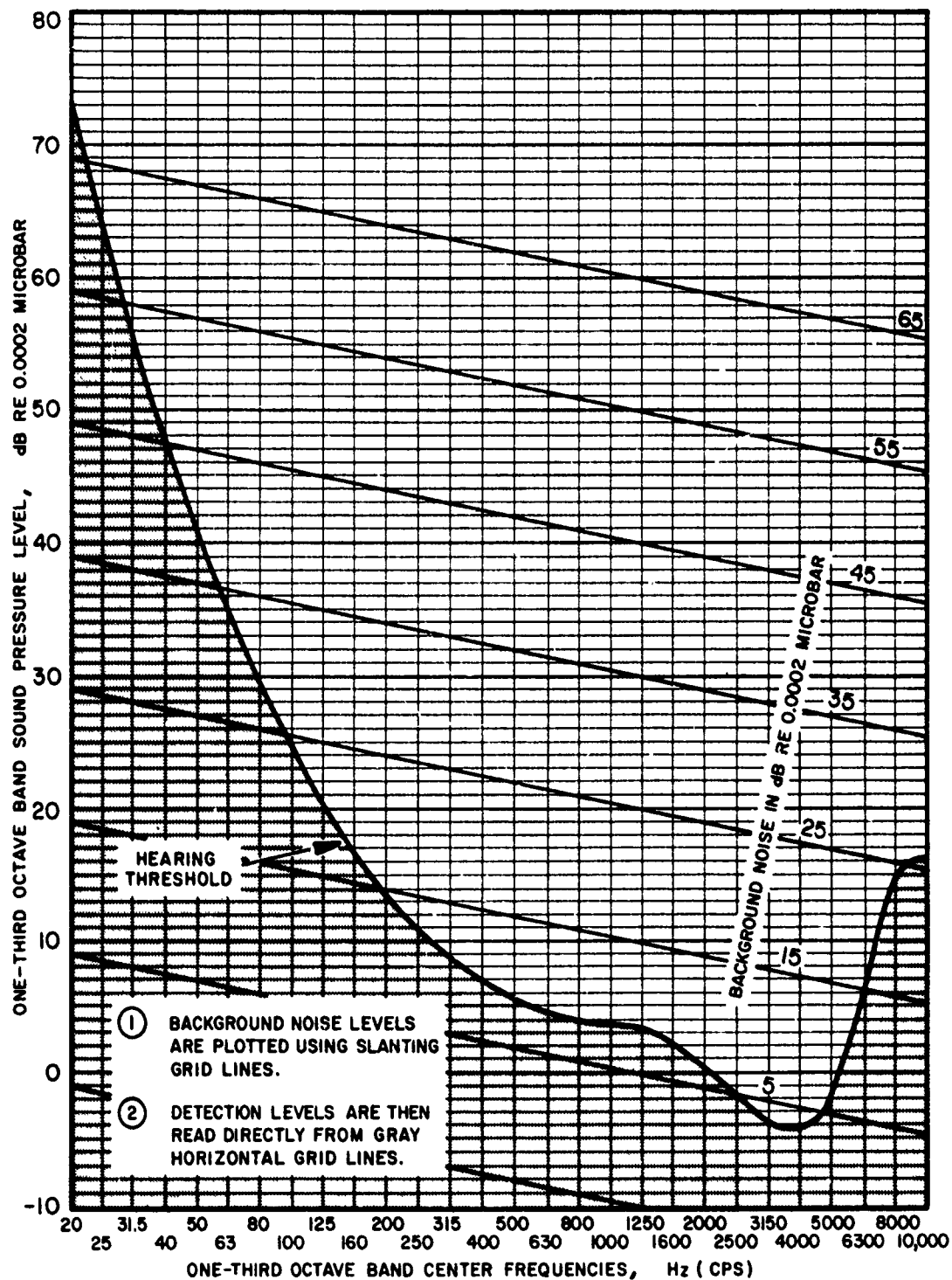
Figure 17. Chart for Predicting Detection Levels (for 50% Correct and 1% False Alarm Rates) Using Background Noise Spectrum in One-Third Octave Bands.

71

After establishing the detection level, the altitude of no detection for a given propeller configuration was obtained using its 1/3 octave band spectral data.

While 1/3 octave data (L_p) was obtained at seven microphone azimuthal positions on a semicircle of 5 foot (1.524 m) radius from the center of the hub, the SPLs (L_p) corresponding to the microphone locations $\theta = 60°$, $90°$, and $120°$ are of primary interest to the prediction of the altitude of no detection. The measured SPLs (L_p) were corrected to a distance of 1 foot (0.3048 m) from the center of the hub by means of the following expression:

$$L_p (1') = L_p (5') + 20 \ Log_{10} (5/1).$$

The L_p at any distance R' from the propeller can be calculated by means of

$$L_p (R') = L_p (1') - \Delta L$$

where ΔL accounts for the attenuation of signal as it travels from the source to the listener in a direction θ. For aural detection analysis, it is approximately equal to

$$\Delta L = 20 \ Log \ R' + K \ R'/1000 \ dB,$$

where the first term on the right side accounts for spherical spreading and the second for atmospheric absorption (classical as well as molecular). The absorption coefficient K varies with the atmospheric conditions as well as the frequency of the sound signal. The K values for atmospheric conditions of 59°F (15°C) and RH 60% were taken from Reference 19. The total attenuation required to make the aircraft undetectable is given by

$$\Delta L \geq L_p (1') - L_D$$

where L_D is the detection level for the given ambient noise. Therefore, for a given sound pressure level spectrum L_p in a direction θ, the detection distance spectrum was obtained by solving the equation

$$20 \text{ Log } R' + K \ R'/1000 = L_p \ (1') - L_D$$

for R' at each 1/3 octave band center frequency. The maximum value of this spectrum of detection distances (R_o) is the distance of interest. After finding R_o, the altitude of no detection (H) is obtained by the formula

$$H = R_o \cos (90° - \theta)$$

where θ is the direction corresponding to L_p. It was found that only the 1/3 octave data corresponding to the directions $\theta = 60°$, $90°$, and $120°$ are important in the computation of the altitude of no detection. Thus, the altitudes of no detection for each propeller configuration for the specified ambient noise spectra (Fig. 4) and atmospheric conditions were computed by hand.

When the altitude of no detection (H) is greater than the cruise altitude, H can also be considered as the slant range in the plane of the propeller. The equivalence between the altitude of no detection and the slant range in the plane of the propeller (perpendicular to flight path for a level flight where the thrust axis is in the direction of flight) for an RPV vehicle flying at 1000 feet (.3048 km) and where H is greater than 1000 feet (.3048 km) is shown in Figure 18. This equivalence is important, especially for RPV vehicles flying near the enemy lines because the ground distance (W) subtended by the two legs H, defines the width of the aural detection "ribbon" laid down by the RPV's noise signature.

Determination of the Slant Range Detection Distances

It is desirable to have as small a slant range distance as possible so that the enemy does not have enough time to take countermeasures before the aircraft reaches it. For the specified ambient noise spectra and the flight conditions, the slant range distances were obtained using a computer program developed by Abrahamson (Ref. 27).

The aural detectability program (Ref. 27) uses as input either the 1/3 octave band or the narrow-band spectral data obtained at the given microphone location. This program was originally developed for helicopters and was suitably modified for use in predicting the forward slant range of propellers. The program computes a slant range detection

73
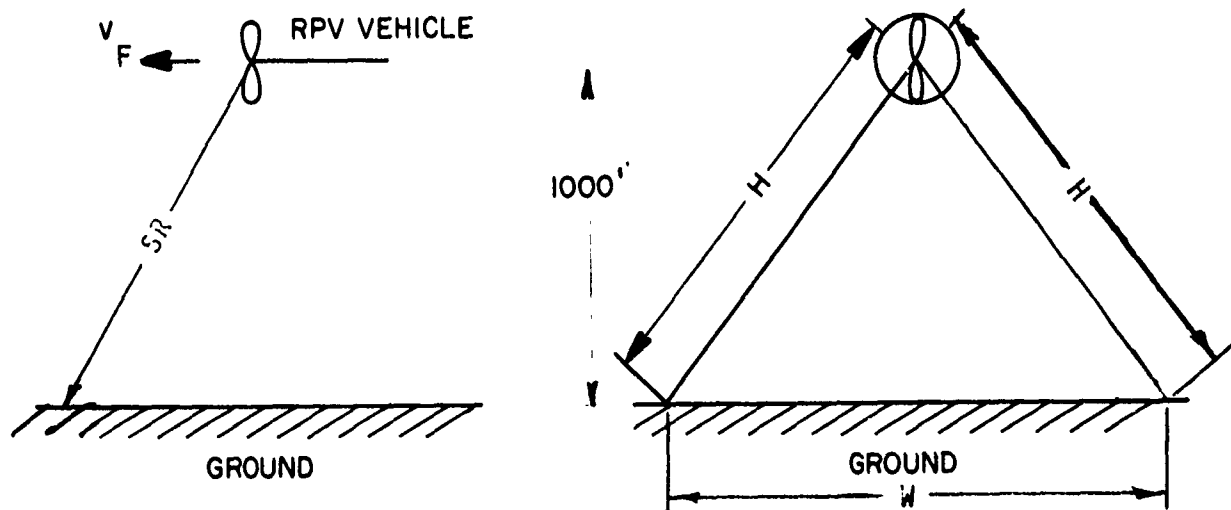
H = ALTITUDE OF NO DETECTION OF RPV AIRCRAFT

SR = SLANT RANGE

W = WIDTH OF DETECTION RIBBON

NOTE: WHEN H IS GREATER THAN THE CRUISE ALTITUDE, H
IS EQUAL TO SR IN THE PLANE OF THE PROPELLER

Figure 18.   Equivalence Between Altitude of No Detection
and Slant Range.

distance spectrum using Ollerhead's detectability criterion (Ref. 29). The program also has the provision where the background noise at the given microphone location can be subtracted from the acoustic signal before the slant ranges are computed. An empirical model for atmospheric attenuation of sound in the lower atmosphere over long distances (that is, for very shallow angles $\theta < 10°$) was also used in addition to the regular spherical spreading and atmospheric absorption. The details of the computer model are given in Reference 27. The output of the program consists of a slant range spectrum which gives the detection distances at various frequencies. The frequency range of interest is divided into several sub-frequency ranges (each roughly equal to the width of a 1/3 octave band) and the computer program gives the detection distances for each sub-frequency range. For each such detection distance, the probability of detection is also given. The slant range distance for a given sub-frequency range is taken as the distance for which the probability of detection is 50%. The peak value of the slant ranges over all the sub-frequency ranges is taken as the slant range detection distance of the propeller configuration for the direction θ, where θ is the angular location of the microphone whose acoustic data is used as input to the computer program.

To take into account the effect of directivity in the determination of slant ranges, the program should compute slant ranges for the data at several microphone angular locations until the retarded slant range computed along the direction θ is equal to the distance between the aircraft and the point of intersection with the ground of a straight line originating at the aircraft at an angle θ with the forward direction. However, the acoustic data of the propeller configurations was obtained at only a finite number of angular locations of the microphone ($\theta = 10°$, $15°$, $20°$, and $30°$) in the forward direction. In order to take into account the effect of directivity on the slant range, a simple procedure was devised. According to this procedure, first, for the given set of flight conditions the slant ranges of a propeller configuration corresponding to the data at microphone angular locations $\theta = 10°$, $15°$, $20°$, and $30°$ are obtained using the computer program as discussed above. Then the retarded values of these slant range distances are marked off along the radial lines originating from the propeller at the given altitude at the corresponding θ to obtain the detection locations. A smooth curve is then drawn through these detection locations and the distance between the propeller and the point of intersection of this curve with

the ground is taken as the directivity-corrected retarded
slant range of the given propeller configuration. The un-
retarded slant range is then obtained using the relations
given in Reference 27. Thus, the directivity-corrected
slant ranges are obtained for each propeller configuration.
The slant range detection distances of all of the propeller
configurations were obtained for a flight altitude of
1000 ft (304.8 m) using the narrow-band spectral data as
input. It is believed that the use of narrow-band spectral
data gives more accurate results than the use of 1/3 octave
band data since the slant range program works internally on
a small constant bandwidth (< 15 Hz) basis.

DISCUSSION OF RESULTS

In this section, the performance and acoustic characteristics of the various propeller configurations tested in both the static condition and in simulated forward flight are discussed. Since the basic purpose of this investigation is to determine the detectability of various propeller configurations at designated operating conditions, the detection characteristics of all the propeller configurations as well as the effects of various parameters on the detection distances are discussed.

PERFORMANCE AND ACOUSTIC CHARACTERISTICS - STATIC TESTS

Several propeller configurations using all blade designs and varying in blade number were tested in the static condition. These configurations can be broadly classified into three categories: free propellers, ducted propellers, and spaced/phased propellers. A propeller typical of each of these categories will be discussed in terms of its performance and general acoustic characteristics. Knowing the general acoustic characteristics of these propellers will help to understand their detectability characteristics.

Free Propellers

A three-bladed propeller with BD3 blade design (see Table 4) is considered here to illustrate the performance and general acoustic characteristics of the free propellers. The performance variables considered are the power absorbed and the figure of merit. Figure 19 shows the effect of rpm (and therefore tip speed) and thrust on the power absorbed and the figure of merit for the three-bladed propeller. As shown in this figure, for a thrust of about 18 pounds (80 newtons) the power absorbed increases and the figure of merit decreases with increase in the rotational speed. However, the figure of merit does not change appreciably with thrust for a given rotational speed. These performance characteristics are fairly typical of all of the free propeller configurations tested in the static condition. These results suggest that the rotational speed is a more important performance parameter than thrust.
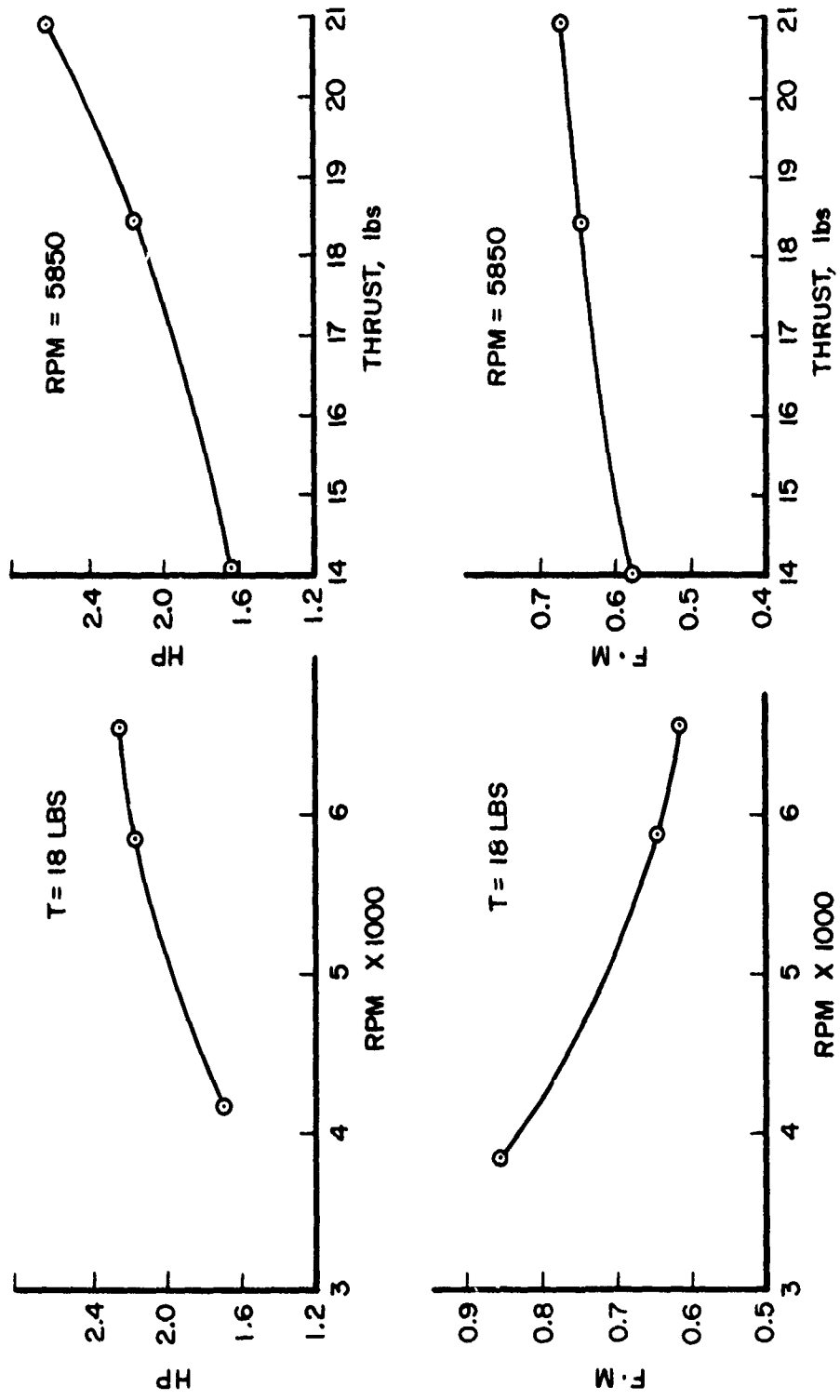
77

Figure 19. Three-Bladed Propeller (BD3 Blade Design) Performance Characteristics.

To illustrate the general acoustic characteristics, narrow-band spectra corresponding to the azimuth locations of θ = 20° and θ = 90° will be presented and discussed. The acoustic signal corresponding to θ = 20° gives a measure of the slant range detection distance of the propeller, as the signal corresponding to this microphone location is representative of the acoustic signal radiated ahead of the propeller. Similarly, the acoustic signal corresponding to θ = 90° is a measure of the altitude of no detection of the propeller configuration. Figure 20 presents the narrow-band spectra (bandwidth 10 Hz) of the three-bladed propeller with the BD3 design [diameter 20 inches (.5048 m), activity factor = 193] for θ = 20° and θ = 90°. These spectra were obtained at the design rpm of 5850 and the design thrust value of 18 pounds (80 newtons). The peaks of sound pressure levels (tones) in these spectra occur at integer multiples of blade passage frequency (293 Hz). This is characteristic of the rotational noise of the propellers. Classical propeller noise theory predicts the existence of tones at the first few harmonics of blade passage frequencies, and these tones are attributed to the steady loads (thrust and drag) on the propeller. Classical theory also predicts a large drop in the SPL with increase in the harmonics of blade passage frequency and relatively lower levels of rotational noise for azimuthal locations near the axis of the propeller. The narrow-band spectra in Figure 20 show, however, the existence of relatively high sound pressure levels at higher harmonics of blade passage frequency. They also show the presence of considerable rotational noise at θ = 20° (which corresponds to an azimuthal location near the axis of the propeller).

The classical propeller theory was based on propellers with a heavy disk loading. In the case of the RPV propellers being considered here, the disk loading is relatively low [5 to 8 lb/ft^2 (74 to 120 newtons/m^2)]. Lightly loaded propellers have very small wake velocities, and in the static condition, the wake of the propeller remains relatively close to the propeller disk. Thus, in the case of the lightly loaded propeller, the wake may interact with the blade, giving rise to unsteady loads on the blade which can generate significant noise at higher blade passage harmonics. Unlike the rotational noise due to steady loads, the tones generated due to unsteady loads radiate ahead of the propeller (i.e., around the axis of the propeller). Barry and Magliozzi (Ref. 7) have found high sound pressure levels at higher harmonics of blade passage frequency in their study of low tip speed propellers. They have shown that these peaks at higher
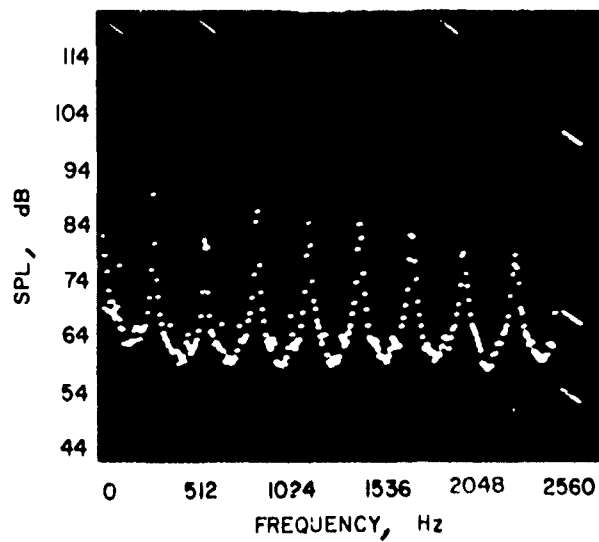
$\theta = 20°$

BLADE PASSAGE FREQUENCY = 293 Hz   B·W = 10 Hz
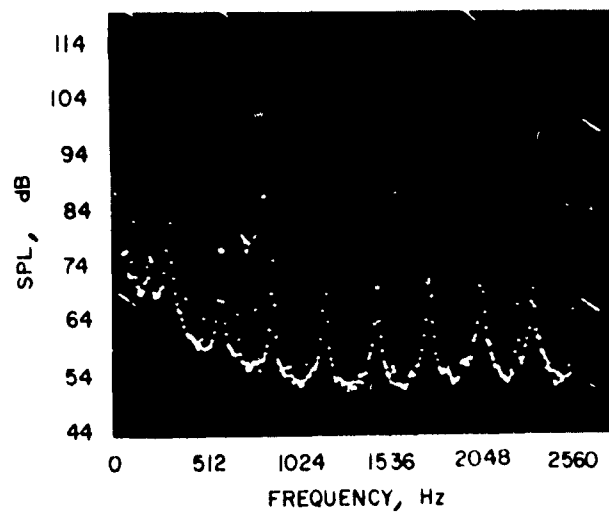
$\theta = 90°$

Figure 20.   Narrow-Band Spectra for Three-Bladed Propeller
                     (BD3 Design) - Static Tests.

harmonics of blade passage frequency were in fact not tones, but were due to narrow-band random noise. It was suggested (Ref. 33) that the source of these peaks is the interaction of the propeller with environmental turbulence. The spectra of Figure 20 clearly show the existence of tones up to at least eight to nine harmonics of blade passage frequency. These may be due to a combination of unsteady loads and the interaction of the propeller with free-stream turbulence in addition to the steady loads.

Figure 20 also shows that for $\theta = 90°$, there is a relatively large drop in SPL between the first and second harmonics of blade passage frequency. This conforms to the pattern suggested by classical propeller noise theory. It also suggests the steady loads (mostly drag) as the dominant source of rotational noise in the plane of the propeller. The distinct tones (see Fig. 20) at higher harmonics of blade passage frequency indicate the presence of rotational noise due to unsteady loads and the interaction of the propeller with free-stream turbulence. However, the levels of these higher harmonic tones in the plane of the propeller are much lower (by about 8 to 10 dB) than those at $\theta = 20°$ indicating a strong directivity.

Figure 21 presents the directivity pattern of the three-bladed propeller for the first few harmonics of blade passage frequency. As shown in this figure, at the first harmonic of blade passage frequency the maximum SPL occurred at $\theta = 30°$ as well as at $\theta = 90°$. However, at the second and third harmonics of blade passage frequency the SPL is minimum in the plane of the propeller. The directivity pattern also shows relatively high SPLs around the axis of the propeller ($\theta = 0°$). The directivity pattern and the characteristics of the narrow-band spectra of the three-bladed propeller are representative of most of the free propellers tested in the static condition.

---

[33] White, Richard P. Jr., The Status of Rotor Noise Technology, One Man's Opinion, Presented at the Specialists Meeting, Helicopter Acoustics, NASA Langley, Hampton, VA, May 22-24, 1978.
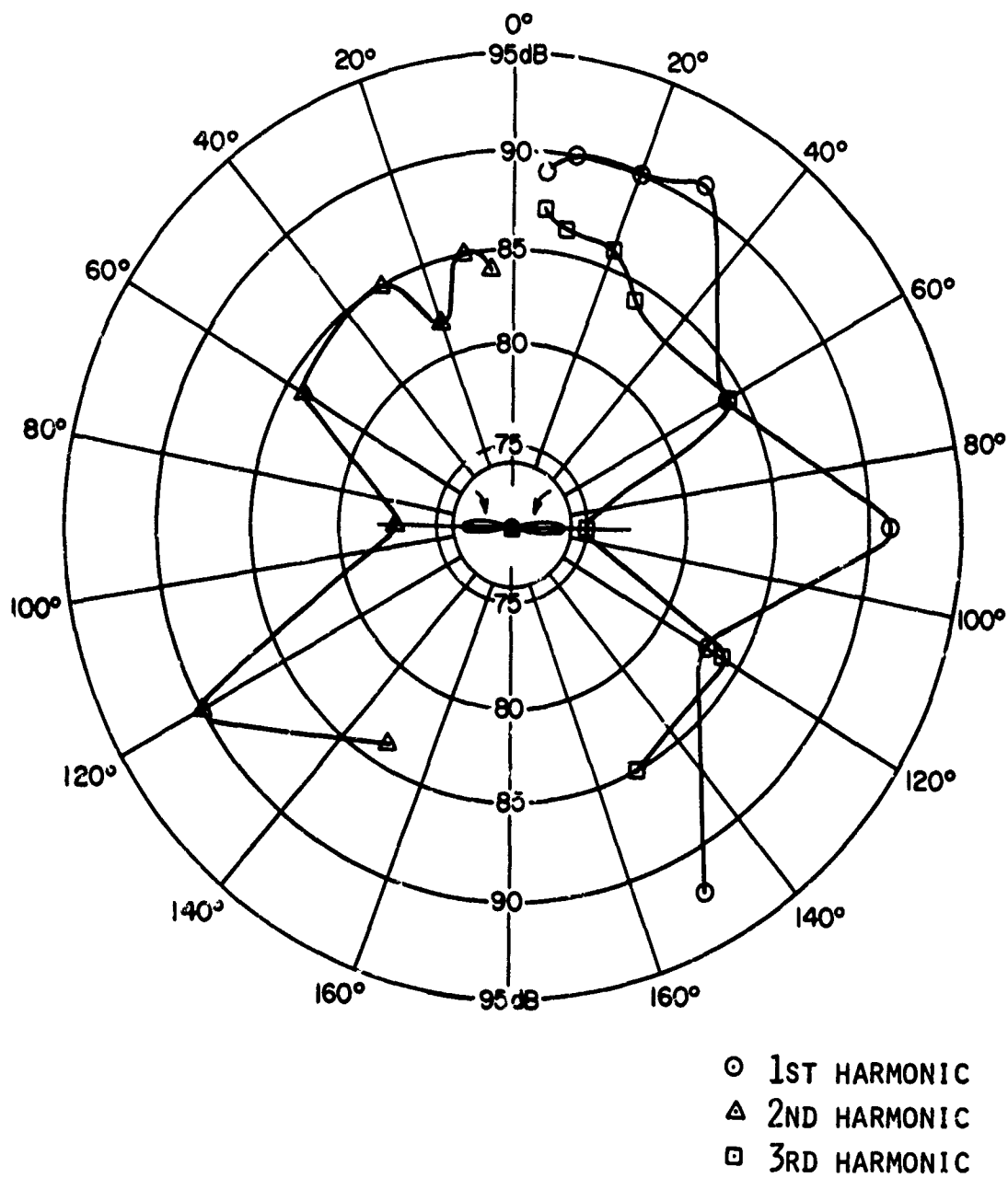
81

Figure 21. Directivity Pattern for Three-Bladed Propeller
Configuration (BD3 Blade Desigr) - Static Tests.

Each free propeller configuration was tested at five desig-
nated operating conditions in the static condition. Using
this data, the effect of tip speed (rpm) and thrust on the
acoustic characteristics of the free propellers can be evalu-
ated. Figure 22 shows the variations of peak SPL with har-
monic number for $\theta = 20°$ and $\theta = 90°$ of a three-bladed BD3
propeller at different rotational speeds. It can be clearly
seen from this figure that at both $\theta = 20°$ and $\theta = 90°$, for
the thrust remaining constant, the SPLs at most of the har-
monic numbers increase with tip speed. This conforms with
the classical theory according to which the propeller noise
increases with tip speed for a given thrust. Figure 22 also
shows that for $\theta = 20°$, at higher tip speed the variation of
SPL with harmonic number exhibits the typical hump pattern
characteristics of the wake interaction. However, this is
not evident at lower tip speeds. In both cases, the wake
velocity is the same since the thrust developed is the same.
However, at higher tip speeds, the ratio of blade rotational
velocity to that of the wake velocity is higher; therefore,
the wake moves down slower with respect to the blade, result-
ing in a stronger blade wake interaction. Figure 23 gives
the variation of SPL with harmonic number for $\theta = 20°$ and
$\theta = 90°$ for three different values of thrust. These spectra
correspond to a rotational speed of 5850 rpm. It can be
inferred from the data presented in Figures 22 and 23 that
the tip speed has a stronger effect than thrust on the acous-
tic characteristics of lightly loaded free propellers.

The performance and acoustic characteristics of the three-
bladed propeller discussed above are representative of the
free propellers tested in the static condition. The acous-
tic spectra of these propellers have shown the existence of
relatively high SPLs at higher (>4) harmonics of blade pas-
sage frequency, especially in the forward direction (azi-
muthal angle $\theta \leq 30°$). These may be due to either the unsteady
loads on the blades caused by wake interaction or the inter-
action of the propeller with free-stream turbulence or both.
It was also shown that tip speed has a significant effect on
the performance and the acoustic characteristics of the
propellers.

Ducted Propellers

Unlike the free propellers, the ducted propellers are char-
acterized by an axisymmetric duct that surrounds the blades
(see Fig. 8) and was designed to develop a significant por-
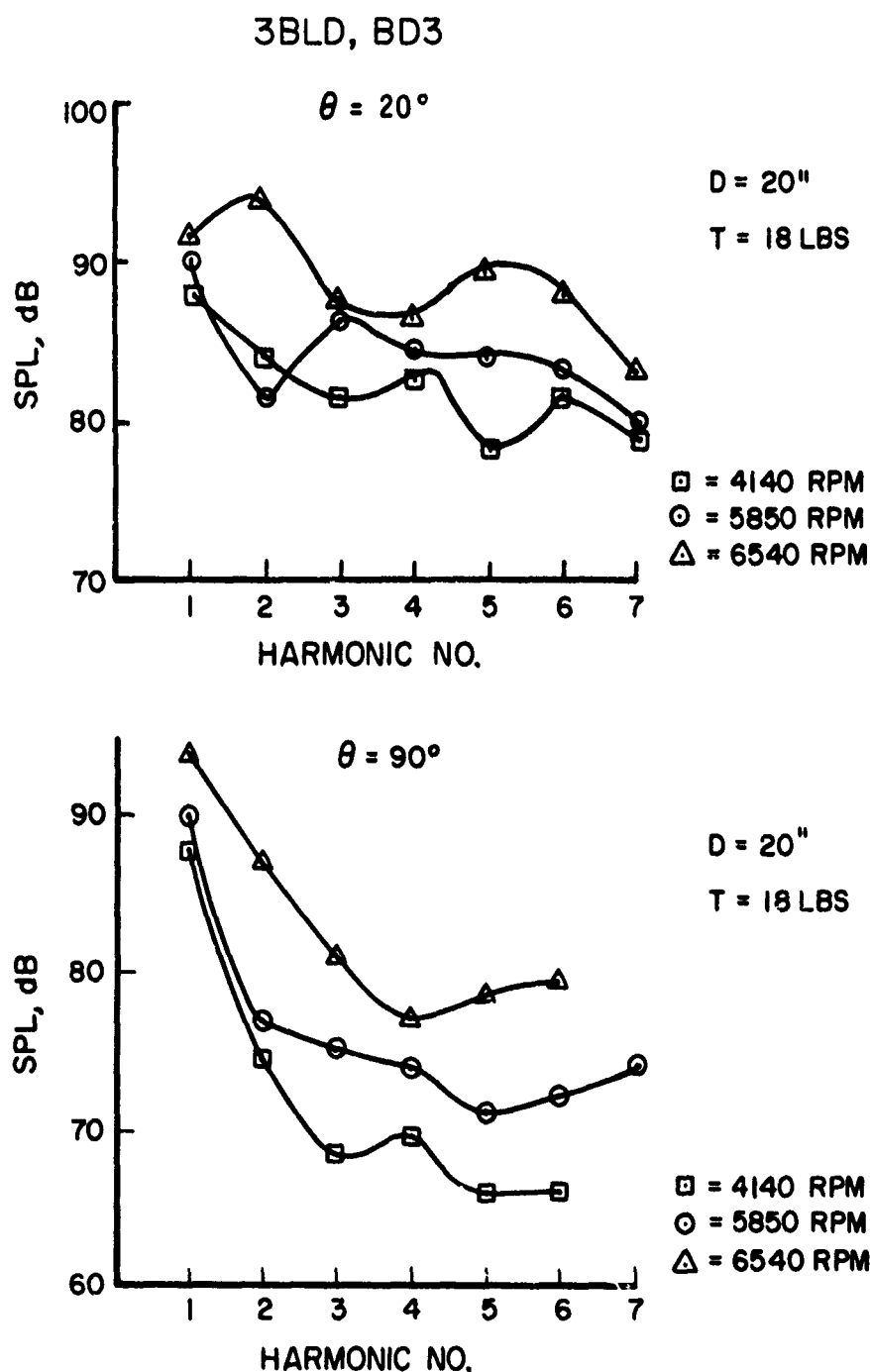tion of the total thrust of the system. The ducts were

Figure 22.   Effect of Tip Speed on the Noise at Harmonics
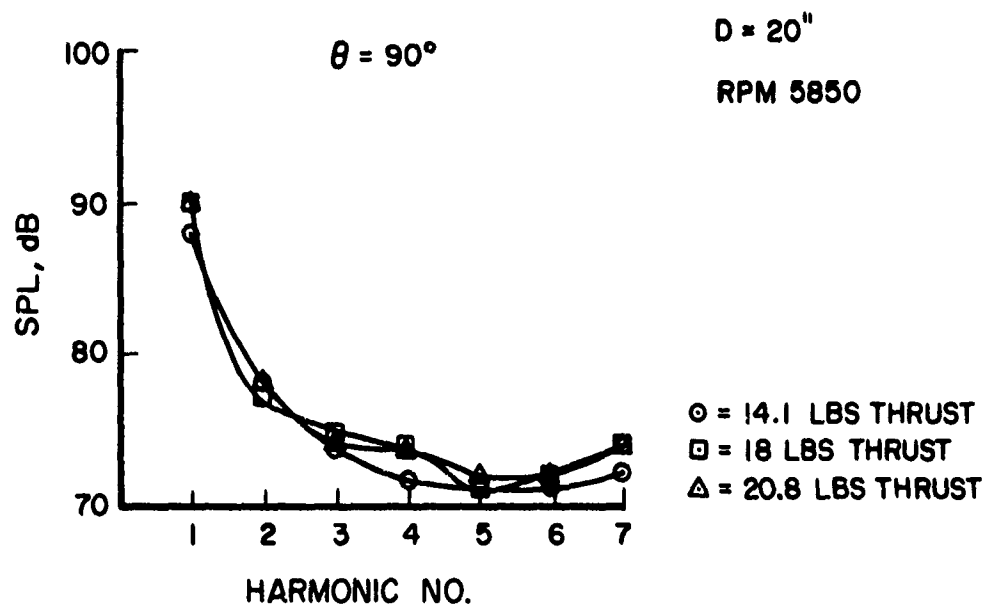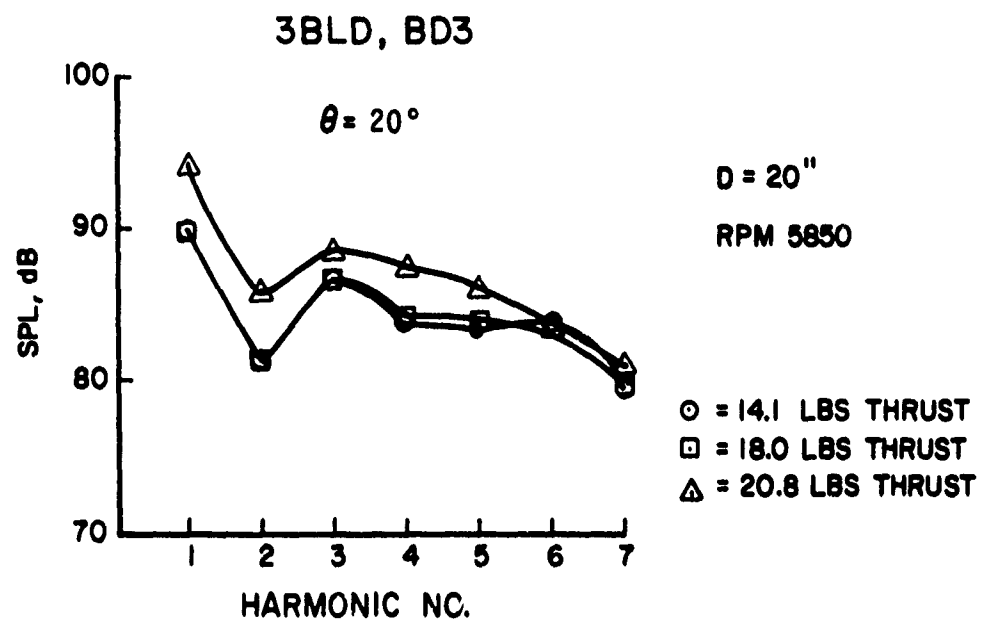of Blade Passage Frequency.

3BLD, BD3

Figure 23.   Effect of Thrust on the Noise.

designed to carry at least 14% of the total thrust at the
design forward velocity and were anticipated to develop at
least 40% of the total thrust in the static test condition.
The performance tests of the ducted propellers in static
condition showed that the thrust augmentation expected of
the ducts did not occur. In fact, the ducted propellers
absorbed more power to develop the same thrust than the free
propellers. It is believed that the low velocity inflow may
have separated from the duct surface ahead of the propeller
plane, which prevented the thrust augmentation from being
realized. The two ducts fabricated to accommodate the large
and small diameter propellers were lined with open cell
acoustic foam over a large portion of the inner surfaces of
the duct. The acoustic foam lining used was relatively rough
and the relatively low energy inflow (static condition) may
have separated at the junction of the hard skin and the foam
lining (see Fig. 8). Because of the elasticity of the foam,
the tip clearance used was somewhat higher than the design
value, which might have also contributed to the degradation
in performance. It is expected that a hard skin duct (with-
out the foam lining) might meet the designed performance
objectives.

Figure 24 presents the narrow-band spectra of the two-bladed
propeller with BD3 blade design [diameter, 20 inches (.5048m),
activity factor = 193] with and without the duct. Both were
run at the same rotational speed (5850 rpm) and developed
approximately the same amount of thrust. For θ = 20°
(Fig. 24a) the SPL at the first blade passage harmonic is
roughly the same for the ducted and free propellers. How-
ever, at higher harmonics of blade passage frequency the
floor level of the spectrum corresponding to the ducted pro-
peller rises by about 10 to 13 dB, indicating the presence
of a strong broad-band noise component which is probably due
to the separated turbulent flow. The 1/3 octave band data
showed that beyond 2 kHz the SPLs of the ducted propellers
are higher than those of the free propellers. Figure 24b
presents a comparison of the narrow-band spectra of the free
and ducted propellers for θ = 90°. For this azimuthal loca-
tion, the presence of a strong random noise component in the
case of the ducted propeller is also apparent, although not
to the degree to which is was apparent at θ = 20°. Also for
θ = 90°, the SPLs at higher harmonics (beyond 3) for the
ducted propellers are 6 to 9 dB higher than those of the
free propellers. At the first blade passage harmonic, the
SPL of the ducted propeller is about 10 dB lower than that
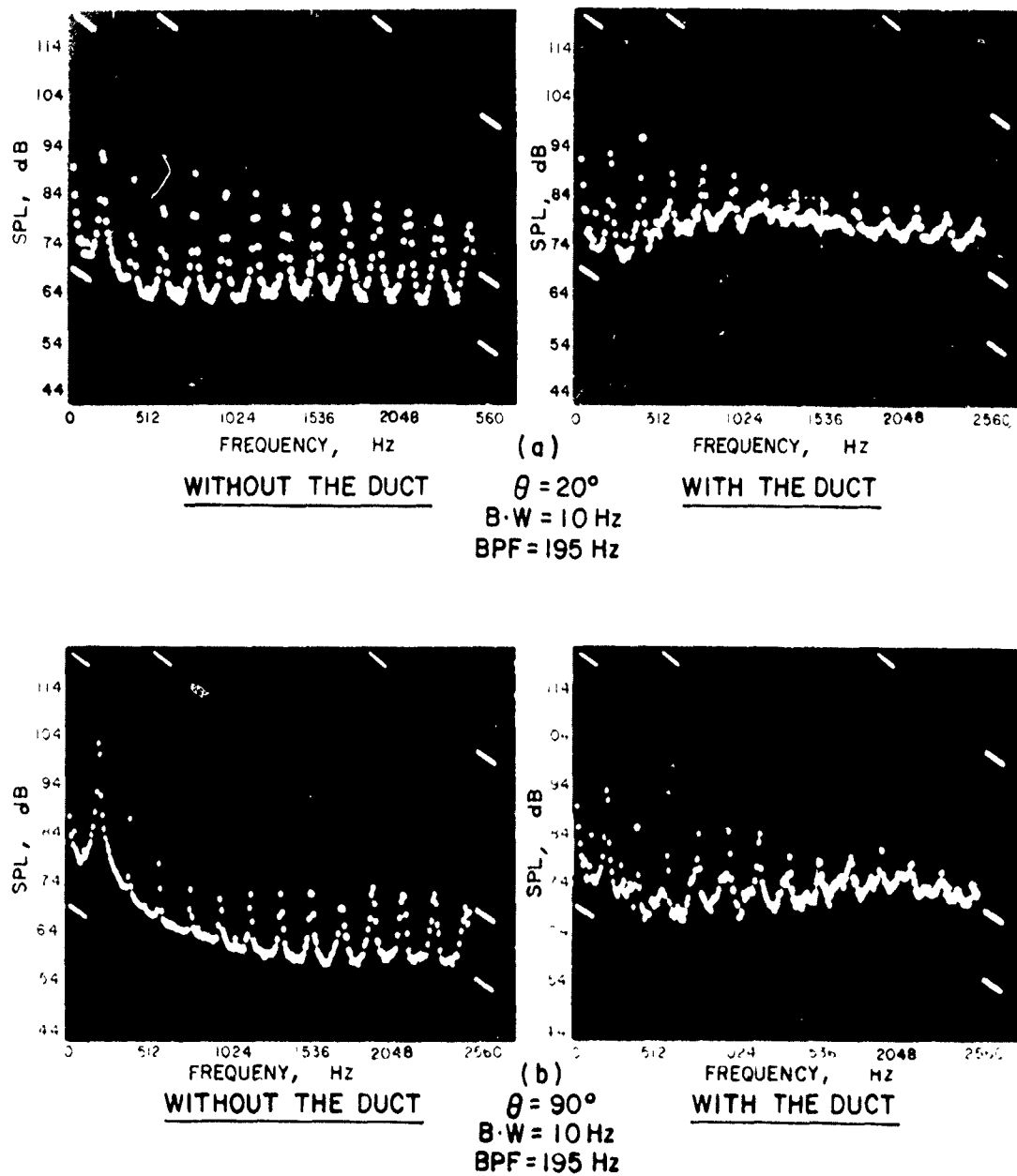
Figure 24. Spectral Comparisons of a Two-Bladed Propeller (BD3 Design) With and Without the Duct.

of the free propeller, which suggests a duct cutoff. Figure 25 presents the directivity pattern of the ducted propeller at a few harmonics of blade passage frequency. Unlike the free propellers (see Fig. 21), the SPLs for the ducted propellers are more uniform all around the azimuth. The SPLs at higher blade passage harmonics (8th harmonic) are relatively high all around the azimuth.

It was found that in the case of the large duct which was used with either the BD2 or BD4 blade design, there was a marginal performance gain. This is believed to be attributable to the lower tip clearances in terms of percent radius that could be obtained with the larger diameter duct. The effects of the large diameter duct on the noise characteristics of the propellers were almost identical to those obtained with the small diameter duct.

On the basis of the results obtained during the static tests, it was concluded that the lack of thrust augmentation and the increased broad-band noise found in the ducted propellers may be due to the separation of the low-energy inflow caused by the acoustic foam lining of the duct. Therefore, in the additional wind tunnel tests conducted later on, the acoustic foam lining was replaced by a hard skin of fiberglass. The results of these tests will be discussed in a later section.

Spaced/Phased Propellers

The spaced/phased propellers are equivalent to a set of closely spaced tandem propellers with the same or different azimuthal spacings between the blades. A four-bladed propeller with BD3 blade design in the spaced configuration consists of two blades in each of two axially spaced disk planes (the axial spacing is about one chord length of the blade at 3/4 radius) with all the blades uniformly spaced around the azimuth (that is, $\Delta\psi = 90°$). The Phase I configuration is essentially the spaced configuration wherein the leading edges of the front blades lead those of the rear by 40° around the azimuth. The Phase II configuration is also a spaced configuration wherein the leading edges of the front blades lead those of the rear by 140°. For the purposes of comparison, the coplanar (all blades lying in the same plane with $\Delta\psi = 90°$), the spaced, and the phased configurations described above were all tested at 5850 rpm and developing 18 pounds (80 newtons) of thrust.
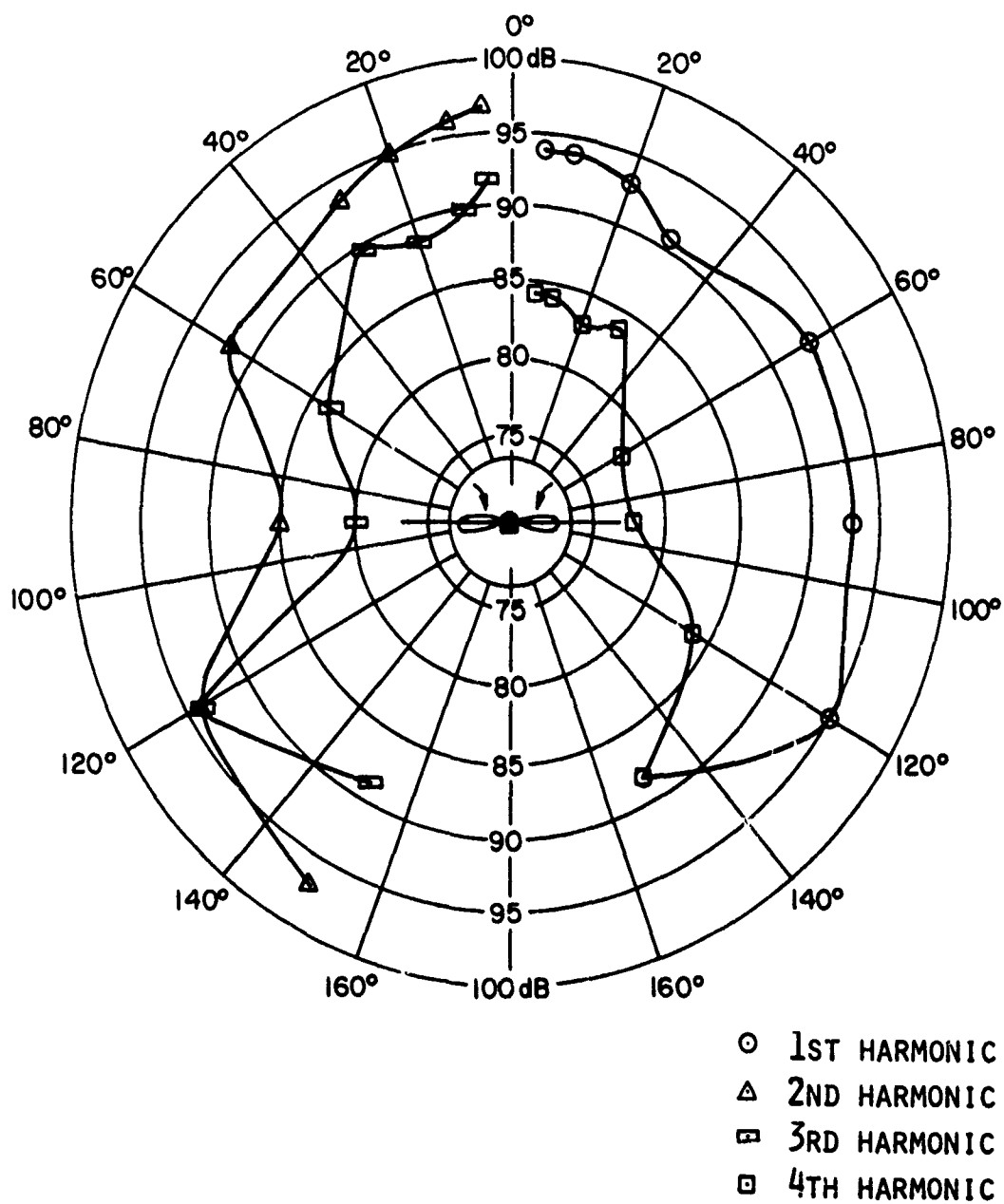
Figure 25. Directivity Pattern of a Two-Bladed Ducted Propeller (BD3 Design).

While no appreciable changes in the performance characteristics were noted between these configurations, the general acoustic characteristics were somewhat different. Figure 26 presents the narrow-band spectra of the coplanar (Fig.26a), spaced (Fig. 26b), Phase I (Fig. 26c), and Phase II (Fig. 26d) configurations of the four-bladed propeller for θ = 20°. As is clearly seen from these spectra, the spaced and phased propellers (Figs. 26b, c, and d) have twice the number of blade passage peaks compared to the coplanar configuration. Similar observations of the effect of separating blade planes were made in the case of variable geometry helicopter rotors (Ref. 31). The fundamental blade passage frequency in the case of spaced and phased configurations is about 195 Hz (half of the coplanar configuration). While the relative sound pressure levels at various harmonics may depend on the axial spacing and the angular phasing of the blades, the advantages of spaced/phased configurations from the point of view of detectability can be significant, since by redistributing the acoustic energy among the lower frequencies the detection distances can be reduced significantly as the ambient noise levels are usually high at lower frequencies. Trends similar to those discussed above were also observed in the spaced/phased configurations of a six-bladed propeller.

PERFORMANCE CHARACTERISTICS - WIND TUNNEL TESTS

Tractor, pusher, and ducted propeller configurations were tested in the wind tunnel. Propellers were tested at different tunnel velocities ranging from 15 ft/sec (4.6 m/sec) to 91 ft/sec (27.74 m/sec). The performance characteristics of all of the propeller configurations were obtained in terms of their propulsive efficiencies at the various tunnel velocities considered. Figure 27 shows the performance characteristics of some of the tractor propeller configurations tested in the wind tunnel at the design rotational tip speed of 510 ft/sec (155.5 m/sec) and the design thrust value of about 18 lbs (80 newtons). These configurations include propellers with variations in blade design, blade radius, and blade number.

As shown in Figure 27, the propulsive efficiencies of all of the propeller configurations increased with an increase in the tunnel velocity and reached their highest values at 91 ft/sec (27.74 m/sec). The tunnel tests were not conducted beyond 91 ft/sec (27.74 m/sec) due to increasing background noise. It is believed that since these propeller configurations were originally designed for a forward velocity of
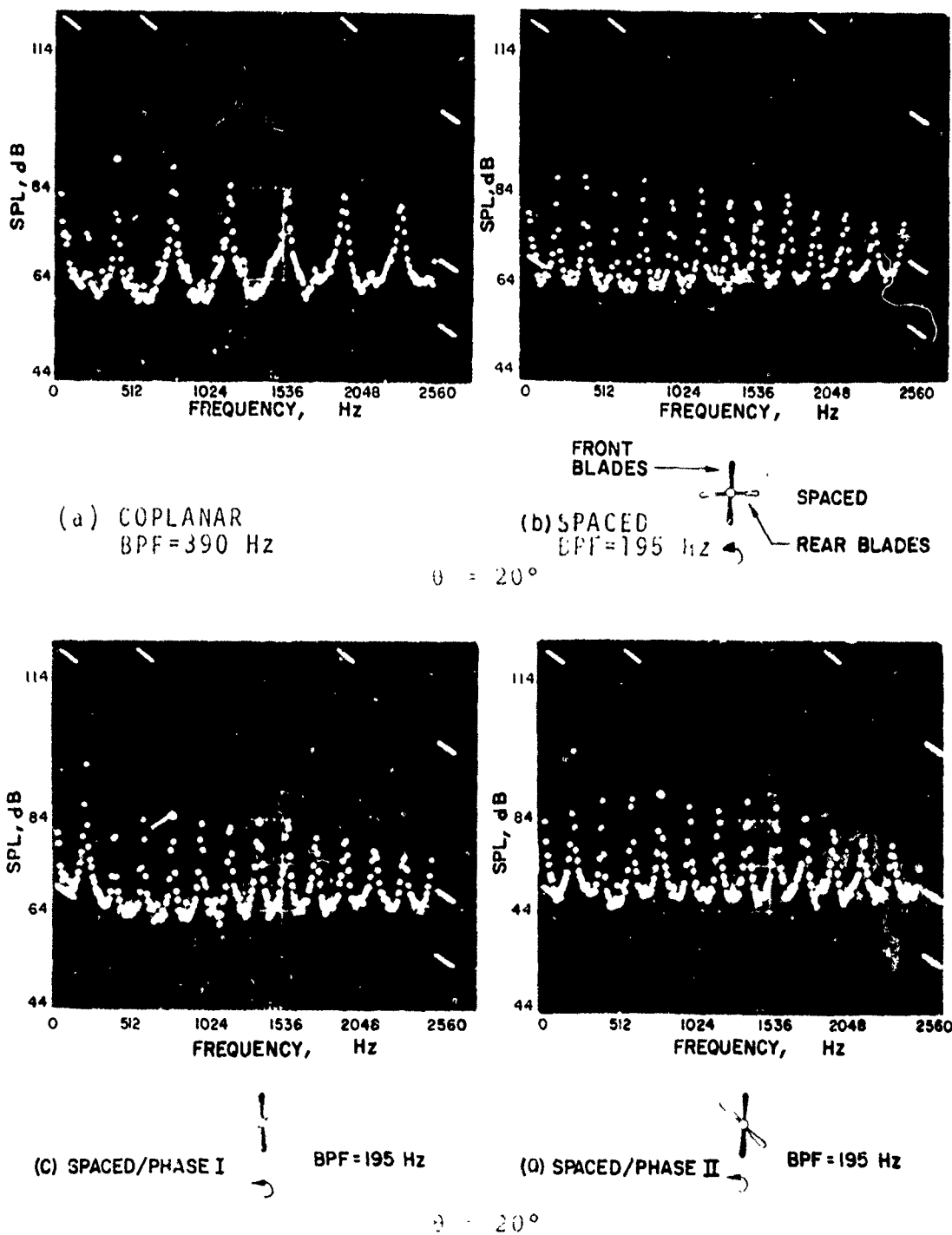
90

Figure 26. Spectral Comparisons of Spaced and Phased Configurations of a Four-Bladed Propeller (BD3 Design).
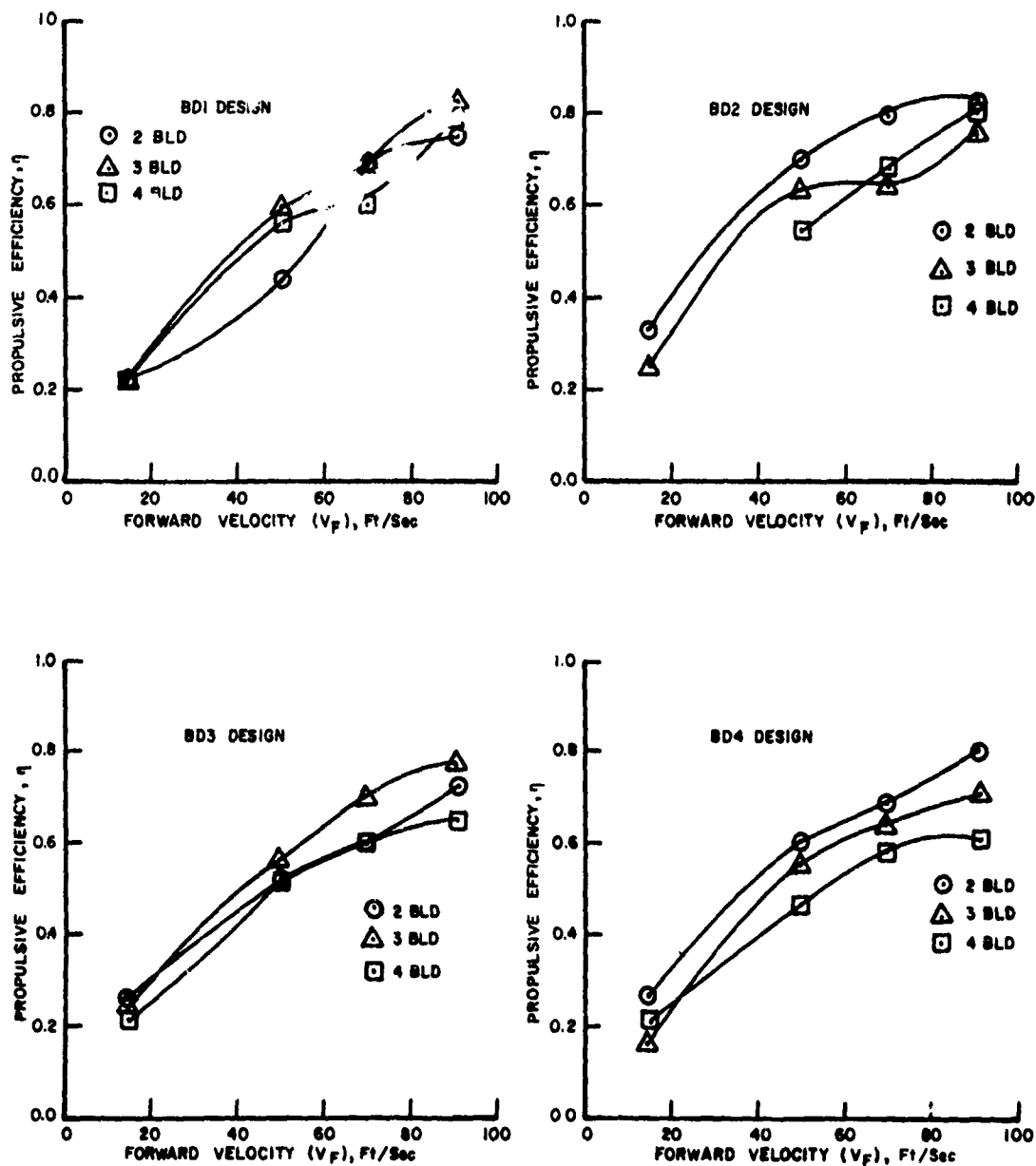
Figure 27. Performance Characteristics of Tractor Propeller
Configurations Tested at Design Tip Speed and
Design Thrust.

92

127 ft/sec (38.6 m/sec), they will attain their highest propulsive efficiencies at 127 ft/sec (38.6 m/sec).

The effect of such parameters as blade design, blade radius, and blade number on the performance characteristics of the propeller configurations can be obtained from a closer examination of Figure 27. As shown, propellers with blade designs BD1 and BD2 have generally higher values of propulsive efficiencies than those of BD3 and BD4. This was anticipated since the blade designs BD1 and BD2 correspond to the optimum performance configurations while the blade designs BD3 and BD4 correspond to the acoustic design variations of the small and large diameter propellers, respectively. The optimum performance blade designs have lower activity factors, higher twists, and larger taper ratios (see Table 4) than their acoustic counterparts. It can also be seen from Figure 27 that three-bladed configurations have the highest propulsive efficiencies in the case of small diameter propellers (BD1 and BD3 designs) while the two-bladed configurations have the highest propulsive efficiencies in the case of large diameter propellers (BD2 and BD4 designs).

To obtain the effect of propeller size (blade radius) on the performance characteristics, propellers of BD3 and BD4 designs are compared. As shown in Figure 27, for a two-bladed propeller an increase in diameter (BD3 to BD4) resulted in an increase in the propulsive efficiency at all flight velocities while for three- and four-bladed propellers an increase in diameter resulted in a marginal decrease in the propulsive efficiency. Among the tractor propeller configurations tested, the two-bladed BD2 propeller had generally the highest propulsive efficiencies while the four-bladed BD4 propeller had generally the lowest propulsive efficiencies at the forward velocities considered. No definitive explanation could be given for some of the performance trends noted above. However, as expected, the optimum performance propellers (BD1 and BD2 designs) were generally more efficient than their acoustic counterparts (BD3 and BD4 designs). The performance characteristics shown in Figure 27 can also be interpreted as efficiency versus advance ratio (J) curves since the tip speed of all of the propellers considered in these curves is the same. However, these curves are different from the general efficiency versus advance ratio curves used in the propeller design charts since these curves are based on a constant thrust condition and therefore each point on any given curve represents a different blade angle.

93

Another nondimensional parameter which is often used in the preparation of propeller design charts is the speed-power coefficient, C_s, which is defined as

$$C_s = \left[\frac{\rho V_F^5}{P' n^2}\right]^{1/5}$$

where ρ is the density in slugs/ft^3, V_F is the forward velocity in ft/sec, P' is the power absorbed in ft-lbs/sec, and n is the rotational speed in revolutions/sec. Figure 28 shows the efficiency versus speed-power coefficient curves of the tractor propeller configurations tested at the design values of thrust and tip speed. These curves generally confirm the performance trends noted in Figure 27. Again, each point on any of these curves (Fig. 28) represents a different blade angle.

In the case of pusher and ducted propeller configurations, torque data was unavailable since these configurations were tested (old wind tunnel tests) without a torque meter to measure the torque absorbed. However, the power absorbed by these configurations was estimated based on the power input to the driving motor and an assumed value for motor efficiency. It was found that at a tunnel velocity of 91 ft/sec (27.74 m/sec) the pusher configurations were less efficient (by about 6 to 8%) than their tractor counterparts. Also, the ducted propeller configurations tested in either the tractor or pusher mode were found to be less efficient than their free (or nonducted) counterparts.

In the case of the ducted configurations considered above, the interior surface of the duct was lined with acoustic foam. It was believed that the lack of thrust augmentation and the consequent reduction in the efficiency of the ducted configurations was due to the separation of flow caused by the interior foam lining of the duct. In the latter series of tests, a three-bladed BD3 propeller configuration with a hard-skin interior duct was tested at a tunnel velocity of 55 ft/sec (16.76 m/sec). The performance data showed that even with the hard skin duct, the expected thrust augmentation was not realized. In fact, the propulsive efficiency of the three-bladed ducted configuration was about 9% less than its nonducted (or free) counterpart. This suggests that the procedure used to design the duct (Ref. 25) may
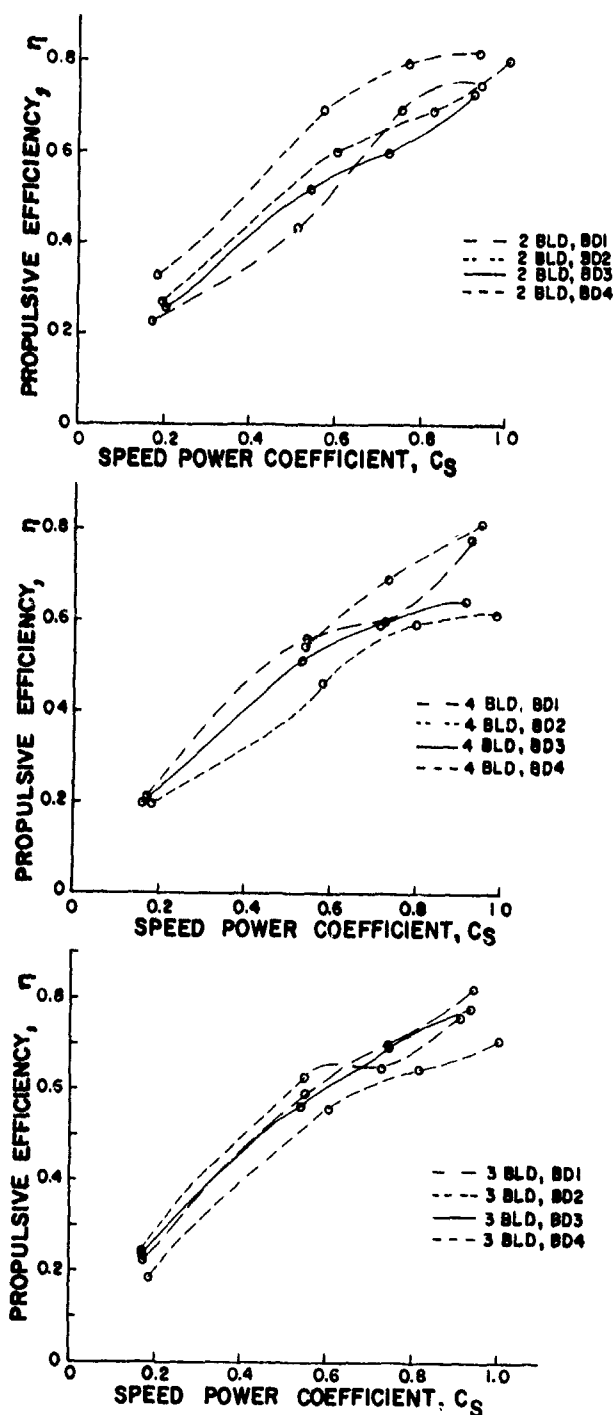
Figure 28. Efficiency Vs Speed-Power Coefficient Curves of
Tractor Propellers Tested at Design Tip Speed and
Design Thrust.

not have been adequate for small-scale RPV propellers.
It is possible that some of the assumptions used in the
design procedure such as the use of an optimum circulation
distribution for propeller blades may have been invalid,
especially with the BD3 blades. The lack of thrust aug-
mentation could also have been due to the nonuniform tip
clearance around the azimuth observed in the case of the
three-bladed ducted propeller configuration. It is possible
that the hard skin duct may have provided the anticipated
thrust augmentation with the optimum performance blades
(BD1 or BD2); however, tests were not conducted with these
propeller blades in the ducted configurations.

Figure 29 shows the effect of tip speed on the performance
characteristics of a two- and three-bladed BD3 propeller
configuration tested in the tractor mode. As expected,
these propellers had their highest propulsive efficiencies
at the design tip speed at most of the forward velocities
considered. However, at low tunnel velocities the three-
bladed configuration was slightly more efficient at the
lower tip speed than at the design tip speed. Figure 30
shows the effect of thrust on the propulsive efficiencies
of a three- and four-bladed BD3 propeller configuration.
These propeller configurations had the highest propulsive
efficiencies at the design thrust of 18 lbs (80 newtons)
and the lowest propulsive efficiencies at the highest thrust
value [36 lbs (160 newtons)] considered. This trend was
observed at all the forward velocities considered (see
Fig. 30).

Summarizing, it can be concluded that at most of the simulated
forward flight velocities considered, the optimum performance
propellers (with blade designs BD1 and BD2) were generally
more efficient than their acoustic counterparts (with blade
designs BD3 and BD4) and that the ducted and pusher configu-
rations were less efficient than the nonducted and tractor
configurations, respectively. It can also be concluded that
at least as far as the tractor configurations are concerned,
the propellers were most efficient at their design values
of thrust and tip speed for most of the forward velocities
considered. As regards the effect of blade number and blade
radius on the performance characteristics of the propellers,
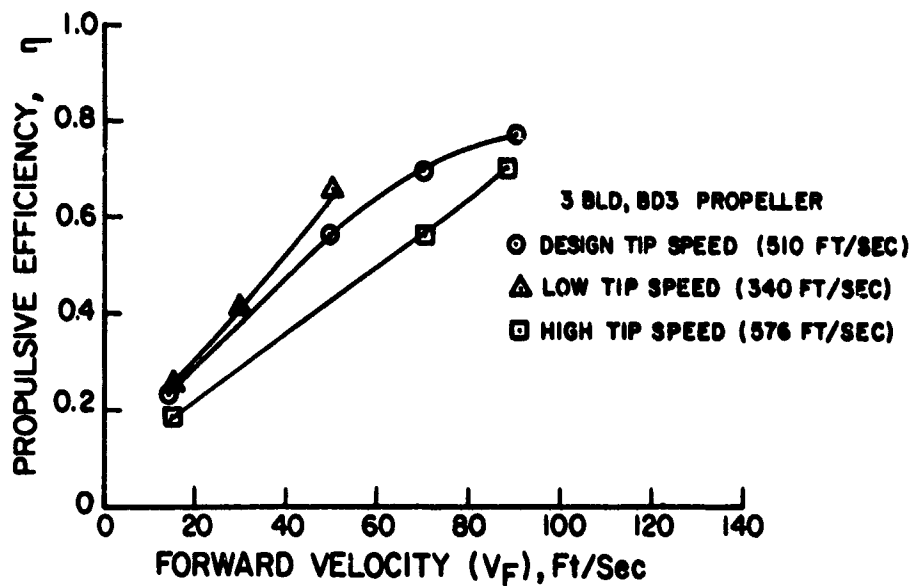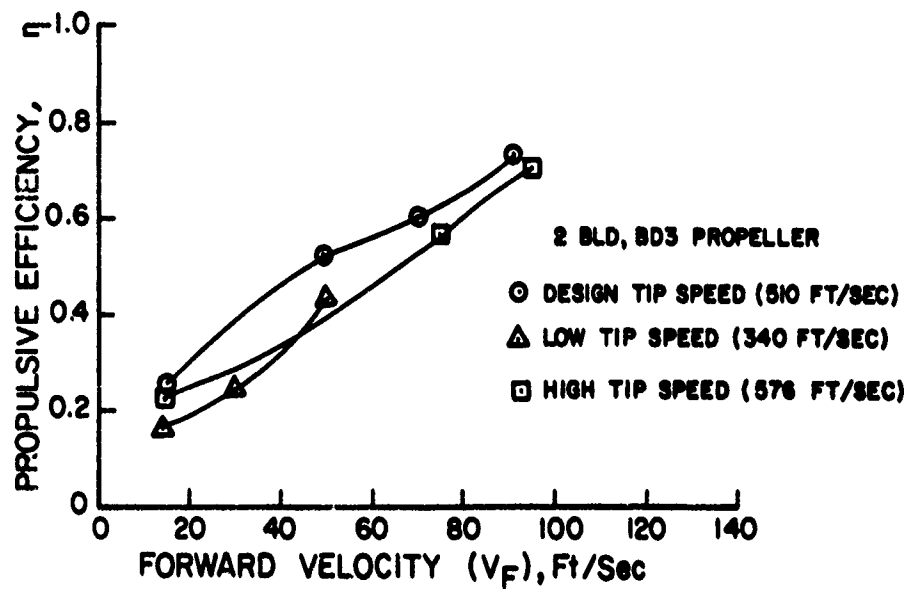no clear trends were observed.

Figure 29.   Effect of Tip Speed on the Performance
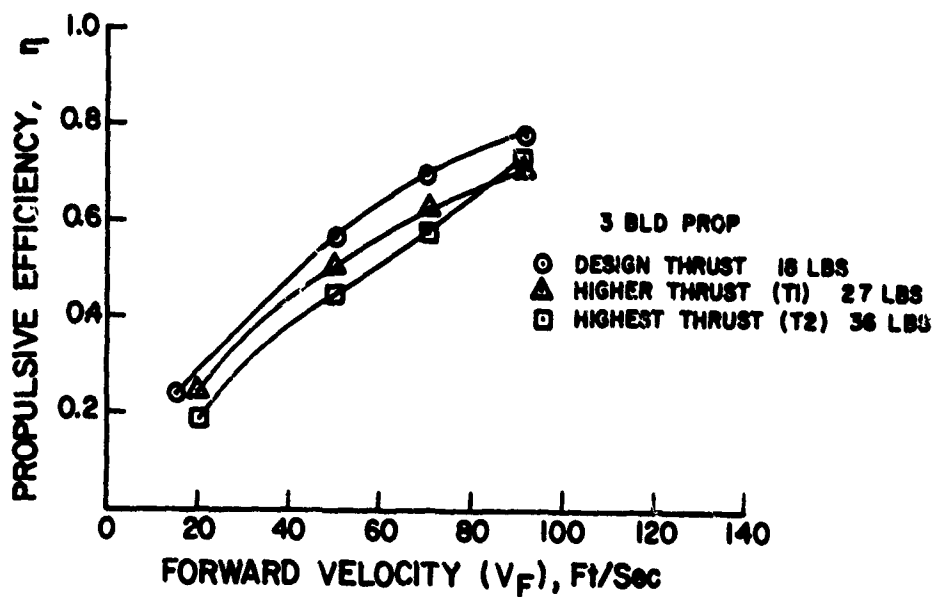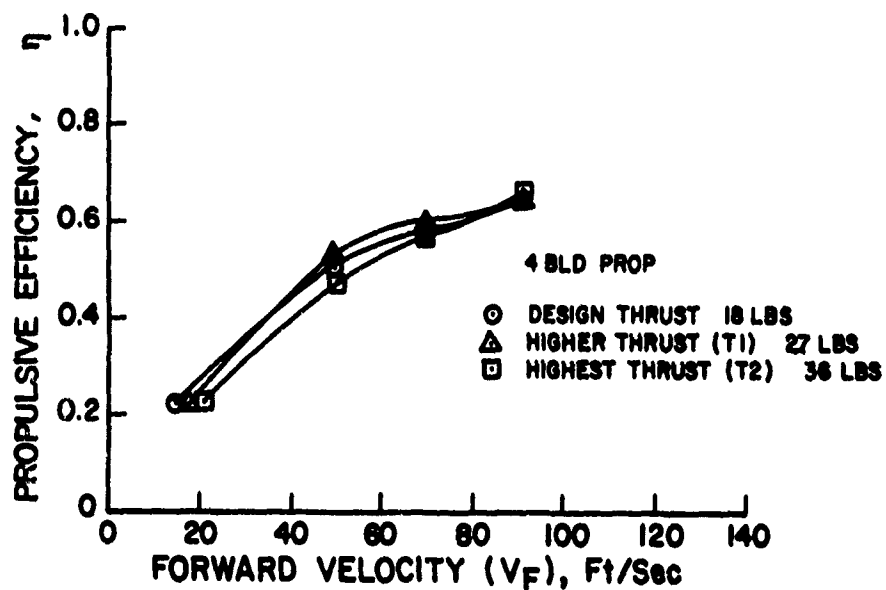   Characteristics of BD3 Propellers.

Figure 30.   Effect of Thrust on the Performance
             Characteristics of BD3 Propellers.

The BD1 and BD2 blades were designed such that a four-bladed propeller with these blades developed about 18 lbs (80 newtons) at a forward velocity of 127 ft/sec (38.6 m/sec). These designs were supposed to give the maximum efficiency (optimum performance) at the design values of thrust and tip speed. These propellers were not tested at a forward velocity of 127 ft/sec (38.6 m/sec) for reasons described before. The test data showed that a four-bladed propeller with these blade designs (BD1 and BD2) will develop only about one-half the design thrust at the design blade angles and the design forward velocity. This apparent discrepancy seriously questions the prediction method used to design the optimum performance blades. It is believed that the extrapolated low Reynolds number airfoil characteristics data (Ref. 24) used in the design procedure may be in error. It may be necessary to use either the recently devised low Reynolds number correction factors (Ref. 16) or more accurate low Reynolds number airfoil data for the successful design of fixed-pitch small-scale propellers like RPV propellers. It is also believed that the application of Theodorsen's method (Ref. 22) to the design of RPV propellers may have overextended the assumptions of the method regarding apparent wake velocity and wake contraction parameters.

With the performance data of RPV propellers generated in this study, an attempt was made to devise a procedure to select the most efficient fixed-pitch propellers for a given set of flight conditions and a given amount of available power. However, a close examination of the performance data show that it is inadequate to develop such a design method. This is mainly because most of the performance data was obtained for a given representative RPV propeller value of thrust and tip speed and therefore the blade pitch angle of a propeller with the highest efficiency for a given set of flight conditions and power available was not determined.

ACOUSTIC CHARACTERISTICS - WIND TUNNEL TESTS

The acoustic characteristics of the propeller configurations tested in the wind tunnel will be presented in terms of the narrow-band spectra of the data obtained at azimuthal locations $\theta = 20°$ and $\theta = 90°$ of the (near) microphone. The data corresponding to the azimuthal locations $\theta = 20°$ and $\theta = 90°$ is representative of the noise propagated forward and sideways, respectively. The data obtained in the

forward direction at the far microphone is not considered, since it is believed that it may have been contaminated by the acoustic reflections off the tunnel walls.

To illustrate the general characteristics of the propellers in simulated forward flight, the spectral data of a three-bladed BD3 propeller tested at the design conditions is considered. Figure 31 shows the acoustic spectra of this propeller configuration at a forward velocity of 15 ft/sec (4.6 m/sec). The spectrum for $\theta = 20°$ shows distinct peaks at harmonics of blade passage frequency over the entire frequency range (0-2.56 kHz), while the spectrum for $\theta = 90°$ shows distinct peaks only at the first three harmonics of blade passage frequency. A comparison of these spectra with those obtained in static tests (see Fig. 20) shows that while the SPLs at the first few harmonics of blade passage frequency remained almost the same, the SPLs at higher harmonics of blade passage frequency were much lower (by about 10 to 15 dB) for 15 ft/sec (4.6 m/sec) than those for the static condition. In fact, for 15 ft/sec (4.6 m/sec) the SPLs at higher harmonics of blade passage frequency (beyond the third) for $\theta = 90°$ were masked by the tunnel background noise (see Fig. 31). This significant drop in SPLs at higher harmonics of blade passage frequency could be due to a more uniform inflow and less wake interaction at 15 ft/sec (4.6 m/sec) than that in the static condition. For the forward velocity of 15 ft/sec (4.6 m/sec), the higher harmonic peaks for $\theta = 20°$ were quite broad (see Fig. 31), indicating the presence of a strong broad-band noise component propagating in the forward direction.

A closer examination of the spectra for a forward velocity of 15 ft/sec (4.6 m/sec) also shows the presence of distinct peaks (referred to as sidebands) at frequencies other than the integer multiples of blade passage frequency. The sidebands were also observed at other tunnel velocities as well as for other propeller configurations. These sidebands generally occurred at harmonics of rotational speed of the driving motor. It is believed that these sidebands are due to either the blade to blade variability or the vibration of the test stand or both.

Figure 32 shows the narrow-band spectra of the three-bladed BD3 propeller at a higher forward velocity of 50 ft/sec (15.24 m/sec). The acoustic characteristics for this velocity are similar to those observed for 15 ft/sec (4.6 m/sec)
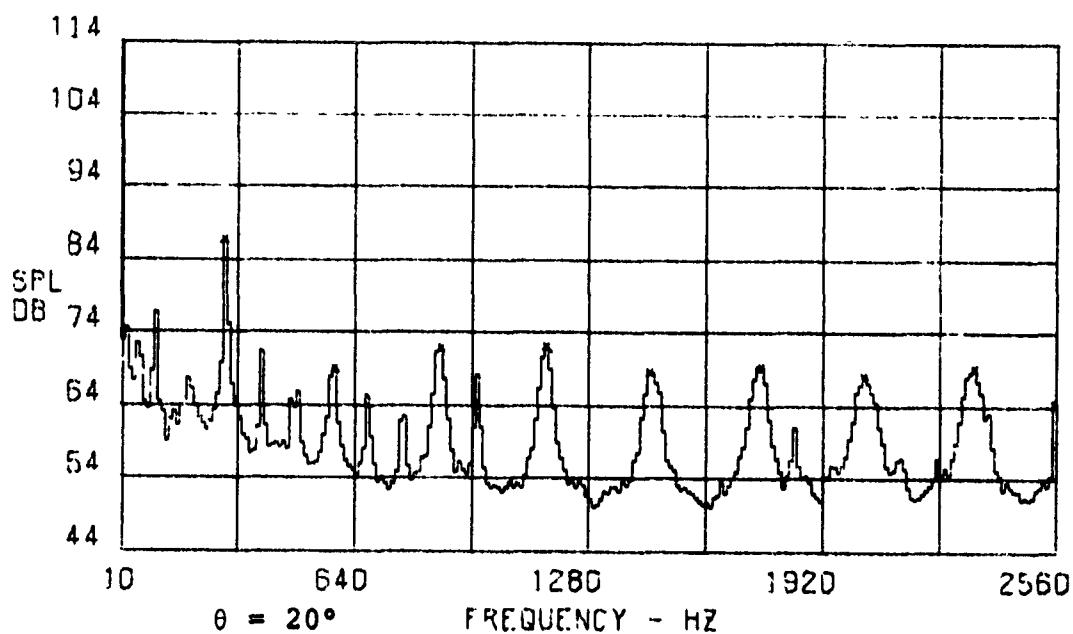
BPF = 292.5 Hz

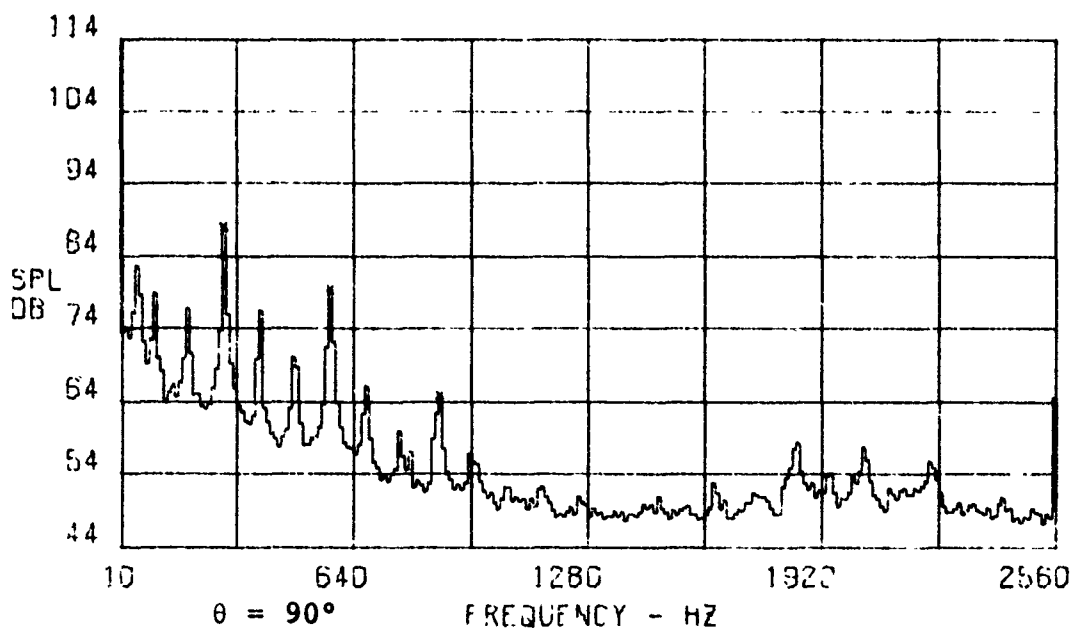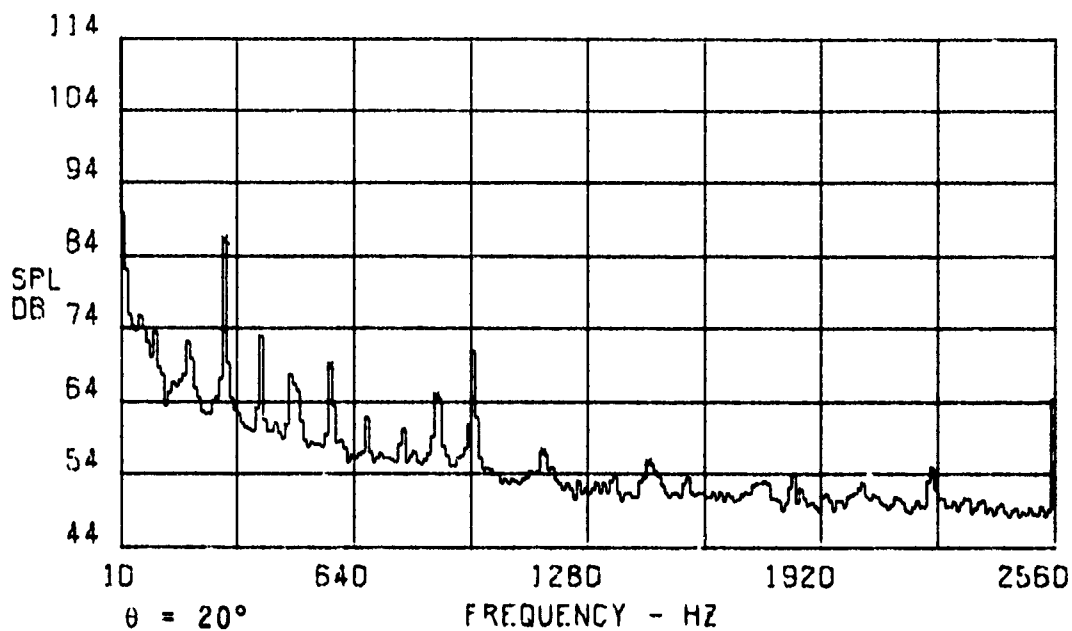Figure 31. Narrow-band Spectra of the Three-Bladed BD3 Propeller at a Forward Velocity of 15 ft/sec (4.6 m/sec).
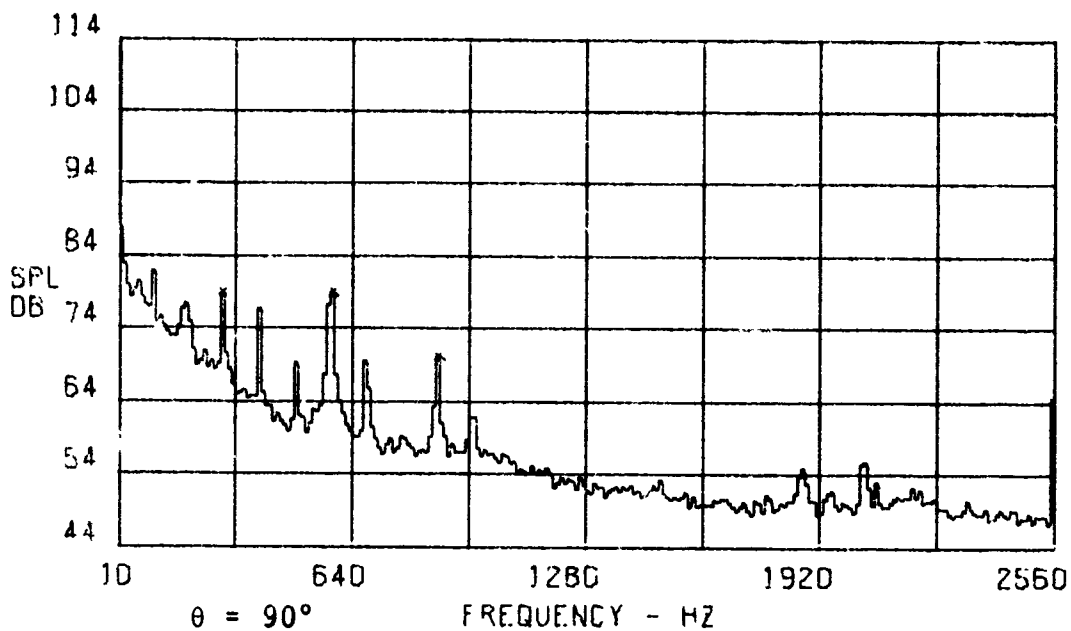
101

BPF = 292.5 Hz

Figure 32. Narrow-band Spectra of the Three-Bladed BD3 Propeller at a Forward Velocity of 50 ft/sec (15.24 m/sec).

except that for θ = 20°, the higher harmonic SPLs for 50 ft/sec (15.4 m/sec) are substantially lower (compare Figs. 31 and 32) than those for 15 ft/sec (4.6 m/sec). It has been well established in the literature that the higher harmonic SPLs are mainly due to wake-induced unsteady loads acting on the blades as well as nonuniform inflow. It has also been known that these higher harmonic SPLs show a strong directivity in the forward direction. Therefore, it is believed that the substantial reduction (of the order of 15 to 20 dB) in the higher harmonic SPLs is due to more uniform inflow and less wake interaction at the forward speed of 50 ft/sec (15.4 m/sec) than at 15 ft/sec (4.6 m/sec).

Figures 33a through 34b show the narrow-band spectra of the three-bladed BD3 propeller configuration at higher forward velocities of 70 ft/sec (21.34 m/sec) and 91 ft/sec (27.74 m/sec) respectively along with the spectra corresponding to the tunnel background noise at these forward velocities. The background noise data was obtained with the blades off and motor running and at the same azimuthal locations of the microphone as those at which the acoustic data of the propellers was obtained. A comparison of the spectra of the three-bladed propeller at 70 ft/sec (21.34 m/sec) with those of the background noise (compare Figs. 33a and 33b) at the same tunnel speed shows that the higher harmonic SPLs for both θ = 20° and θ = 90° were completely masked by the background noise. In fact, these spectra show that only the first two blade passage harmonic SPLs were substantially higher (about 6 to 15 dB) than the corresponding background noise spectral levels.

The tunnel background noise levels increase with the tunnel velocity, and at a velocity of 91 ft/sec (27.74 m/sec) the spectra show (see Figs. 34a and 34b) that the SPLs at the first two harmonics of blade passage frequency were only 3 to 8 dB higher than the corresponding background noise levels. Fortunately, the detection distances of the propeller configurations (as will be shown later) are mostly determined by the SPLs at the first few harmonics (first or second) of blade passage frequency and therefore the tunnel background will not have a strong influence on the detection distances. However, because of the higher background noise levels, the variation of the higher harmonic SPLs with forward velocity at higher tunnel velocities could not be determined. It is believed, however, that with increasing forward velocities the higher harmonic SPLs will continue to decrease perhaps at a slower rate due to an increasingly uniform inflow and decreasing wake-induced effects.
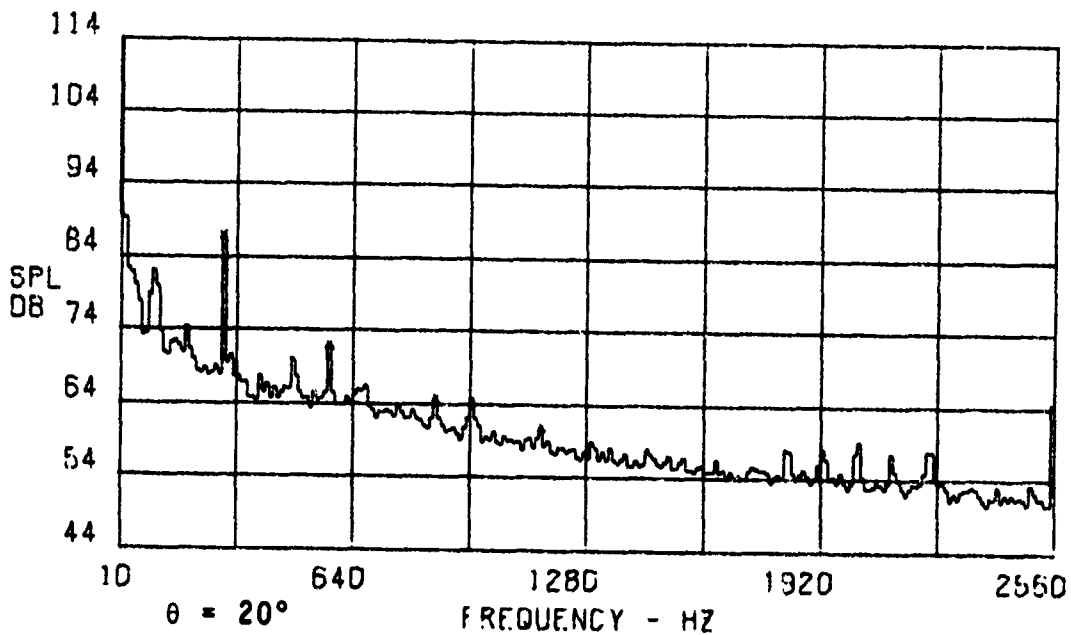
BPF = 292.5 Hz
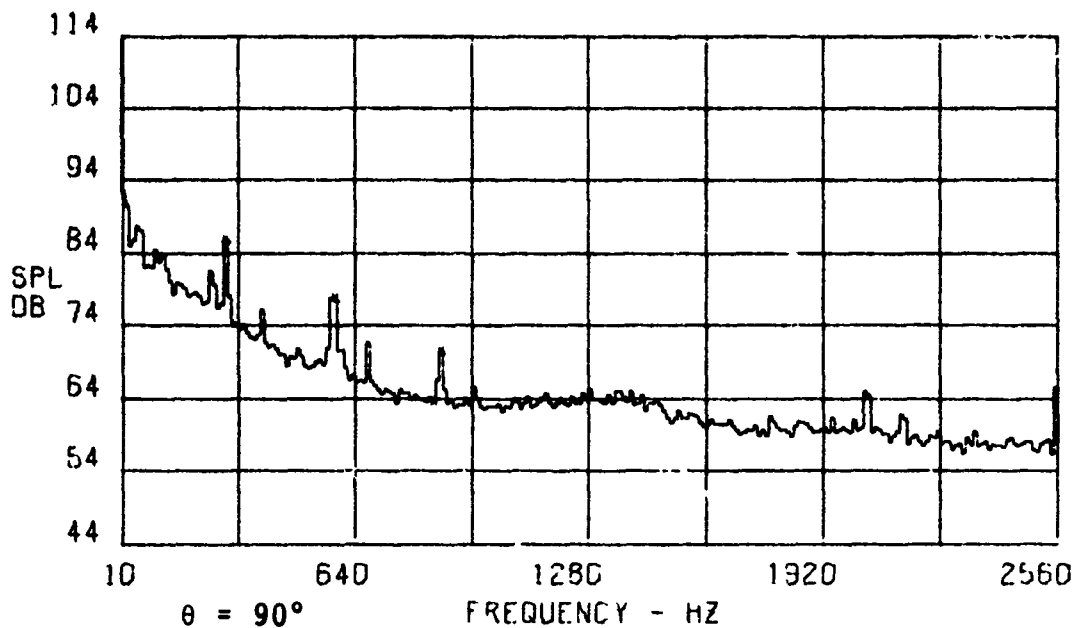
a. Forward Velocity - 70 ft/sec (21.34 m/sec).

Figure 33. Narrow-band Spectra of the Three-Bladed
BD3 Propeller.
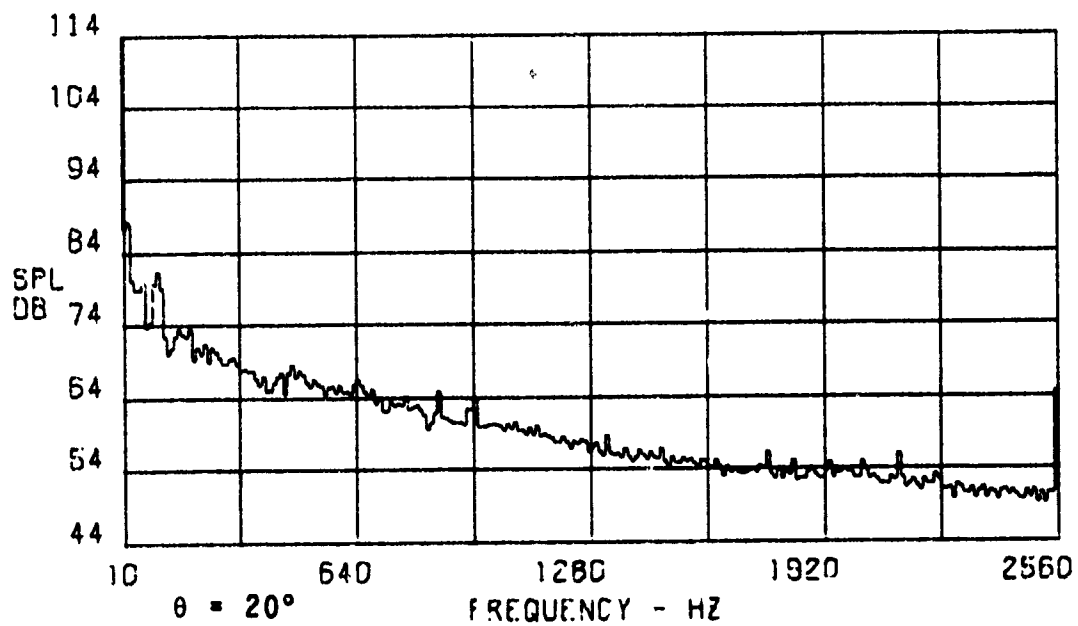
BPF = 292.5 Hz
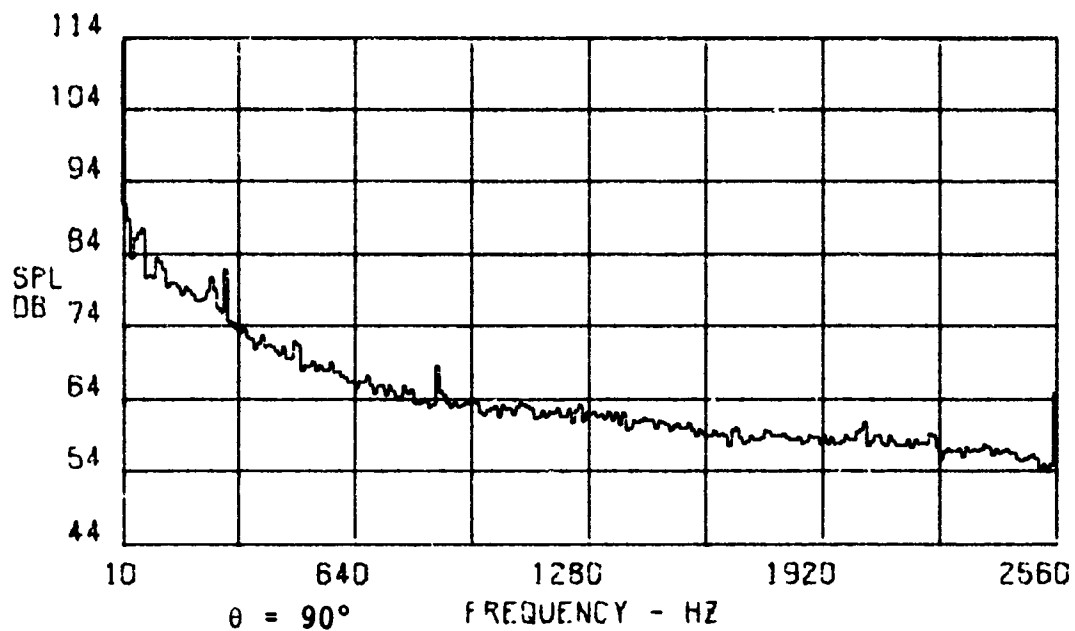
b. Tunnel Background Noise at 70 ft/sec (21.34 m/sec).

Figure 33. Continued.

105
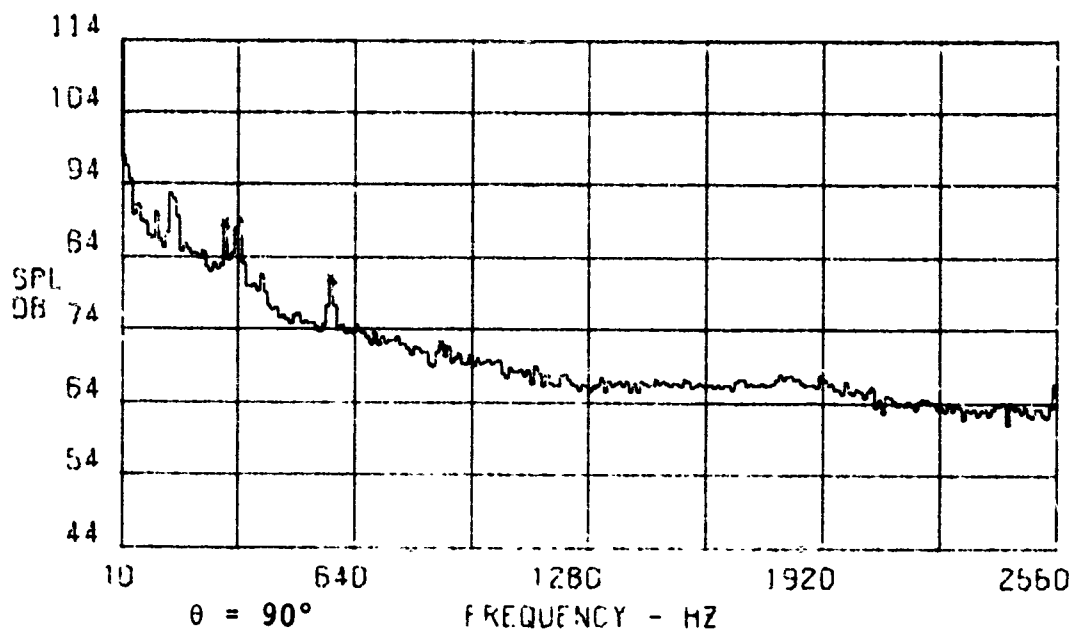
a. Forward Velocity of 91 ft/sec (27.74 m/sec).

Figure 34. Narrow-band Spectra of the Three-Bladed BD3 Propeller.

θ = 20° FREQUENCY - HZ

BPF = 292.5 Hz

θ = 90° FREQUENCY - HZ
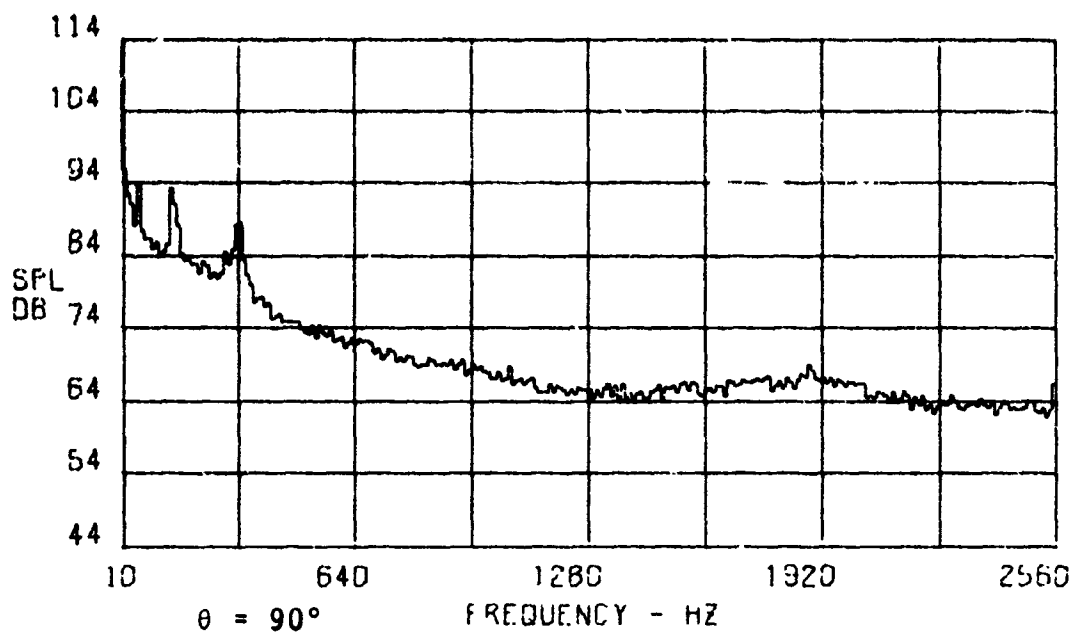
b. Tunnel Background Noise at 91 ft/sec (27.74 m/sec).

Figure 34. Continued.

107

Full-scale flight tests show a decrease in higher harmonic
levels with an increase in flight speeds; this trend is at
least partially confirmed by the present tunnel tests in the
range of velocities of 15 ft/sec (4.6 m/sec) to 50 ft/sec
(15.24 m/sec). Figure 35 shows the variation of the SPLs at
the first three harmonics of blade passage frequency with
forward velocity for θ = 20° and θ = 90°. The dashed lines
in these figures indicate that the noise levels in question
might have been affected by the background noise. It can
be seen from Figure 35 that the SPLs at the first two or
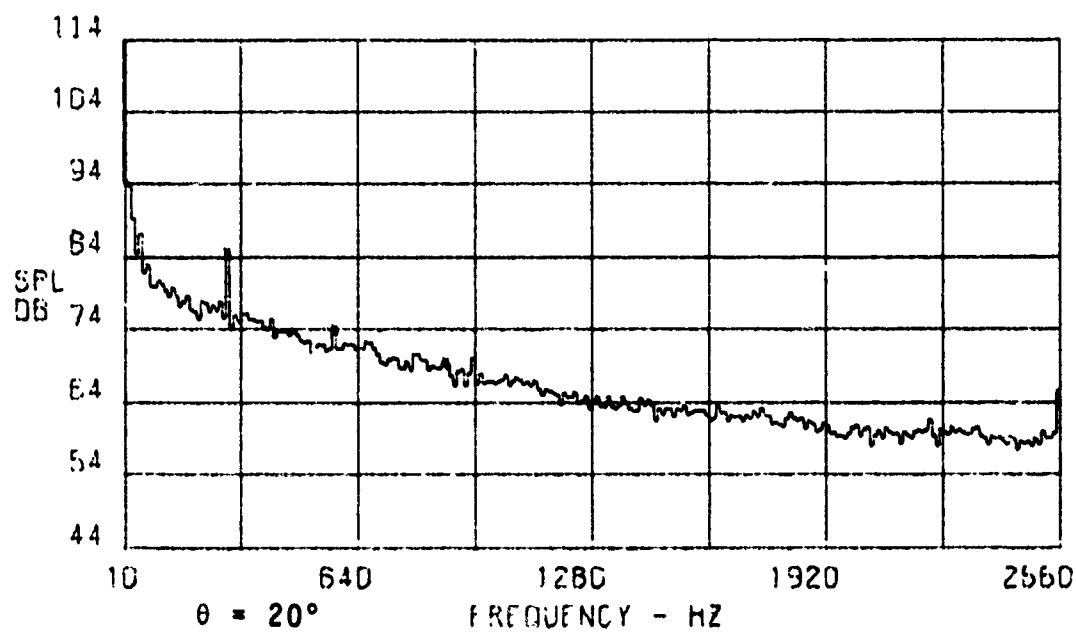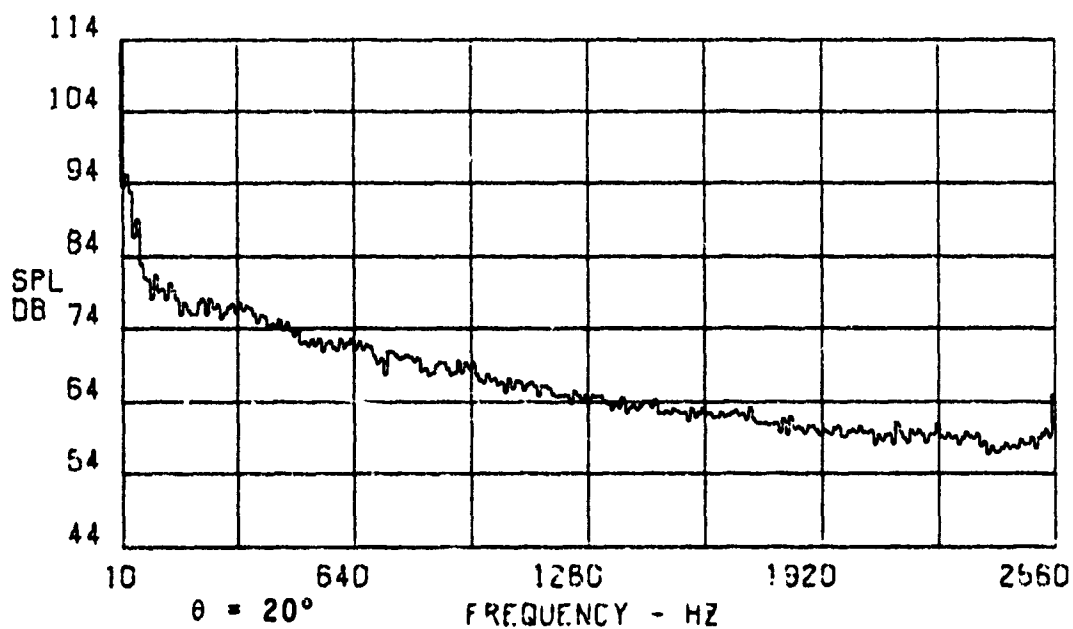three harmonics of blade passage frequency varied much more
slowly with changes in forward velocity than those at the
higher blade passage frequencies. This is partially because
the steady blade loads which contribute mainly to the lower
harmonic SPLs remained relatively constant with forward
velocity changes, since the thrust developed by each propeller
configuration was kept the same at all the forward velocities
considered in the tests.

Figure 36 gives the directivity patterns of the three-bladed
BD3 propeller at the first two harmonics of blade passage
frequency for different forward velocities. At most of the
forward velocities considered, these directivity patterns
showed relatively high SPLs in the forward direction
(10° ≤ θ ≤ 20°) as well as in the plane of the propeller
(θ = 90°). Figure 36 also shows that the directivity pat-
tern of the propeller was not significantly affected by
the changes in forward velocity.

The general acoustic characteristics discussed above are
fairly typical of the tractor propeller configurations tested
in the wind tunnel at the design tip speed of 510 ft/sec
(155.5 m/sec) and the design thrust of 18 lbs (80 newtons).
The three-bladed BD3 propeller was also tested at off-design
conditions. The general acoustic characteristics of the
three-bladed BD3 propeller at off-design conditions were
similar to those discussed above. Figures 37 and 38 show the
variation of lower harmonic SPLs of the three-bladed BD3
propellers with forward velocity at an off-design tip speed
of 576 ft/sec (175.6 m/sec) and an off-design thrust value of
36 lbs (160 newtons) respectively. These figures clearly
show that for both θ = 20° and θ = 90°, these variations were
similar to those observed at the design conditions.

Two propeller configurations (4 BLD, BD1 and 2 BLD, BD2) were
also tested in the pusher mode at a forward velocity of
91 ft/sec (27.74 m/sec). These pusher configurations were
tested at design conditions with and without the addition of
an upstream wing. Figures 39a and 39b show the narrow-band
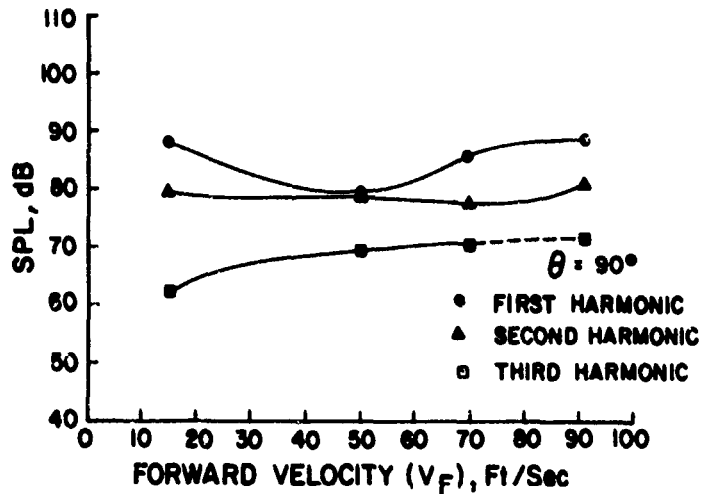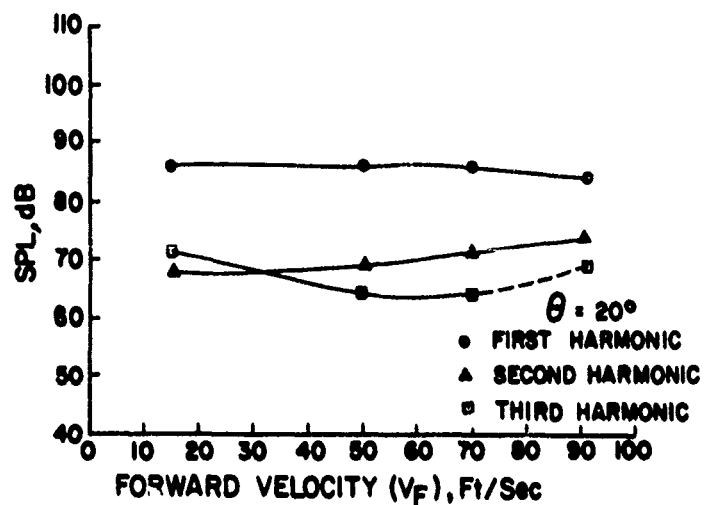
Figure 35. Variation of Harmonic SPLs With Forward Velocity
of a Three-Bladed BD3 Propeller.
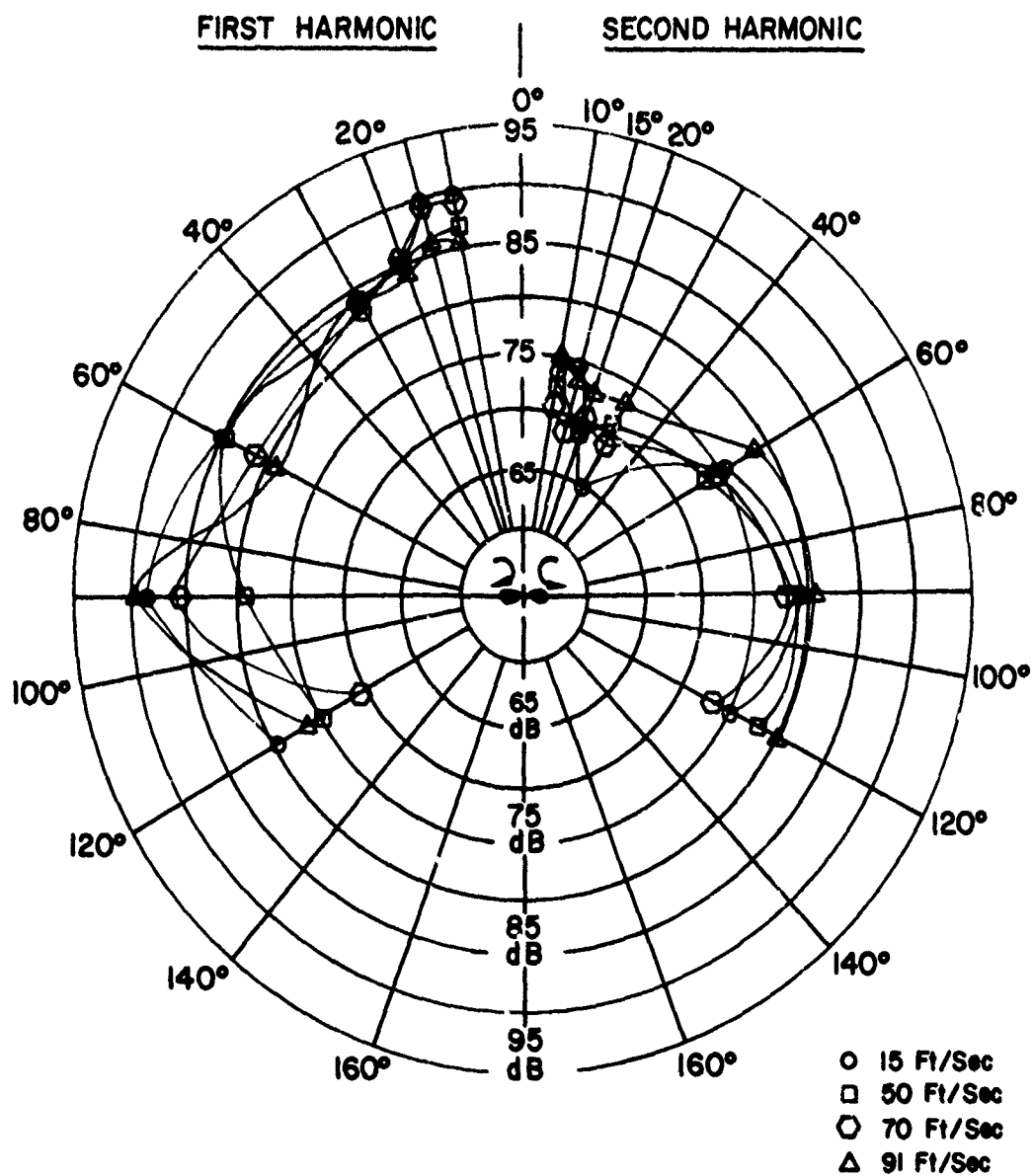
Figure 36. Directivity Patterns of a Three-Bladed BD3 Propeller at Different Forward Velocities.

110
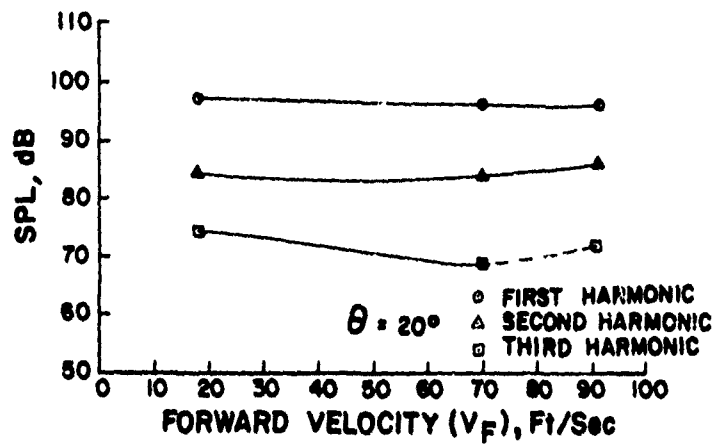
Figure 37. Variation of Lower Harmonic SPLs With Forward
            Velocity of a Three-Bladed BD3 Propeller at an
            Off-Design Tip Speed of 576 ft/sec (175.6 m/sec).

111

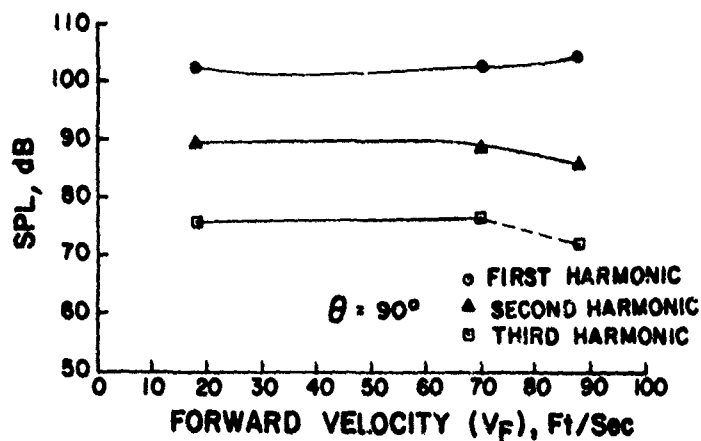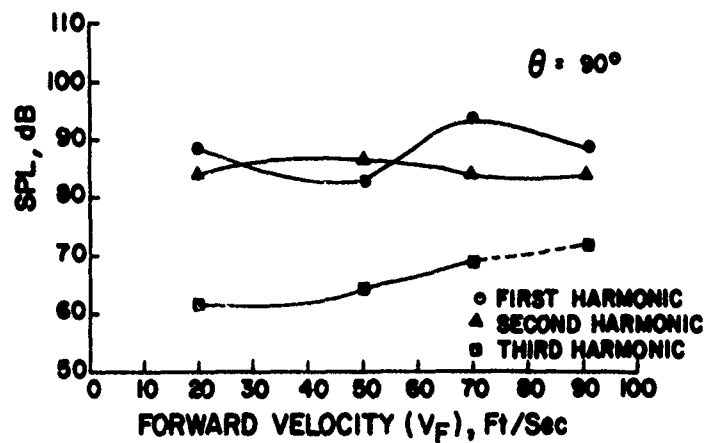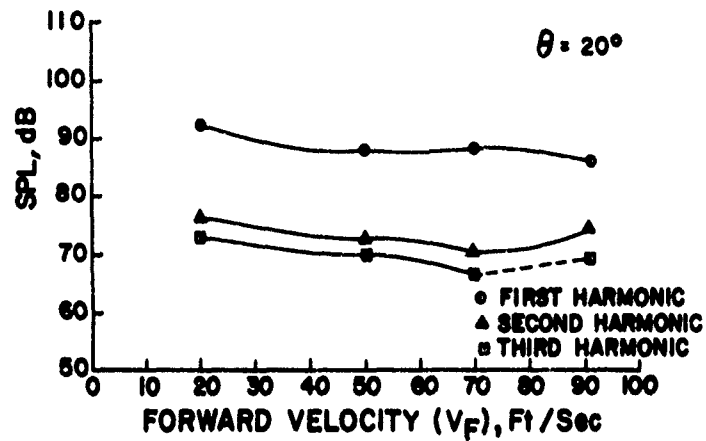Figure 38. Variation of Lower Harmonic SPLs With Forward Velocity of a Three-Bladed BD3 Propeller at an Off-Design Thrust Value of About 36 lbs (160 newtons).

spectra of a four-bladed BD1 propeller in both tractor and pusher configurations. As shown in Figure 39a, for $\theta = 20°$, the harmonic SPLs of the propeller in the pusher mode were substantially higher (by about 6 to 10 dB) than those of its tractor counterpart. In the tractor configuration, the harmonic levels were masked by the background noise. The addition of an upstream wing in the inflow resulted in only a slight increase in the harmonic levels over those of the propeller without an upstream wing. A comparison of the spectra for $\theta = 90°$ shows (see Fig. 39b) that the differences in harmonic SPLs between the tractor and pusher modes were not very significant. These results suggest that the turbulence generated by the forebody resulted in a much greater change in the fluctuating lift of the propeller than it did to the drag. This result is somewhat puzzling, as one would expect that since the propeller efficiency is lower in the pusher mode, the noise in the plane of the propeller ($\theta = 90°$) would increase more than that in the thrust direction. Considering that turbulence would generate unsteady lift forces and thus unsteady indirect drag forces, one would also conclude that the noise in the propeller plane would increase as much as in the thrust direction. Since neither of these explanations fit the trend of the results, the reason the experimental data varied as it did could not be ascertained. The acoustic data of the two-bladed BD2 propeller in the pusher mode generally confirmed the above results except that the differences of the harmonic SPLs between the tractor and pusher modes are smaller than those of the four-bladed BD1 propeller.

A few propellers were also tested in the ducted configuration. Two sets of ducts were used: one with an interior foam lining and the other with a hard-skin fiberglass interior surface. Only a three-bladed BD3 propeller was tested with the hard-skin duct. This test was conducted at the design conditions and at a forward velocity of about 50 ft/sec (15.24 m/sec). Figures 40a and 40b give the acoustic spectra of this propeller in the ducted and free (non-ducted) configurations. These spectra clearly show that the ducted configurations were much noisier than their free counterparts. Specifically, the higher harmonic SPLs of the ducted configuration were about 5 to 12 dB higher than those of the free propeller in the forward direction ($\theta = 20°$) as well as the plane of the propeller ($\theta = 90°$). These results suggest the presence of large fluctuating loads on the blades which might have occurred due to a more turbulent inflow. It is believed, however, that the smooth interior surface of the duct is unlikely to generate such a strong turbulent inflow.

113
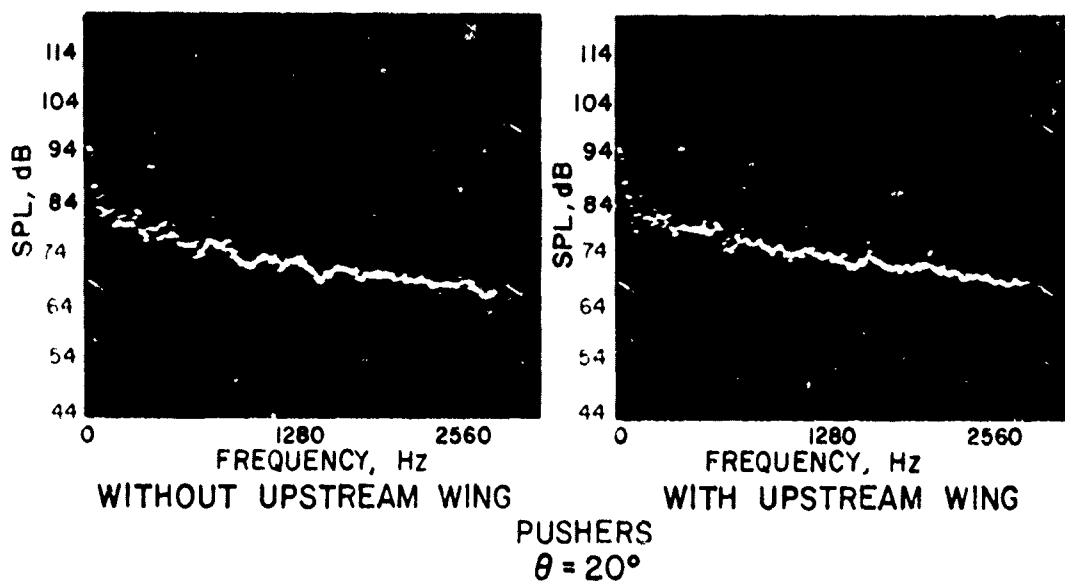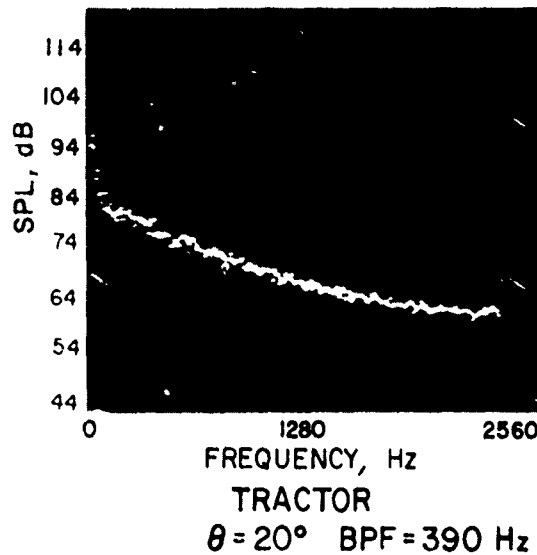
a. Forward Velocity of 91 ft/sec (27.74 m/sec).

Figure 39. Narrow-band Spectra of a Four-Bladed BD1 Propeller.
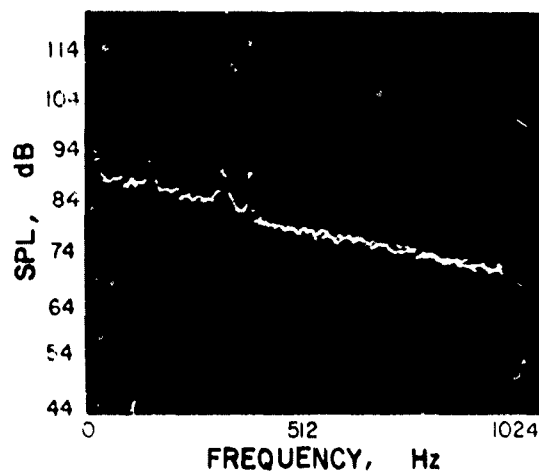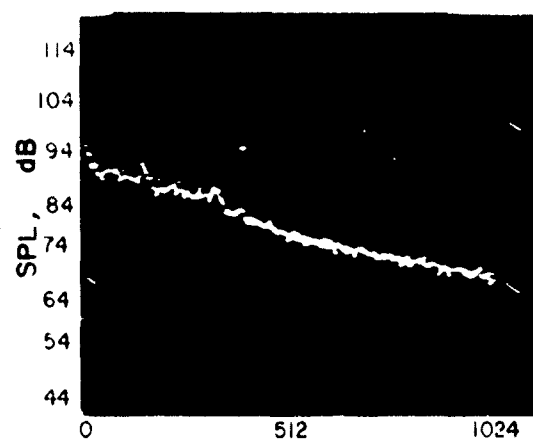
b. Forward Velocity of 91 ft/sec (27.74 m/sec).

Figure 39. Continued.
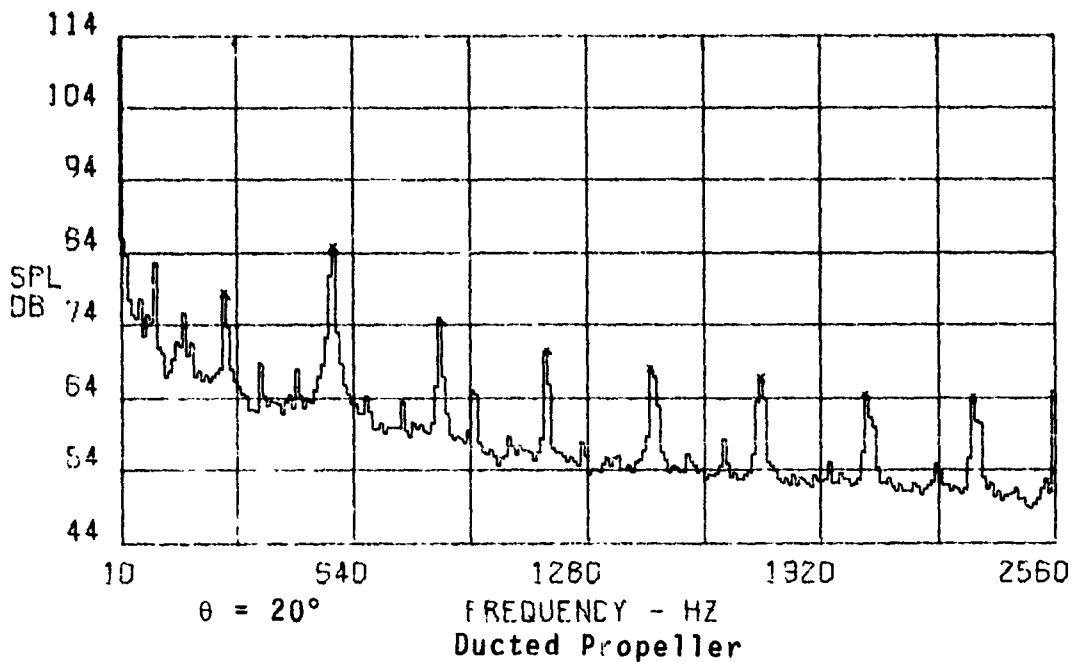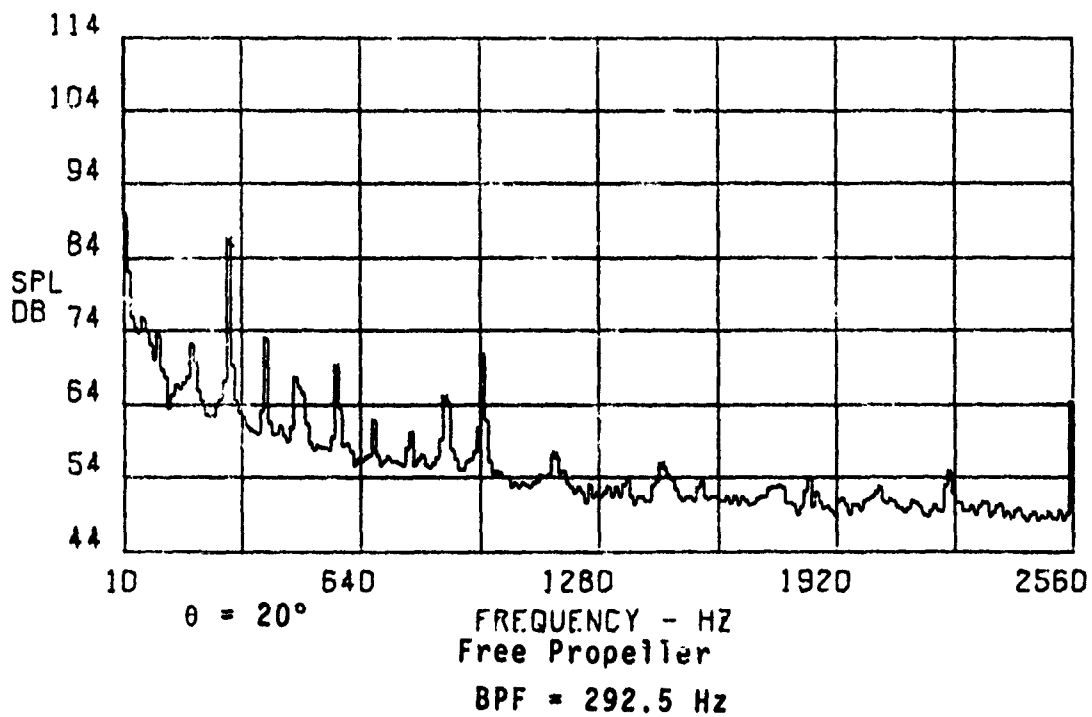
a. Forward Velocity of 50 ft/sec (15.24 m/sec).

Figure 40. Narrow-band Spectra of a Three-Bladed BD3 Propeller.

116

θ = 90°   FREQUENCY - HZ
Free Propeller

BPF = 292.5 Hz

θ = 90°   FREQUENCY - HZ
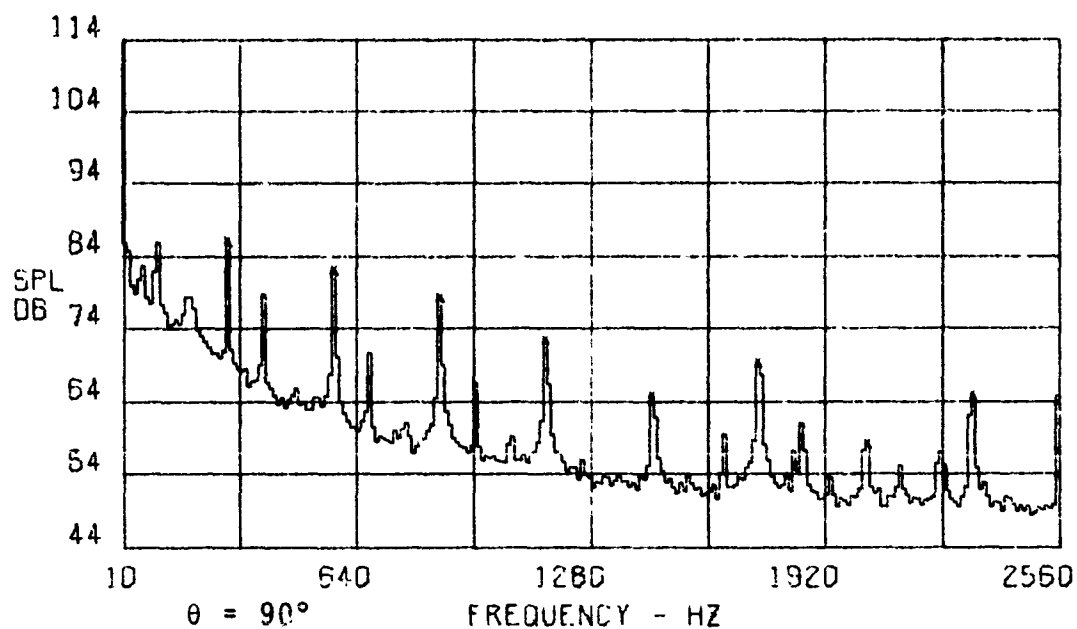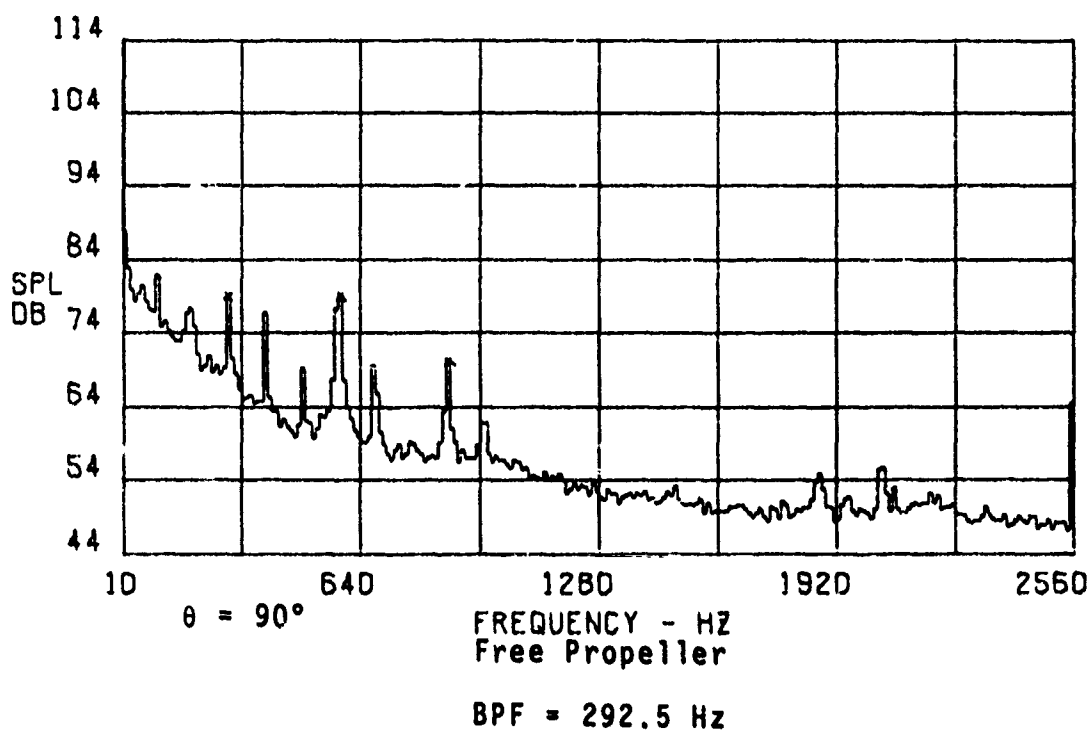
b. Forward Velocity of 50 ft/sec (15.24 m/sec).

Figure 40.   Continued.

117

The configurations tested with a duct with interior foam lining showed the same general acoustic characteristics as the one with hard skin duct. A rational explanation could not be given for the increased noise levels associated with the ducted configurations. Figures 41a and 41b give the narrow-band spectra of a four-bladed ducted propeller (with foam-lined duct) in the tractor and pusher modes at a forward velocity of 91 ft/sec (27.74 m/sec). The spectra for $\theta = 20°$ show that the harmonic SPLs at the first two or three harmonics of blade passage frequency of the pusher configurations were significantly higher (6 to 12 dB) than those of the tractor configurations, while the SPLs at higher harmonics of blade passage frequency showed only a marginal difference between the tractor and pusher modes. The spectra for $\theta = 90°$ (in the plane of the propeller) did not show any significant difference between the tractor and pusher modes except for a moderate (4 to 6 dB) increase in the pusher mode at the first harmonic of blade passage frequency. Again, a rational explanation could not be given for this behavior. However, the ducted and pusher configurations generally were noisier than their free and tractor counterparts respectively. Also, the addition of an upstream wing did not seem to increase the noise levels of pusher configurations to any significant degree.

Acoustic Trends in Forward Flight

The acoustic trends will be obtained at two forward velocities: 15 ft/sec (4.6 m/sec), which is representative of low speed forward flight, and 70 ft/sec (21.34 m/sec), which is representative of moderate speed forward flight. The data at 70 ft/sec (21.34 m/sec) was specifically chosen over that at 91 ft/sec (27.74 m/sec) since the former is less contaminated by the tunnel background noise. It is believed that the trends obtained at 70 ft/sec (21.34 m/sec) will be representative of those at higher velocities such as 127 ft/sec (38.6 m/sec), which was the design flight speed of most of the propeller configurations. The acoustic data at both $\theta = 20°$ and $\theta = 90°$ will be examined. All the acoustic trends will be based on the narrow-band acoustic data of only the tractor propeller configurations.

Effect of Blade Design

The total effect of such parameters as blade activity factor, taper ratio, and twist has been identified as the effect of blade design. It is believed, however, that the blade activity factor plays a more significant role among the parameters

TRACTOR
$\theta = 20°$ B·W=IO Hz
BPF = 390 Hz
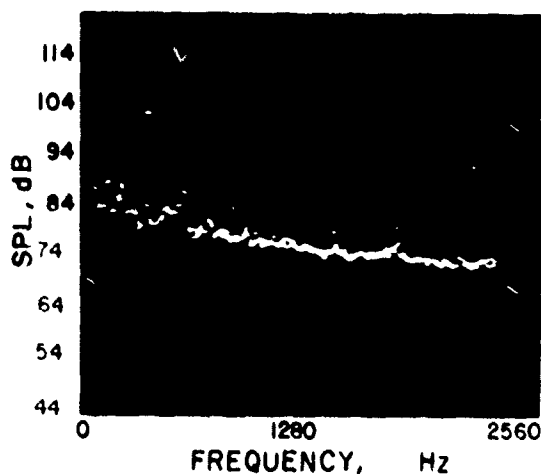
WIHTOUT UPSTREAM WING

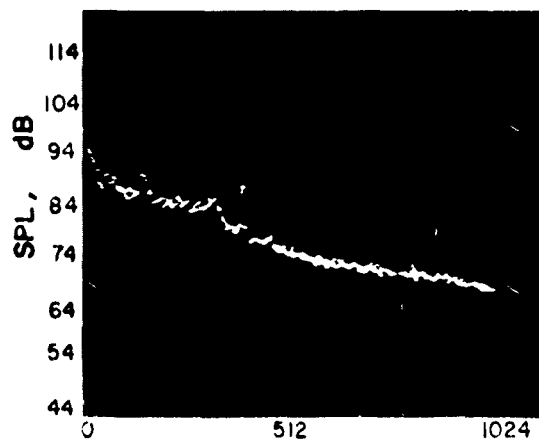WITH UPSTREAM WING

$\theta = 20°$
PUSHERS

a.   Forward Velocity of 91 ft/sec (27.74 m/sec).

Figure 41.   Narrow-band Spectra of a Four-Bladed BD1 Ducted Propeller.
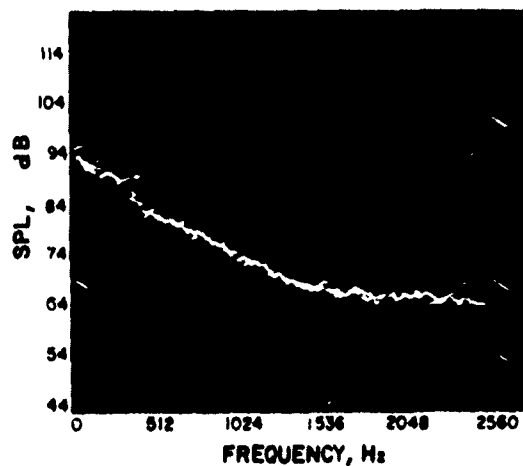
TRACTOR
$\theta = 90°$ B·W=10 Hz
BPF = 390 Hz
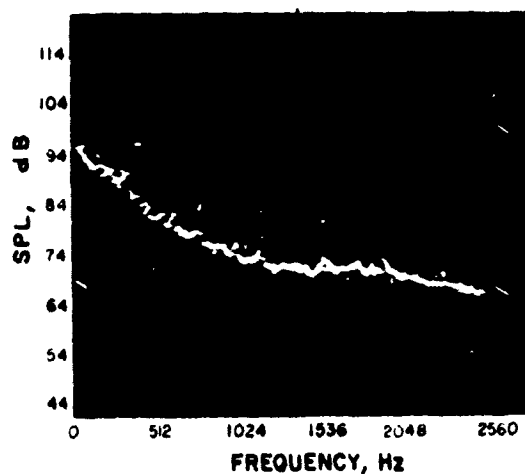
WITHOUT UPSTREAM WING   WITH UPSTREAM WING
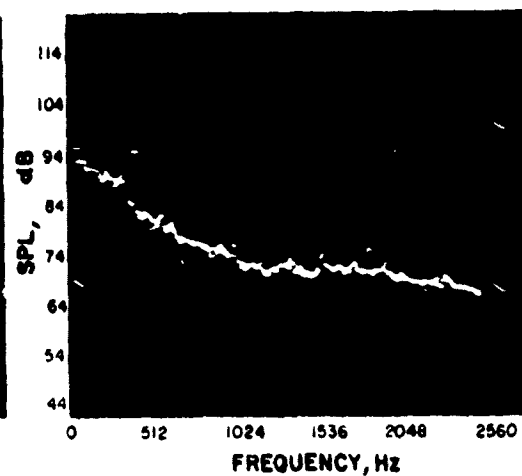
$\theta = 90°$
PUSHERS

b.   Forward Velocity of 91 ft/sec (27.74 m/sec).

Figure 41.   Continued.

120

mentioned above. Among the propeller configurations tested, there were basically four blade designs; two of those (BD1 and BD3 propellers) correspond to the small diameter propellers while the remaining two (BD2 and BD4 propellers) correspond to the large diameter propellers. The characteristics of these blade designs were listed in Table 4. To determine the acoustic trends, it is necessary to vary a given parameter while the other parameters are kept constant. In this case, the comparisons will be made between BD1 and BD3 propellers and BD2 and BD4 propellers. Propellers with BD3 and BD4 acoustic blade designs have wider blade chords (larger activity factors) and lower blade twists than those with BD1 and BD2 performance blade designs, respectively. The comparisons will be made for a three-bladed configuration at the design values of thrust and tip speed. Figures 42 and 43 show the effect of blade design on a three-bladed propeller in terms of SPLs at various harmonic numbers of blade passage frequency. The dashed lines in these figures indicate that the harmonic SPLs in question might have been affected by the tunnel background noise. As shown in Figure 42, the blade design did not have a strong effect on the SPLs. However, at both of the forward velocities considered, the propeller with BD3 blade design (wider chord blades) had slightly higher SPLs (about 2 to 3 dB) than that with BD1 blade design. This is generally true for noise propagated in the forward direction ($\theta \approx 20°$) as well as the noise propagated in the plane of the propeller ($\theta = 90°$). Essentially similar trends were also observed in the case of the large diameter propellers. As shown in Figure 43, the propeller with BD4 blade design (wider blade chords) had slightly higher SPLs. This trend was also observed with propellers with a different number of blades (2 or 4). In general, such blade parameters as activity factor, twist, and taper ratio did not have a major effect on the noise output of RPV propellers in forward flight. However, unlike the trends observed for large-scale propellers, propellers with wider chord blades and lower twists had slightly higher SPLs, at least at the lower harmonics of blade passage frequency.

Effect of Propeller Diameter

The effect of propeller diameter was obtained by comparing the acoustic data of propellers with blade designs BD3 and BD4. As was shown in Table 4, the only difference between the two designs is the blade radius which increases from 10 in (.254 m) for the BD3 blades to 13 in (.33 m) for the BD4 blades. Figure 44 shows the harmonic SPLs of a three-bladed propeller with blade designs BD3 and BD4 tested at the design values of tip speed and thrust. It can be seen from Figure 44 that at the forward velocity of 15 ft/sec (4.6 m/sec), the larger
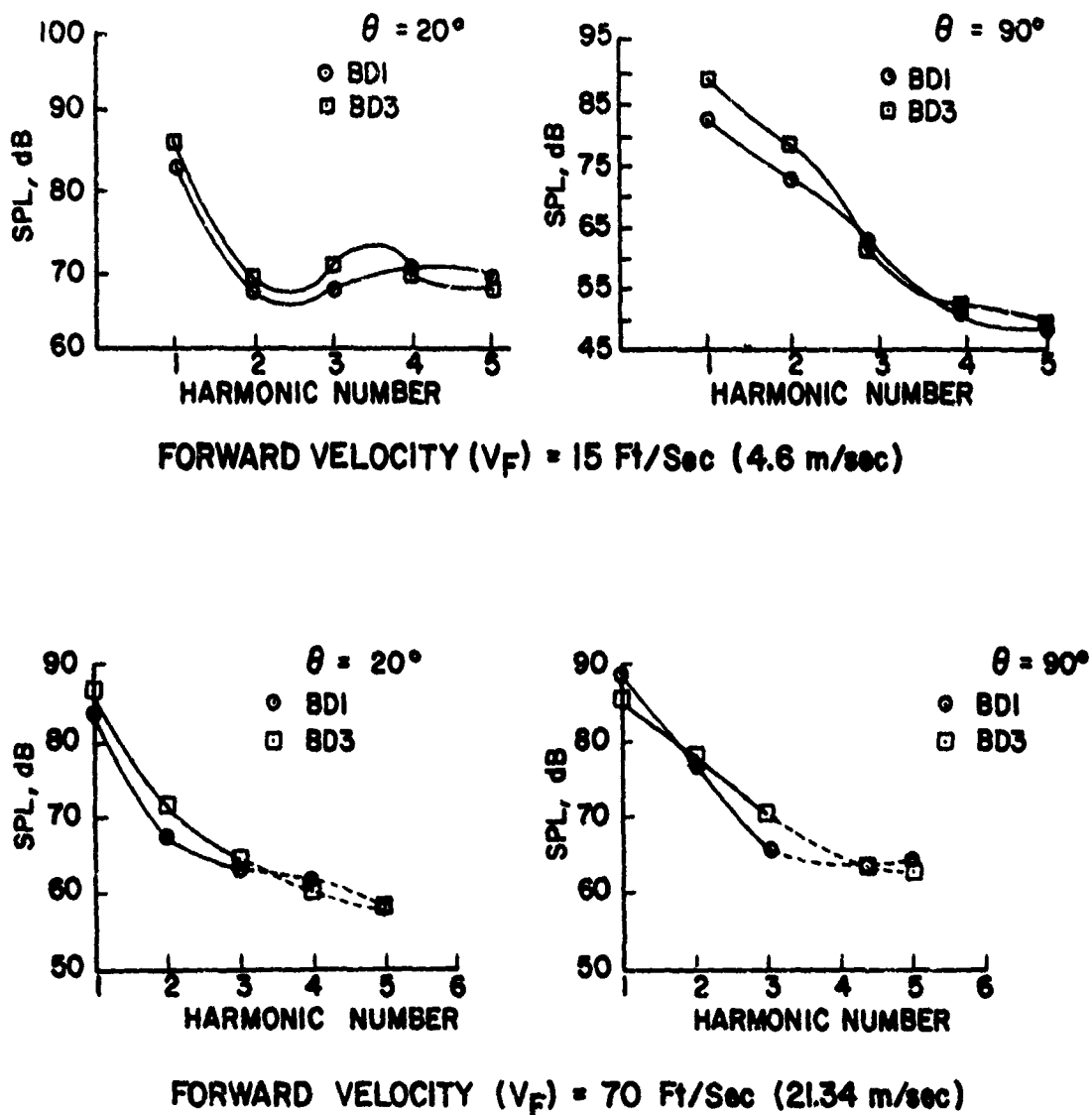
Figure 42. Effect of Blade Design on a Small Diameter
Three-Bladed Propeller.
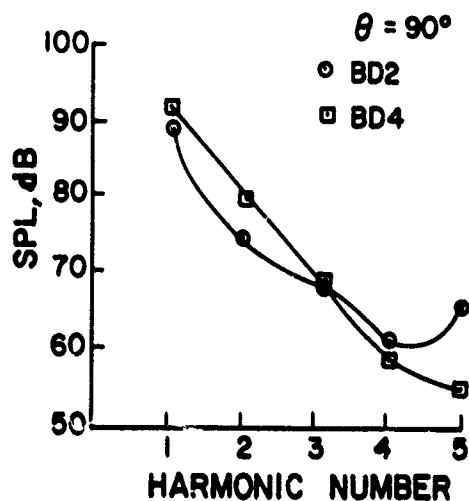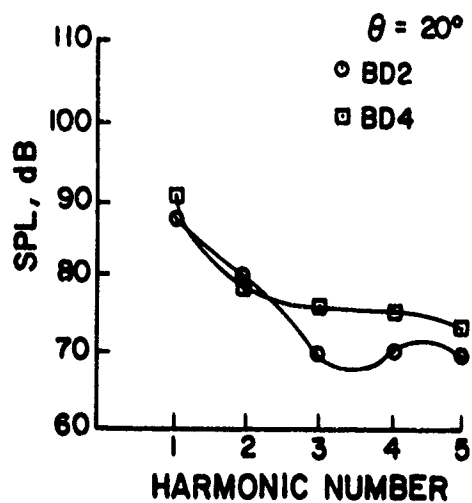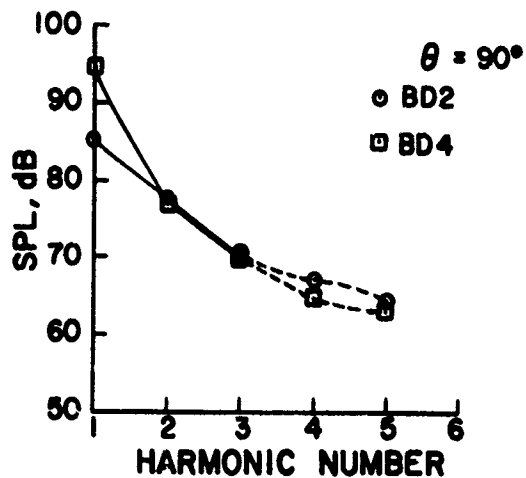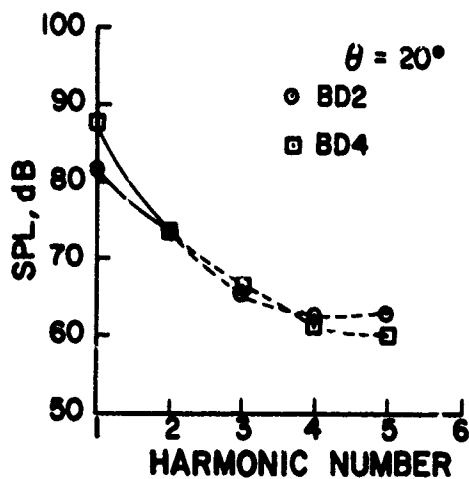
Figure 43. Effect of Blade Design on a Large Diameter
Three-Bladed Propeller.
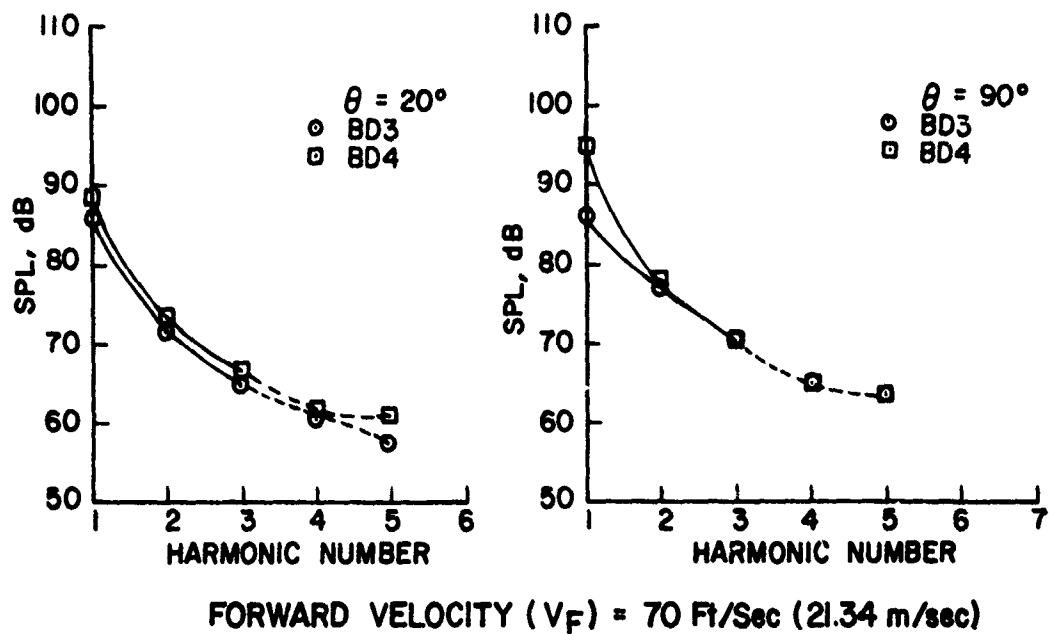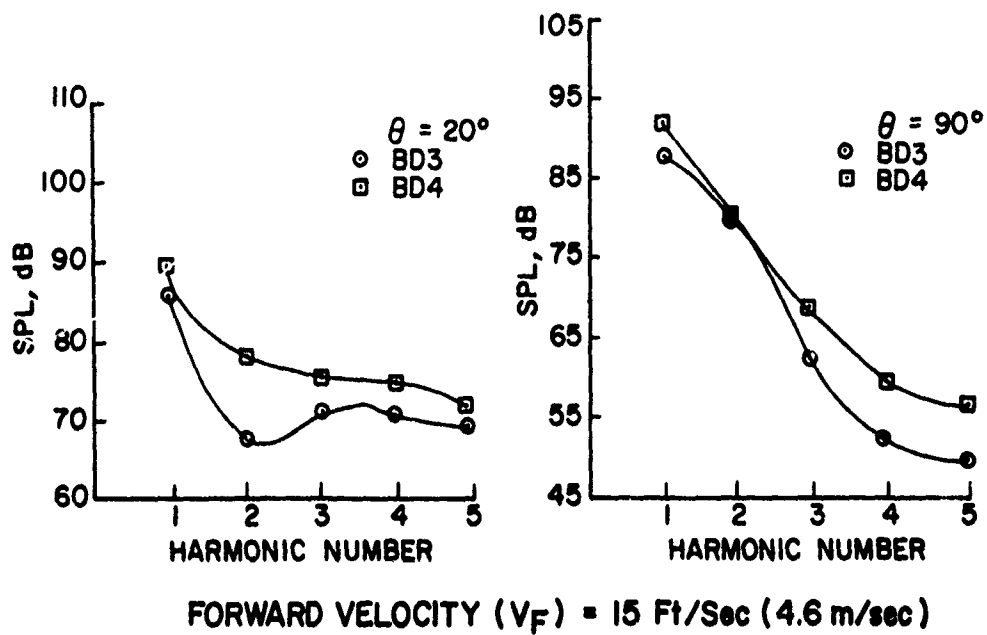
Figure 44.   Effect of Propeller Diameter on a Three-Bladed
             Propeller.

124

diameter propeller (BD4) had higher SPLs for both of the azi-
muthal locations ($\theta = 20°$ and $\theta = 90°$) considered. At the
higher forward velocity of 70 ft/sec (21.34 m/sec), the pro-
peller diameter did not have a strong effect on the harmonic
SPLs. However, the larger diameter propeller had slightly
higher SPLs (see Fig. 44). Similar trends were also observed
with propellers with different blade numbers (2 or 4). In
addition, the acoustic data obtained at a lower tip speed of
340 ft/sec (103.6 m/sec) showed that the larger diameter pro-
pellers had much higher SPLs (5 to 10 dB) for the noise propa-
gated in the forward direction ($\theta = 20°$). The trend observed
for these small-scale RPV propellers is quite different from
that of the large-scale propellers where the larger diameter
propellers were found to have lower SPLs. The propellers with
different diameters considered here had different values of
blade passage frequency, since these were tested at the same
tip speed. This may have a strong bearing on the detection
distances which depend on the SPLs as well as the frequencies
at which they occur. In general, for a given tip speed, an
increase in the diameter was not beneficial as far as small-
scale RPV propeller noise characteristics were concerned.

Effect of Blade Number

The effect of blade number on the harmonic SPLs was obtained
for the sr ll diameter BD3 propellers and the large diameter
BD4 prope.. rs. Again the comparisons were based on the acous-
tic data obtained at the design values of tip speed and thrust.
Figure 45 shows the effect of blade number on the harmonic
SPLs of a BD3 propeller. As shown in Figure 45, an increase
in the blade number generally resulted in a decrease in the
harmonic SPLs at both of the forward velocities considered.
The effect of blade number was stronger for the noise in the
plane of the propeller ($\theta = 90°$) than in the forward direction
($\theta = 20°$). In fact, for $\theta = 90°$, the three-bladed propeller
had significantly lower harmonic SPLs (by about 5 to 14 dB)
than the two-bladed propeller. The differences in SPLs be-
tween a three- and four-bladed propeller were not that signif-
icant. At the forward velocity of 15 ft/sec (4.6 m/sec), the
four-bladed propeller had the highest SPLs for $\theta = 20°$ at
higher harmonics of blade passage frequencies. Similar trends
were also observed for the large diameter BD4 propellers (see
Fig. 46). Generally, for a given tip speed and thrust an in-
crease in the blade number had a beneficial effect on the
harmonic levels of the small-scale RPV propellers, at least for
higher forward flight velocities. This was also confirmed by
the acoustic data of propellers with BD1 and BD2 blade designs
as well as the data obtained at other tip speeds. Again, it
should be noted that for a given rotational speed, different
blade numbers result in different values of blade passage
frequency.
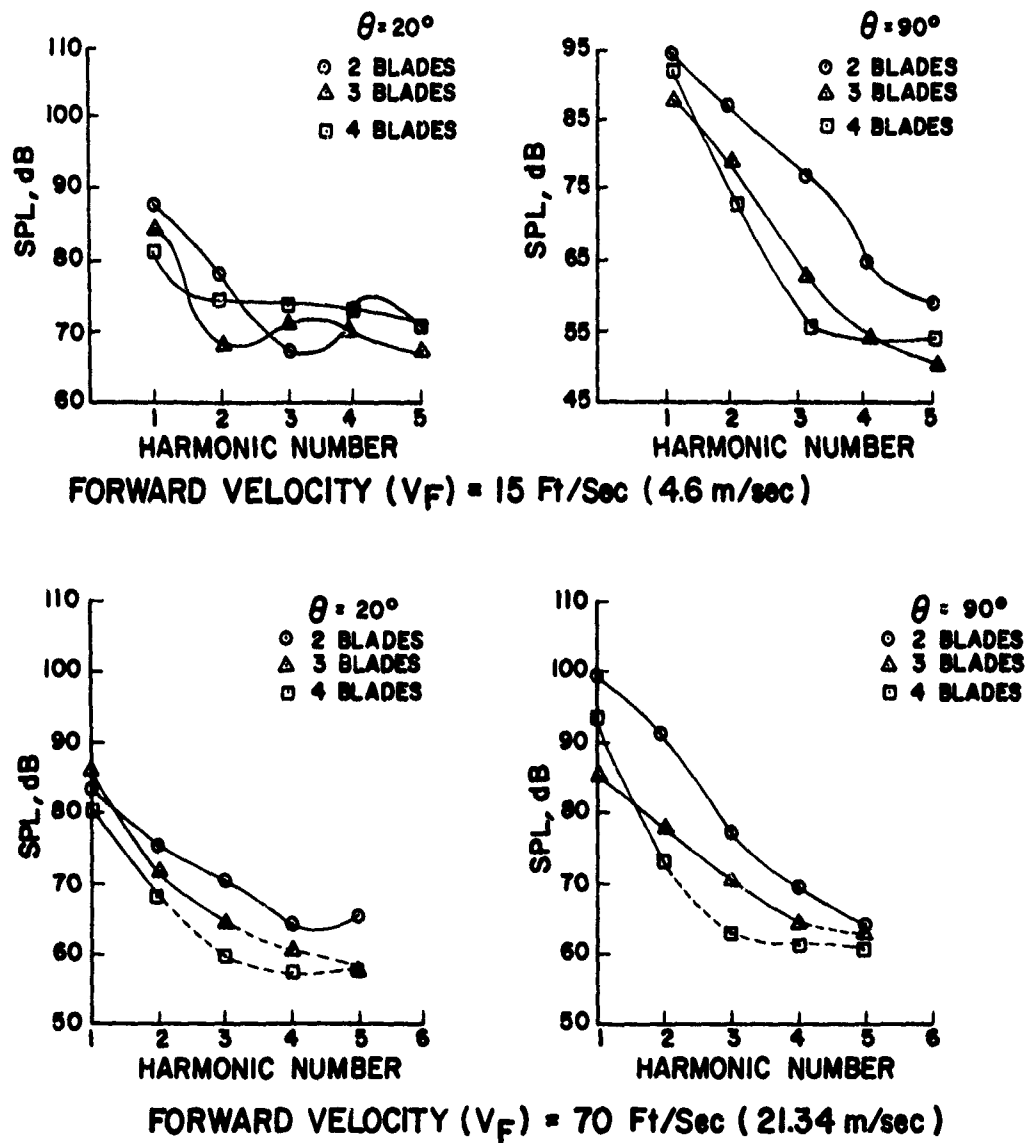
Figure 45.   Effect of Blade Number on the Small Diameter
(BD3) Propeller.
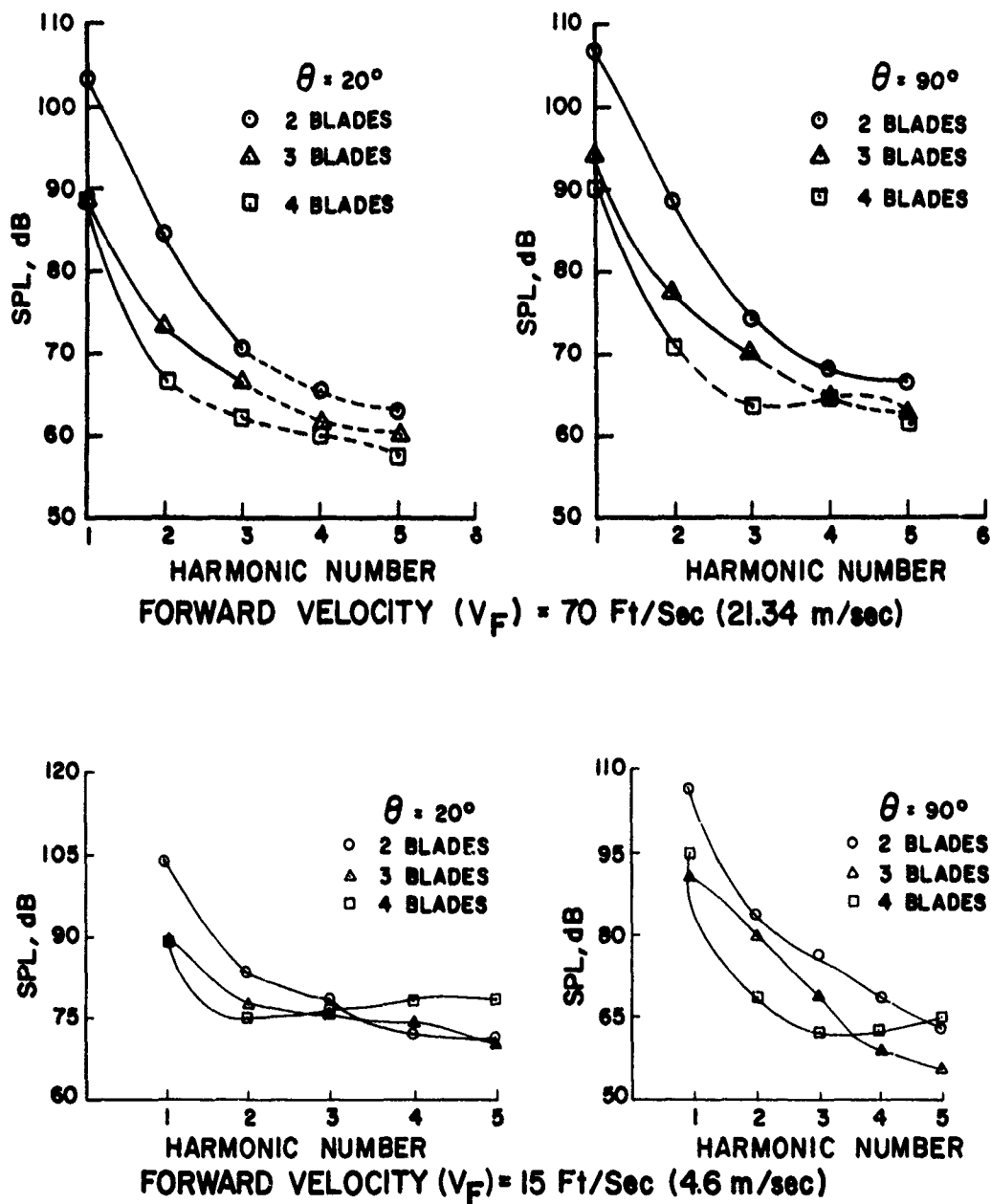
Figure 46.   Effect of Blade Number on the Large Diameter
             (BD4) Propeller.

127

Effect of Tip Speed

Only BD3 propellers were tested at three different tip speeds: the design tip speed of 510 ft/sec (155.5 m/sec), a lower tip speed of 340 ft/sec (103.6 m/sec), and a higher tip speed of 576 ft/sec (175.6 m/sec). The propellers at lower tip speed were not tested beyond a forward velocity of 50 ft/sec (15.24 m/sec). The comparisons were again based on the acoustic data obtained at the design value of thrust. Figure 47 shows the effect of tip speed on the harmonic SPLs of a three-bladed BD3 propeller at a forward velocity of 15 ft/sec (4.6 m/sec). As expected, the tip speed had a significant effect on the SPLs at various harmonics of blade passage frequency. As shown in Figure 47, for $\theta = 20°$, an increase in the tip speed of about 13% from the design value resulted in a large increase in SPLs (about 3 to 16 dB) depending upon the harmonic number, while a decrease of 33% in the tip speed resulted in a much larger decrease in SPLs at various harmonic numbers. The effects were not as high for $\theta = 90°$. In fact, the differences in SPLs between the design and lower tip speeds were very small except for that at the second harmonic number. However, even for $\theta = 90°$, an increase in the tip speed resulted in significant increases in harmonic SPLs. Similar trends were also observed for a two-bladed propeller. These trends showed that between the lower tip speed of 340 ft/sec (103.6 m/sec) and the higher tip speed of 576 ft/sec (175.6 m/sec), the SPLs increased anywhere between 5 to 25 dB depending upon the harmonic number. Figure 48 shows the effect of tip speed at higher forward velocities. At a forward velocity of 50 ft/sec (15.24 m/sec), a reduction in tip speed resulted in a significant decrease in SPLs (see Fig. 48), at least at lower harmonic numbers. The data at the lower tip speed for higher harmonic numbers was masked by the tunnel background noise, and therefore clear trends could not be established for these harmonic numbers. Similarly, at a forward velocity of 70 ft/sec (21.34 m/sec) an increase in the tip speed resulted in a significant increase in SPLs (see Fig. 48) at lower harmonic numbers, while the data for the higner harmonic numbers was masked by the tunnel background noise; therefore a clear trend could not be established. It is believed, however, that for these higher harmonic numbers, the trends will be similar to those obtained at the lower harmonic numbers, but the changes will be much smaller. Generally the tip speed had a very strong effect on the acoustic characteristics of small-scale RPV propellers in forward flight, at least in the range of tip speeds considered.
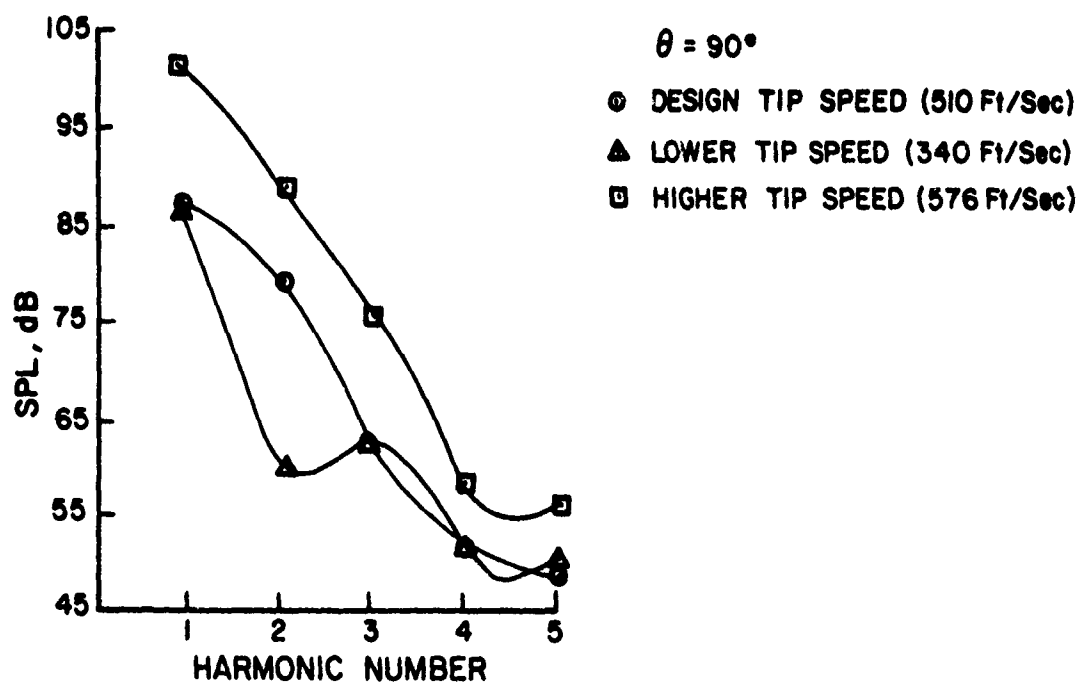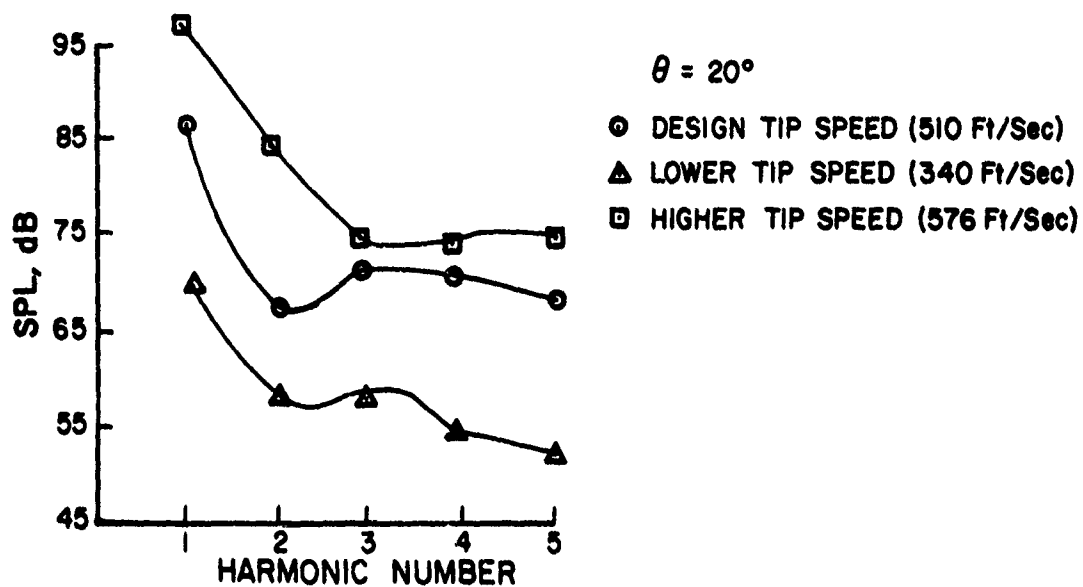
Figure 47. Effect of Tip Speed on a Three-Bladed BD3 Propeller at a Forward Velocity of 15 ft/sec (4.6 m/sec).
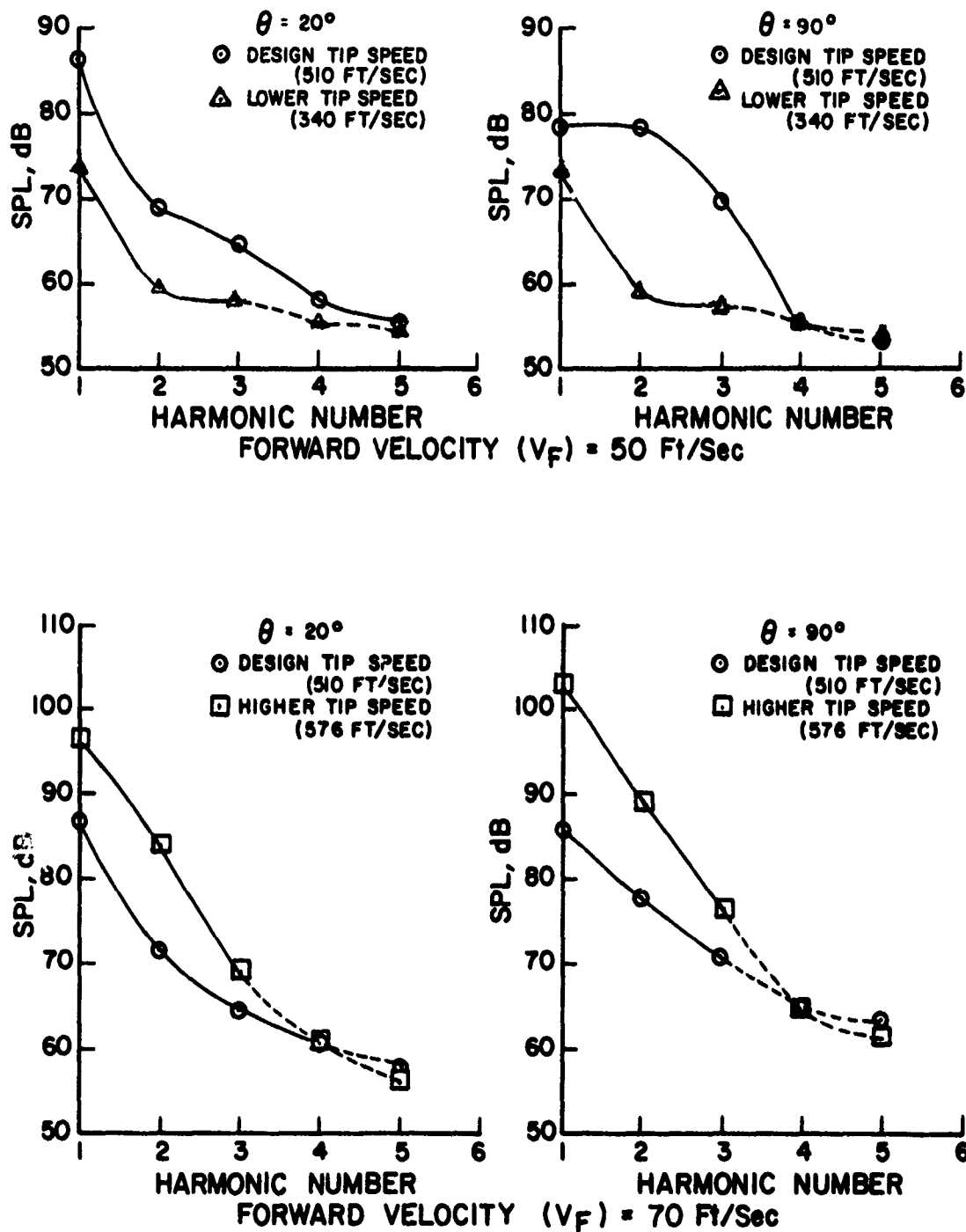
Figure 48. Effect of Tip Speed on a Three-Bladed BD3 Propeller.

Effect of Thrust

Figure 49 shows the effect of increasing thrust on the harmonic levels of a three-bladed BD3 propeller in forward flight tested at the design value of tip speed. At a forward velocity of 15 ft/sec (4.6 m/sec), for $\theta = 20°$ as well as $\theta = 90°$, an increase in thrust resulted in a moderate increase in harmonic SPLs. In fact, increasing the thrust from 18 lbs (80 newtons) to 40 lbs (178 newtons) resulted in an increase of about 3 to 6 dB (see Fig. 49) in the harmonic SPLs. However, the effect of thrust on the harmonic SPLs for $\theta = 20°$ was negligible at a forward velocity of 70 ft/sec (21.34 m/sec). Nevertheless, an examination of the acoustic data for $\theta = 10°$ at this velocity showed that there was an increase of about 5 dB in the harmonic SPLs as the thrust was increased from 18 lbs (80 newtons) to 29 lbs (129 newtons) while there was a marginal decrease (of the order of 1 to 2 dB) when the thrust was increased from 29 lbs (129 newtons) to 36 lbs (160 newtons). A rational explanation cannot be given for this peculiar trend. For $\theta = 90°$, at 70 ft/sec (see Fig. 49) a 100% increase in the thrust value resulted in a 5 dB increase in the SPLs for the first two harmonic numbers. The effect of thrust on a four-bladed BD3 propeller was much smaller. In the case of a four-bladed propeller, doubling of the thrust value resulted in only a marginal increase (of the order of 1 or 2 dB) in the SPLs at all of the forward velocities except 91 ft/sec (27.74 m/sec). Thus, the effect of thrust on the harmonic SPLs seemed to vary with blade number and forward velocity. Generally, the effect of thrust was more significant on the SPLs at the first two or three harmonic numbers. This was expected since, according to the classical propeller theory, the steady thrust load contributes primarily to the SPLs at the lower harmonic numbers.

In the range of thrust values considered, for a given tip speed an increase in the thrust value resulted in an increase of the harmonic SPLs, though the amount of increase seems to depend on parameters such as blade number and forward velocity.

Summary

As far as the acoustic characteristics of RPV propellers in forward flight are concerned, the tip speed is a very potent parameter. Parameters such as blade radius, activity factor, and blade number have a relatively weaker effect on the noise output. The acoustic trends observed in small-scale RPV propellers are not necessarily the same as those observed in large-scale propellers.

131
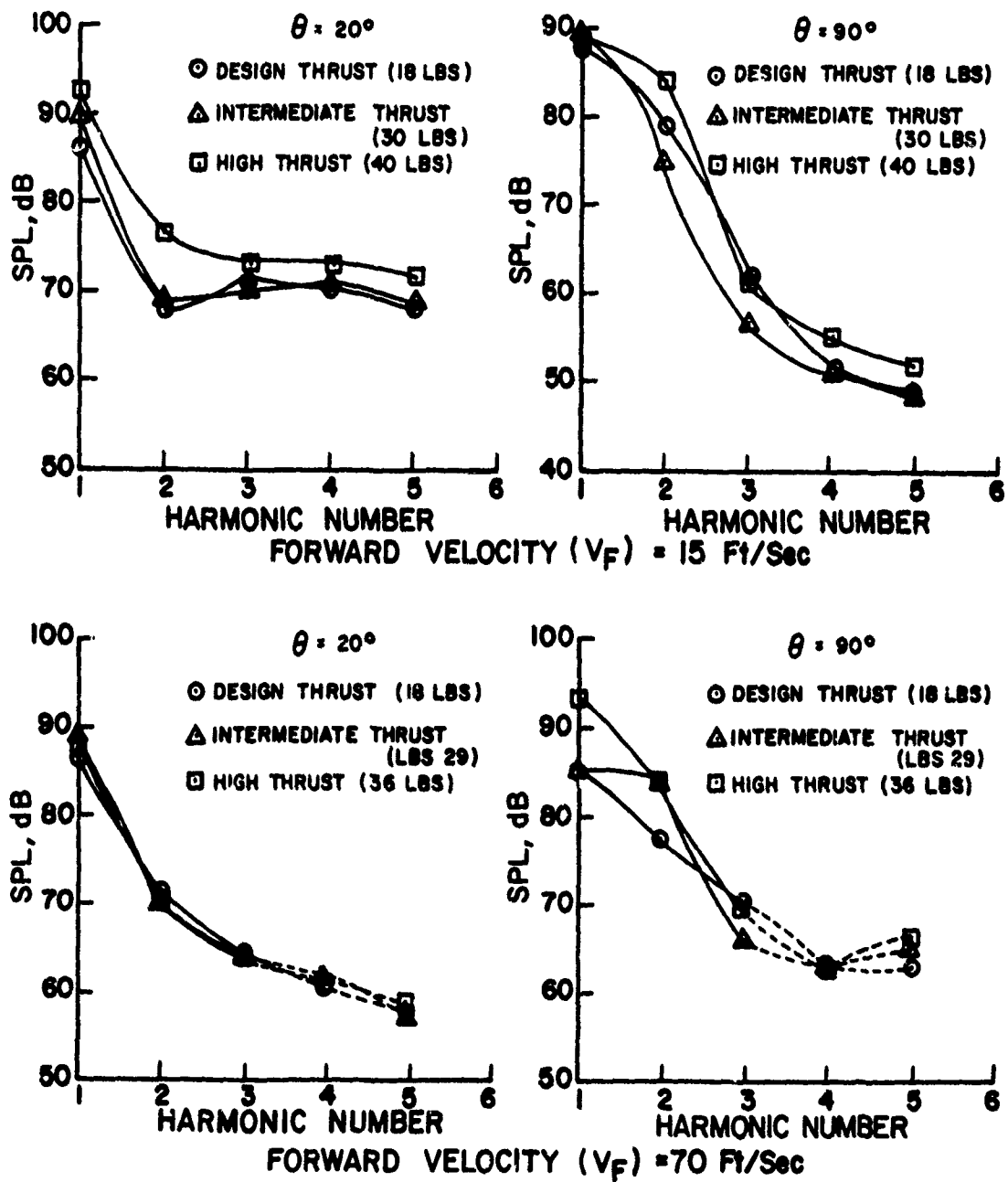
Figure 49. Effect of Thrust on a Three-Bladed BD3 Propeller.

132

DETECTABILITY CHARACTERISTICS

Using the procedures described in an earlier section, the
detection distances (slant range and altitude of no detec-
tion) of each propeller configuration were computed for a
temperature of 59°F (15°C) and a relative humidity of 60%.
Slant ranges were computed for a flight altitude of 1000 ft
(305 m). The low ambient noise spectrum (see Fig. 4) was
used in the computations of the detection distances. The
moderate and high ambient noise spectra (see Fig. 4) were
not used since preliminary calculations have shown that for
the given set of flight conditions, some of the low noise
propeller configurations flying at an altitude of 1000 ft
(305 m) will not be detected on the ground when these ambi-
ent noise spectra are used. However, the similarity of the
different ambient noise spectra of Figure 4 suggests that
the detectability trends obtained with the low ambient noise
spectrum will also be valid for the moderate as well as the
high ambient noise spectra.

The detection distance of a given propeller is strongly
dependent on the difference in dB (ΔdB) between the measured
SPL of the acoustic signal of the propeller at a given fre-
quency; the higher the difference (ΔdB), the larger the de-
tection distance. The frequency of the acoustic signal also
plays a major role in the determination of detection distance;
the higher the frequency, the greater the atmospheric attenu-
ation due to classical and molecular absorption of the signal.
For a given propeller acoustic signal level, the lower the
frequency at which it occurs, the smaller will be the differ-
ence (ΔdB) between this signal level and the ambient SPL,
since the ambient spectra (see Fig. 4) have higher SPLs at
lower frequencies. For the same propeller acoustic signal
level, it can be seen from Figure 4 that the difference be-
tween the propeller and ambient SPLs (ΔdB) will be much
larger at higher frequencies (> 1000 Hz). However, the
large atmospheric attenuation (classical and molecular
absorption) associated with high frequency signals will
result in low detection distances. This suggests that for
propellers, the detection might occur in the mid-frequency
range (200 < f < 1000 Hz). In fact, the computations have
shown that most of the propellers would be detected at either
the first, second, or third harmonic of their blade passage
frequency which usually fall in the mid-frequency range.

The acoustic spectra of most of the propeller configurations
tested were characterized by high rotational noise peaks at
the lower harmonics of their blade passage frequency and a
relative lack of strong broad-band noise levels at higher

133

frequencies. This explains why most propeller configurations would be detected at the lower harmonics (first, second, or third) of their blade passage frequency. It is to be noted that small changes (of the order of 3 to 5 dB) in the lower harmonic SPLs of propellers can cause relatively larger changes in the detection distance since in the absence of classical and molecular absorption in the atmosphere, an increase of 6 dB in the acoustic signal will result in doubling of the detection distance. However, the atmospheric absorption usually tempers these large changes in these detection distances, and in most cases an increase of 6 dB in the acoustic signal will result in only a moderate increase in the detection distance (anywhere from 20 to 60% depending on the frequency). (The detectability trend data that will be discussed in the following pages will closely parallel the acoustic trend data of the lower harmonic SPLs of the propellers).

Detection distances were obtained for almost all of the propeller configurations tested in the latter series of tunnel tests (see Table 10) as well as for a few of the tractor, pusher, and ducted configurations tested in the earlier series of tunnel tests (see Tables 8 and 9). It can be seen from Table 10 that in the latter series of tunnel tests, a few propeller configurations were not tested at 91 ft/sec (27.74 m/sec); therefore, in the development of detectability trend data, in some instances it became necessary to combine the data from the two series of wind tunnel tests. This resulted in seemingly inconsistent trends in some cases, as will be shown later.

Effect of Forward Velocity

Detection distances for each tractor propeller configuration tested at the design values of thrust and tip speed were obtained for four different forward velocities ranging from a very low value of 15 ft/sec (4.6 m/sec) to a moderate value of 91 ft/sec (27.74 m/sec). Tables 11 and 12 give the slant ranges and the altitudes of no detection, respectively, for all of the tractor propeller configurations tested at the design conditions and various forward velocities. Propulsive efficiency of each propeller configuration was also given in these tables to provide a quick comparison of the performance and detectability trend data.

The acoustic data of the propeller configurations tested at the design conditions showed large changes in the higher harmonic SPLs with forward velocity. However, it is the variation of lower harmonic SPLs with forward velocity that

134

TABLE 11

SLANT RANGES (SR) AND PROPULSIVE EFFICIENCIES (η) OF THE TRACTOR PROPELLERS TESTED AT THE DESIGN TIP SPEED AND THRUST

V_F / PROP. CONFIG.	≈15 Ft/Sec		50 Ft/Sec		70 Ft/Sec		91 Ft/Sec	
	η	SR, Ft(m)	η	SR, Ft(m)	η	SR, Ft(m)	η	SR, Ft(m)
2BLD,BD1	.227	6400 (1951)	.435	6600 (2012)	.697	6525 (1989)	.752*	8090* (2466)
3BLD,BD1	.221	5275 (1608)	.589	5500 (1676)	.697	5670 (1390)	.821	5430 (1655)
4BLD,BD1	.214	3975 (1212)	.562*	6400* (1951)	.603	3944 (1202)	.787*	6740* (2054)
2BLD,BD2	.328	5725 (1745)	.697	6975 (2126)	.801	6145 (1873)	.827*	6530* (1990)
3BLD,BD2	.245	4100 (1250)	.629	5740 (1750)	.645	6750 (2080)	.759	7350 (2240)
4BLD,BD2	----	----	.548	6305 (1922)	.695	8255 (2516)	.814	6620 (2018)
2BLD,BD3	.258	7600 (2316)	.520	5030 (1533)	.601	7930 (2417)	.735*	9600* (2926)
3BLD,BD3	.236	6315 (1925)	.564	5545 (1690)	.697	5820 (1774)	.773	4800 (1463)
4BLD,BD3	.199	5480 (1670)	.515	6690 (2039)	.595	7365 (2245)	.649	5245 (1599)
2BLD,BD4	.268	7900 (2408)	.602	7645 (2330)	.692	7505 (2288)	.804	7670 (2338)
3BLD,BD4	.183	6115 (1864)	.559	6470 (1972)	.644	7180 (2188)	.708	7350 (2240)
4BLD,BD4	.196	7055 (2150)	.466	8505 (2592)	.593	8255 (2516)	.616*	9935* (3028)

* DATA POINT -- EARLIER SERIES OF WIND TUNNEL TESTS

DETECTION DISTANCES BASED ON LOW AMBIENT NOISE (FIG. 4)

TABLE 12
ALTITUDES OF NO DETECTION (AND) AND PROPULSIVE
EFFICIENCIES (η) OF THE TRACTOR PROPELLERS
TESTED AT THE DESIGN TIP SPEED AND THRUST

V_F / PROP. CONFIG.	≈ 15 Ft/Sec		50 Ft/Sec		70 Ft/Sec		91 Ft/Sec	
	η	AND, Ft(m)	η	AND, Ft(m)	η	AND, Ft(m)	η	AND, Ft(m)
2BLD,BD1	.227	5885 (1794)	.435	9730 (2966)	.697	8920 (2719)	.752*	14615* (4455)
3BLD,BD1	.221	3500 (1067)	.589	3970 (1210)	.697	5125 (1562)	.821	3500 (1067)
4BLD,BD1	.214	7050 (2149)	.562*	9130* (2783)	.603	9460 (2883)	.787*	13890* (4234)
2BLD,BD2	.328	7330 (2234)	.697	8075 (2461)	.801	6985 (2129)	.827*	11720* (3572)
3BLD,BD2	.245	3270 (997)	.629	2310 (704)	.645	2830 (863)	.759	5830 (1777)
4BLD,BD2	----	----	.548	6145 (1873)	.695	2590 (789)	.814	----
2BLD,BD3	.258	7050 (2149)	.520	9730 (2966)	.601	9730 (2966)	.735*	14615* (4455)
3BLD,BD3	.236	5620 (1713)	.564	5025 (1532)	.697	3970 (1210)	.773	5415 (1650)
4BLD,BD3	.199	10130 (3088)	.515	10830 (3301)	.595	10830 (3301)	.649	10130 (3088)
2BLD,BD4	.268	13975 (4260)	.602	12810 (3904)	.692	12810 (3904)	.804	13975 (4260)
3BLD,BD4	.183	5050 (1539)	.559	4190 (1277)	.644	6385 (1946)	.708	7120 (2170)
4BLD,BD4	.196	10115 (3083)	.466	8635 (2632)	.593	7955 (2425)	.616*	15535 (4735)

* DATA POINT -- EARLIER SERIES OF WIND TUNNEL TESTS

DETECTION DISTANCES BASED ON LOW AMBIENT NOISE (FIG. 4)

determine the effect of forward velocity on the detection distances. A close examination of the detection distances in Tables 11 and 12 shows that in most cases the forward velocity has a significant effect on slant ranges as well as altitudes of no detection. It can also be seen that the variation of either the slant range or the altitude of no detection with forward velocity seems to depend on the type of propeller and its parameters such as blade number, blade radius, etc.

An examination of the slant ranges of various propeller configurations (see Table 11) shows that there are essentially two sets of propellers: one in which the slant range at the highest forward velocity of 91 ft/sec (27.74 m/sec) is approximately the same as that at the lowest forward velocity (near static condition) of 15 ft/sec (4.6 m/sec); the other in which the slant ranges at the two extremities of the forward velocities are quite different. In the first group fall such propeller configurations as three-bladed BD1, four-bladed BD3, and two-bladed BD4 (see Table 11). Among these configurations, in some cases such as the four-bladed BD3 propeller the slant ranges at the intermediate forward velocities [50 ft/sec (15.24 m/sec) and 70 ft/sec (21.34 m/sec)] are quite different from those at the extreme values of forward velocity, while in the case of the two-bladed BD4 propeller the slant ranges remain almost uniform over the range of forward velocities considered.

An examination of the acoustic data showed that for the propeller configurations discussed above the lower harmonic SPLs in the forward direction ($\theta = 10°$, 15° or 20°) varied with forward velocity in the same manner as that of slant ranges. For a propeller such as the two-bladed BD1, the slant range remains more or less uniform (see Table 11) up to a forward velocity of 70 ft/sec (21.34 m/sec) followed by a sharp increase at 91 ft/sec (27.74 m/sec). However, in this particular instance the slant range at 91 ft/sec (27.74 m/sec) was computed using the acoustic data from the earlier series of tunnel tests. This raises some questions regarding the use of the acoustic data from the earlier series of tunnel tests in combination with that from the latter series of tunnel tests. In fact, in the case of a four-bladed BD1 propeller (see Table 11) the use of the two sets of data resulted in a much stronger variation in the slant range with forward velocity. Both series of tunnel tests were conducted in exactly the same manner and there is apparently no reason why they shouldn't provide a compatible set of acoustic data. This can only be resolved with further testing. In the absence of any further additional tunnel tests, the slant range trend

137

data of the propellers where both sets of acoustic data was used may not be very accurate and therefore, must be viewed with caution.

Table 11 also shows that for propeller configurations such as three-bladed BD4, three-bladed BD2, and four-bladed BD4, slant range monotonically increases with the forward velocity. An examination of the acoustic data of these propellers in the forward direction (θ = 10°, 15° or 20°) shows that the lower harmonic SPLs of these configurations also increase monotonically with forward velocity. A rational explanation could not be ascertained for this behavior of the lower harmonic SPLs. Of all the propeller configurations tested at the design conditions, the three-bladed BD3 propeller had the least slant range [4800 ft (1463 m)] at the forward velocity of 91 ft/sec (27.74 m/sec). It was also the only configuration where the slant range at 91 st/sec (27.74 m/sec) is much less than that at 15 ft/sec (4.6 m/sec). Figure 50a shows the variation of the slant ranges with forward velocity of four different propeller configurations (each with a different blade design) tested at the design conditions. These curves clearly show some of the trends discussed above.

One of the main reasons for testing propellers at four different forward velocities was to obtain sufficient trend data to extrapolate it to higher forward velocities which could not be considered in the tunnel tests because of the higher tunnel background noise associated with them. However, except for the two-bladed BD4 propeller (see Fig. 50a and Table 11) it is doubtful whether the slant ranges can be extrapolated to higher forward velocities. The validity of such an extrapolation can only be confirmed by additional tunnel tests at higher forward velocities.

Unlike the slant range, the altitude of no detection of each propeller configuration is determined by the lower harmonic SPLs of the noise in and near the plane of the propeller. Figure 50b shows the variation of altitude of no detection with forward velocity of the same four propeller configurations that were used in Figure 50a. A comparison of Figure 50a and Figure 50b shows that except for the two-bladed BD4 propeller, the overall variations of slant ranges and altitudes of no detection with forward velocity are quite different from each other though in a smaller range of forward velocities [70 ft/sec (21.34 m/sec) to 91 ft/sec (27.74 m/sec)] they may be similar. A comparison of slant ranges and altitudes of no detection of other propeller configurations (see Tables 11 and 12) also confirms the above trend. This suggests that the variation of lower harmonic SPLs with forward velocity in the forward direction (θ = 10°, 15° or 20°) is in

138
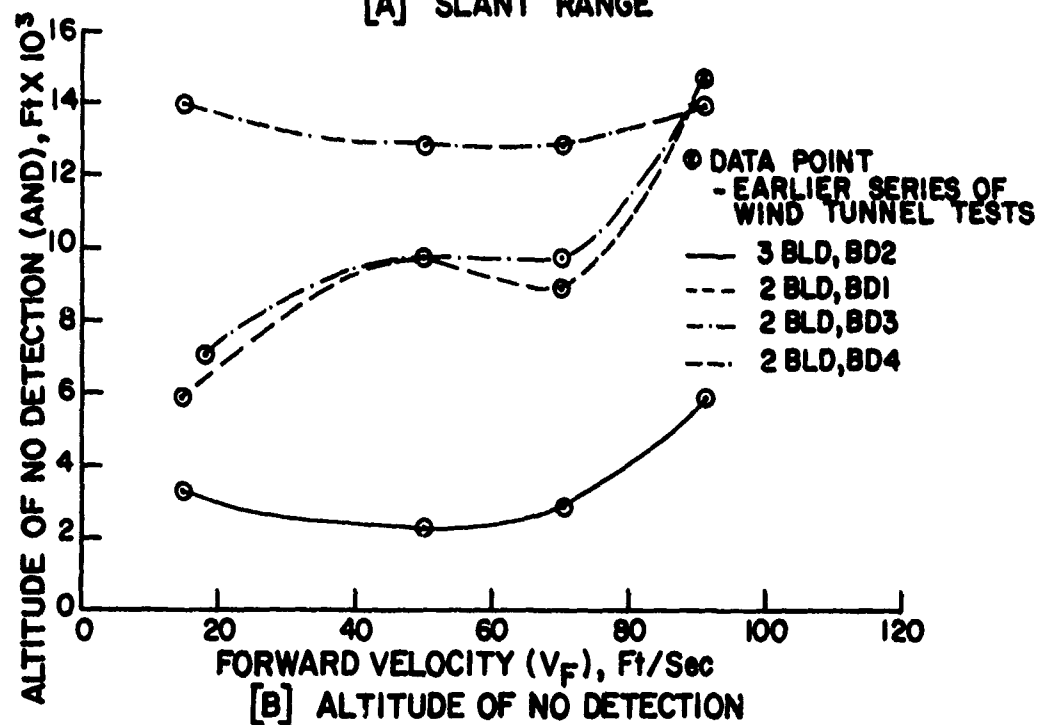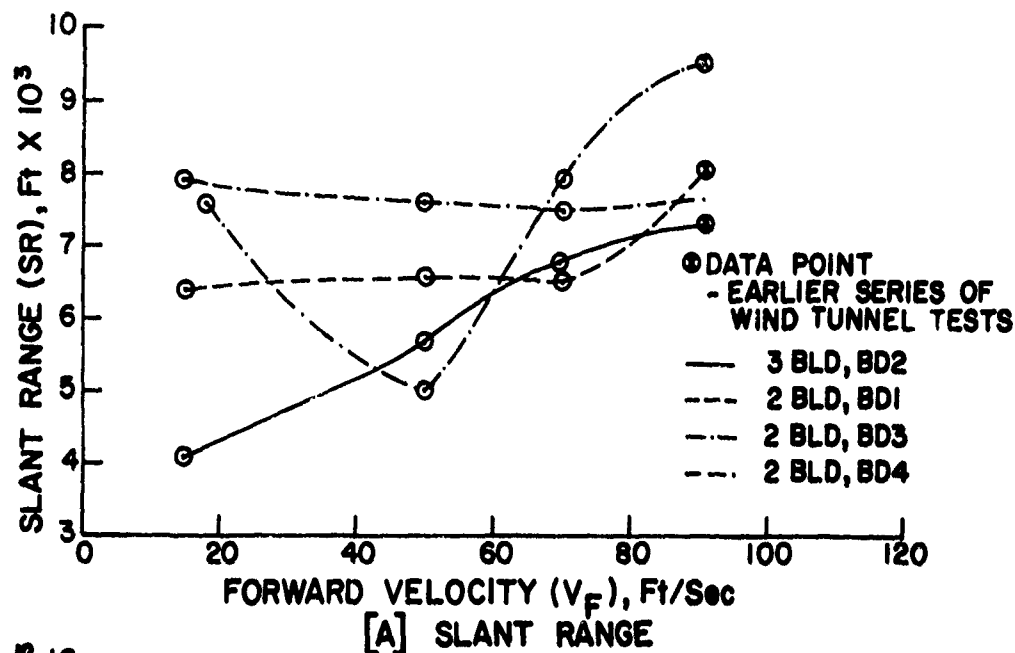
Figure 50.   Effect of Forward Velocity on the
             Detection Distances.

general different from that in the plane of the propeller
(θ = 90°). As was the case with the slant ranges, there were
propeller configurations such as three-bladed BD1, three-
bladed BD3, four-bladed BD3, and two-bladed BD4 where the
altitudes of no detection at 15 ft/sec (4.6 m/sec) and
91 ft/sec (27.74 m/sec) are roughly the same. It can be
clearly seen from Table 12 that the use of acoustic data
from the earlier series of tunnel tests at 91 ft/sec (27.74
m/sec) usually resulted in much larger values of altitudes
of no detection compared to those at 70 ft/sec (21.34 m/sec),
again raising doubts about the accuracy of the trend data of
propellers where such data was used. A closer examination of
the data in Table 12 suggests that, in general, the forward
velocity has a significant effect on the altitudes of no de-
tection of RPV propellers, though the degree of the effect
seems to depend on the type of propeller. Among the propel-
lers tested at the design conditions, the three-bladed BD1
propeller had the lowest altitude of no detection [3500 ft
(1067 m)] at the forward velocity of 91 ft/sec (27.74 m/sec),
while the three-bladed BD2 propeller had the lowest altitude
of no detection at other forward velocities considered.

In summation, the forward velocity has a significant effect
on the detection distances (slant ranges as well as altitudes
of no detection) of RPV propeller configurations, though the
degree of the effect seems to depend on the type of the pro-
peller and its parameters such as blade design, blade number,
etc. For a given propeller configuration the variations of
the slant ranges and the altitutdes of no detection with for-
ward velocity may be quite different from each other. It
was also shown that for some of the propeller configurations
tested at the design conditions, the detection distances at
a forward speed of 91 ft/sec (27.74 m/sec) were roughly the
same as those at near static conditions [15 ft/sec (4.6 m/sec)],
though they can be quite different from the detection dis-
tances at intermediate forward speeds. In the absence of
availability of data at high forward speeds, the extrapolation
of the available detectability data to higher forward speeds
may be in error. Considering both performance and detecta-
bility, the three-bladed BD1 propeller seems to be the best
among the configurations tested at design conditions with gen-
erally high propulsive efficiencies and low detection distances
at most of the forward velocities considered.

Having examined the effect of forward velocity on detection
distances, the effect of parameters such as blade design,
blade number, blade radius, tip speed and thrust on the de-
tection distances will now be discussed. The conclusions
regarding the effect of these parameters will generally

140

be based on the detectability trend data obtained using the acoustic data of the latter series of wind tunnel tests since this data is believed to be more accurate and consistent.

Effect of Blade Design

As was done in the trend studies of the acoustic data, the effect of blade design on detectability will be obtained by comparing results for propellers having different blade designs but the same diameter. Figure 51a shows the variation of the slant range with velocity of three-bladed propellers with different blade designs. In the case of small diameter three-bladed propellers (BD1 and BD3), the BD3 propeller has generally higher slant ranges than the BD1 propeller at all forward velocities except 91 ft/sec (27.74 m/sec). However, this trend is not always true if two- and four-bladed propellers are also considered (see Table 11). There does not seem to be a clear overall trend in the small diameter propeller results except that propellers with wide blade chords (BD3 design) have slightly higher slant ranges than those with narrow blade chords (BD1 design). However, it can easily be seen from Table 11 that among the large diameter propellers with two, three, and four blades (BD2 and BD4 designs), propellers with wide chords (BD4 design) have generally much higher slant ranges than those with narrow chords (BD2), though the difference in the slant ranges depends on the forward velocity of interest.

The trends noted above generally hold also for the altitudes of no detection of these propellers. As shown in Figure 51b among the large diameter three-bladed propellers, the propeller with the BD4 design (wide chords) has significantly higher altitudes of no detection than the propeller with the BD2 design (narrow chord).

Of the two-, three- and four-bladed tractor RPV propellers tested at the design conditions, propellers with wider blade chords (higher activity factor) are generally more detectable than those with the narrower chords (lower activity factor) at most of the forward velocities considered, though the degree of detectability seems to depend on such parameters as blade number and diameter. This trend is different from that for the large-scale propellers where the propellers with wide chord blades were found to be slightly less detectable (Ref. 7).

141
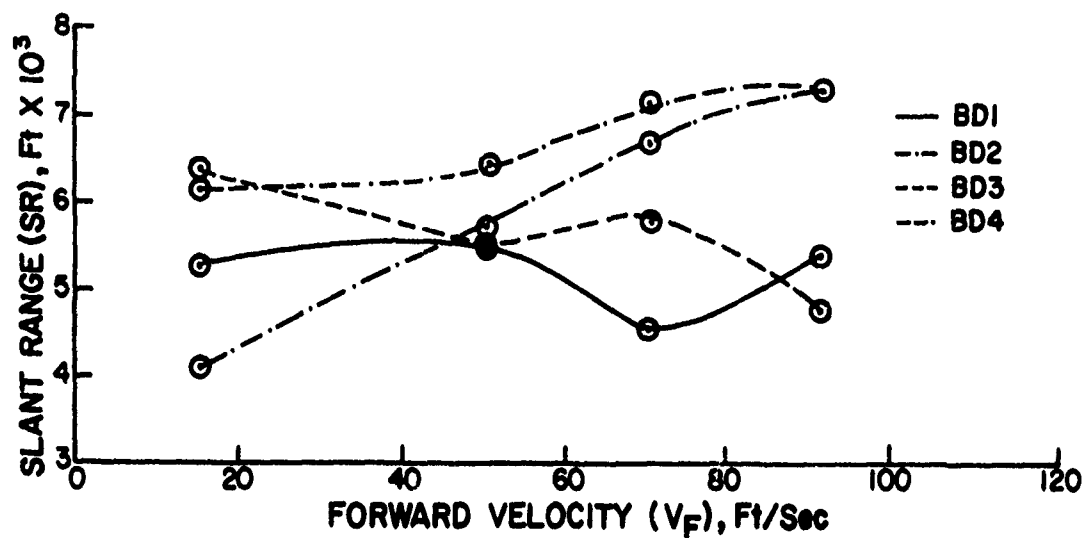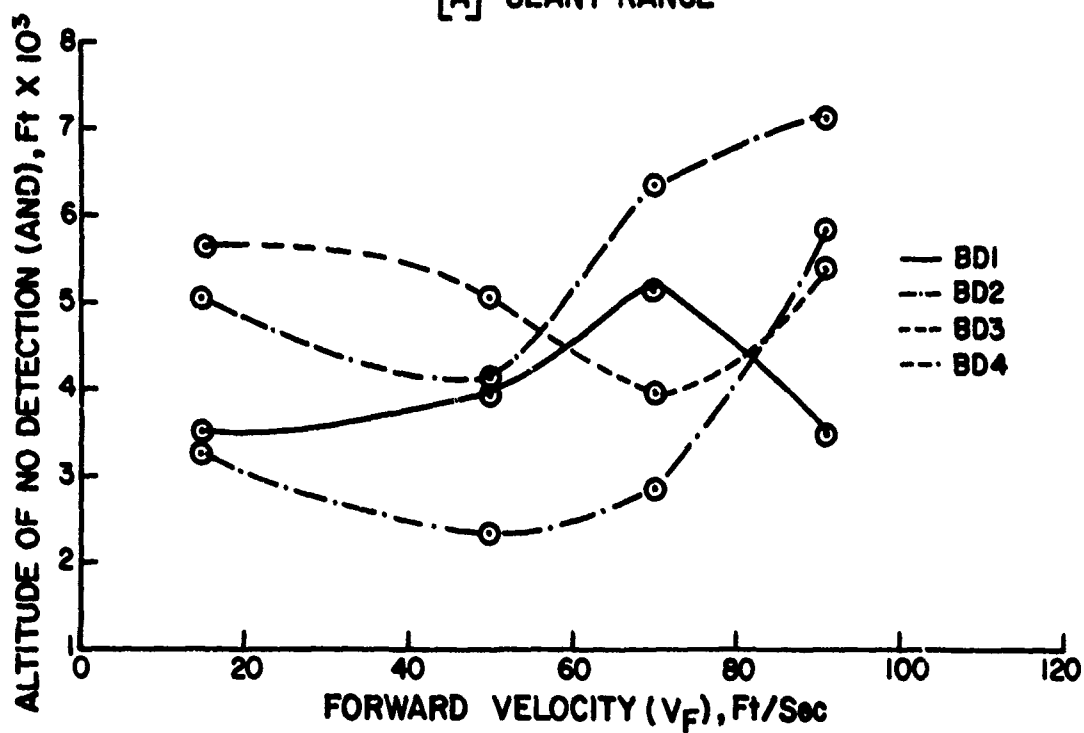
Figure 51.   Effect of Blade Design/Diameter on the Detection
             Distances of a Three-Bladed Propeller.

Effect of Diameter

The effect of diameter can be obtained by comparing the detection distances of propellers with blade designs BD3 and BD4. The only difference between these two designs is the blade radius which is 10 in (.254 m) for BD3 blades and 13 in (.33 m) for BD4 blades. It can be seen in Figure 51a that, for a three-bladed propeller, an increase in diameter resulted in a significant increase in the slant range at all of the forward velocities except 15 ft/sec (4.6 m/sec). This is also generally true for two- and four-bladed propellers (see Table 11) at most of the forward velocities considered. However, as far as the altitude of no detection is concerned, an increase in diameter was not always detrimental. As shown in Figure 51b, for a three-bladed propeller at lower forward velocities, an increase in diameter resulted in a smaller altitude of no detection. This was also found to be the case for a four-bladed propeller (see Table 12). However, at high forward velocities and for a two-bladed propeller at all forward velocities except 91 ft/sec (27.74 m/sec), the larger diameter propellers (BD4 design) had higher altitudes of no detection than the smaller diameter (BD3 design) propellers (see Table 12). In all of the comparisons discussed above, the tip speed as well as thrust of the propeller was kept constant. The trends noted above for small-scale RPV propellers are opposite those that have been observed for large-scale propellers (Ref. 7). A rational explanation could not be ascertained for this reversal in the trends.

Effect of Blade Number

Figures 52a and 52b show the effect of blade number on the detection distances (slant ranges and altitudes of no detection, respectively) of a BD3 propeller tested at the design values of tip speed and thrust. It can be seen from Figure 52a that at the higher forward velocities, the three-bladed propeller had lower slant ranges than either the two- or four-bladed propeller and that at other forward velocities considered, slant ranges are not that much higher than those of the two- or four-bladed propellers. The data in Table 11 shows that this is generally true for other blade designs as well. Figure 52b shows that the three-bladed propeller is clearly the best of the BD3 propellers with the lowest altitudes of no detection at all the forward velocities considered. The three-bladed propellers had generally the lowest altitudes of no detection for all blade designs (see Table 12) at most of the forward velocities considered. In the comparisons made above, the increase in the blade number increases the total

143
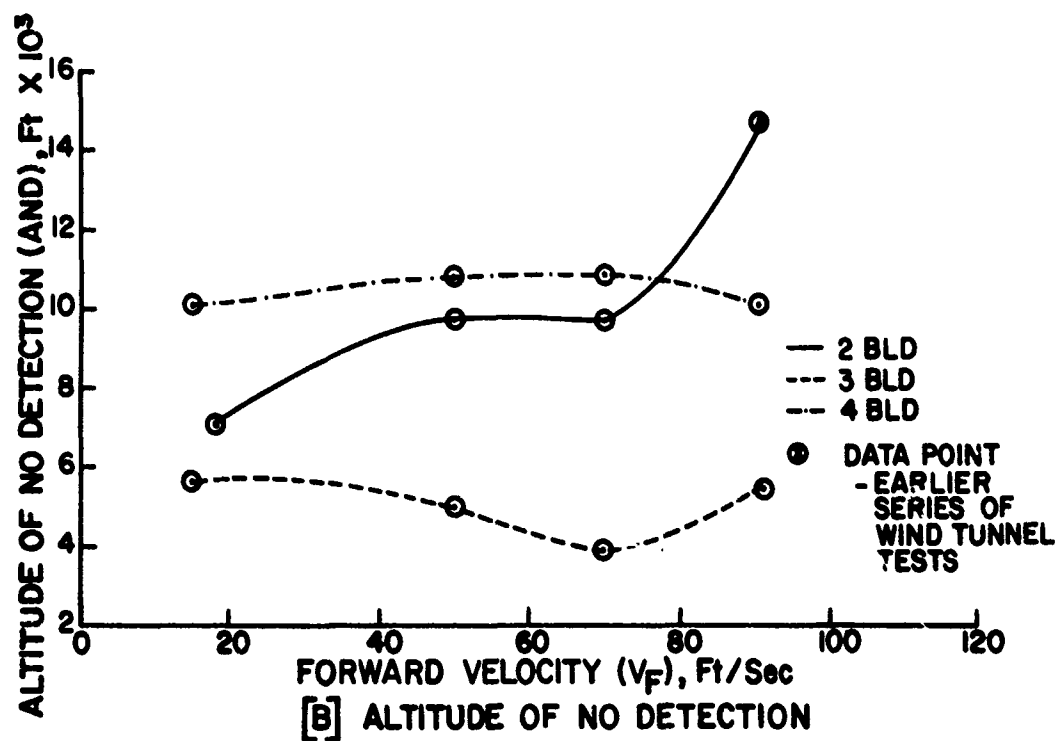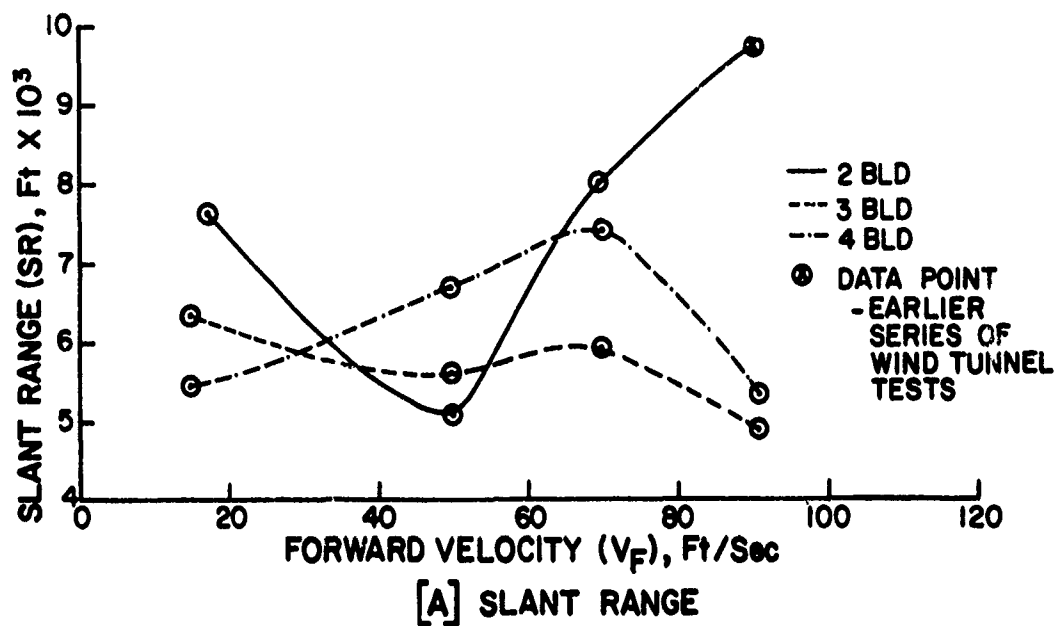
Figure 52.   Effect of Blade Number on the Detection Distances of a BD3 Propeller.

activity factor (and solidity) of a propeller with a given
blade design. Among the propellers tested at the design con-
ditions, three-bladed propellers are generally less detectable
than either two- or four-bladed propellers at most of the for-
ward velocities considered.

Effect of Tip Speed

Figures 53a and 53b show the effect of tip speed on the detec-
tion distances of a three-bladed BD3 propeller tested at the
design thrust value. As would be expected, tip speed had a
significant effect on the slant ranges and altitudes of no
detection at all the forward velocities considered. Table 13
lists the slant ranges and altitudes of no detection of pro-
pellers for three different tip speeds. As shown in Figure 53a,
a 13% increase in the tip speed from the design value of
510 ft/sec (155.5 m/sec) resulted in an increase in slant range
of anywhere from 30% to 70% depending upon the forward velocity.
The data in Table 13 shows that a 33% decrease in the tip speed
from the design value resulted in a significant reduction in
the slant ranges of propellers. The trends in altitudes of no
detection are similar to those discussed above. It can be seen
from Figure 53b that a 13% increase in the tip speed from the
design value resulted in much sharper increases in the alti-
tudes of no detection of about 2.5 to 4 times those at the de-
sign tip speed, depending upon the forward velocity. However,
as shown in Figure 53b, a 33% decrease in the tip speed from
the design values resulted in relatively modest reductions in
the altitudes of no detection. A rational explanation could
not be ascertained for this behavior. In general, tip speed
is one of the most potent parameters as far as the detecta-
bility of RPV propellers is concerned, though the tip speed
seems to have different degrees of effect on the slant ranges
and altitudes of no detection.

Effect of Thrust

Figures 54a and 54b show the effects of thrust on the de-
tection distances (slant ranges and altitudes of no detec-
tion, respectively) of a three-bladed BD3 propeller tested
at the design tip speed for different forward velocities.
As would be expected, an increase of thrust generally re-
sulted in significant increases in the detection distances,
though the amount of increase seems to depend on the for-
ward velocity. This can be seen in Figure 54a where a
100% increase in thrust resulted in an increase of slant
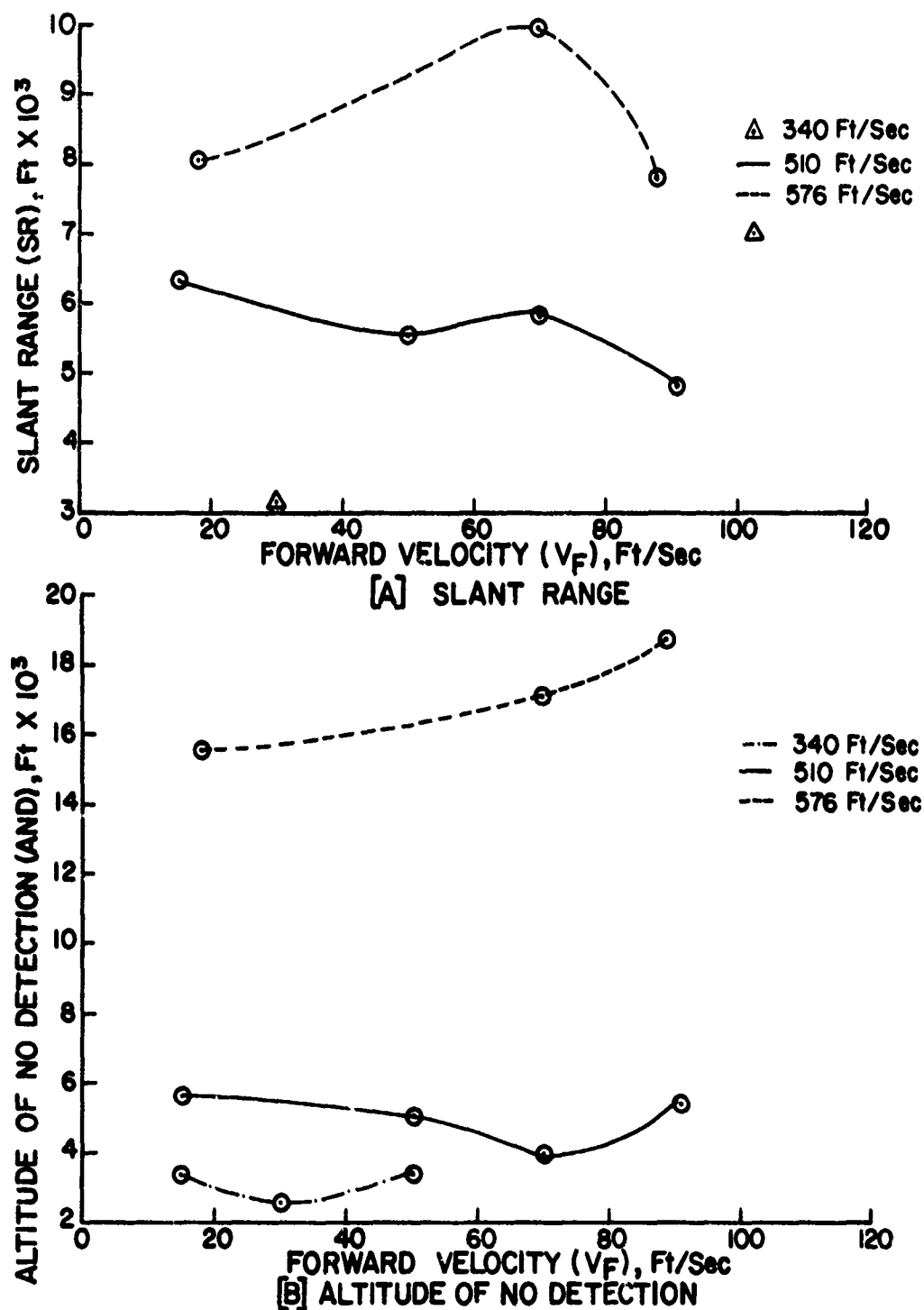
Figure 53. Effect of Tip Speed on the Detection Distances of a Three-Bladed BD3 Propeller.

TABLE 13

VARIATION OF SLANT RANGES (SR), ALTITUDES OF NO DETECTION (AND), AND PROPULSIVE EFFICIENCIES (η) OF A FEW TRACTOR PROPELLERS TESTED AT THE DESIGN THRUST

V_F PROP. CONFIG.	Tip speed, Ft/sec (m/sec)	≈15 Ft/Sec			30 Ft/sec			50 Ft/sec			70 Ft/Sec			≈88 Ft/sec		
		η	SR, Ft(m)	AND, Ft(m)	η	SR, Ft(m)	AND, Ft(m)	η	SR, Ft(m)	AND, Ft(m)	η	SR, Ft(m)	AND, Ft(m)	η	SR, Ft(m)	AND, Ft(m)
2BLD,BD3	510 (155.5)	.258	7600 (2316)	7050 (2149)	---	----	----	.520	5030 (1533)	9730 (2966)	.601	7930 (2417)	9730 (2966)	.735	9600* (2926)	14615* (4455)
	340 (103.6)	.163	4440 (1353)	2405 (733)	.247	2965 (904)	3720 (1134)	.448	----	2995 (913)	---	----	----	---	----	----
	576 (175.6)	.243	----	10595 (3229)	---	----	----	---	----	----	.577[b]	6630[b] (2021)	13525[b] (4122)	.715[d]	----	13090[d] (3990)
3BLD,BD3	510 (155.5)	.236	6315 (1925)	5620 (1713)	---	----	----	.564	5545 (1690)	5025 (1532)	.697	5820 (1774)	3970 (1210)	.773	4800 (1463)	5415 (1650)
	340 (103.6)	.258	----	3410 (1039)	.420	3120 (951)	2665 (812)	.662	----	3410 (1039)	---	----	----	---	----	----
	576 (175.6)	.186	8080 (2463)	15535 (4735)	---	----	----	---	----	----	.537	9960 (3036)	17110 (5215)	.710	7800 (2377)	18780 (5724)
4BLD,BD3	510 (155.5)	.199	5480 (1670)	10130 (3088)	---	----	----	.515	6690 (2039)	10830 (3301)	.595	7365 (2245)	10830 (3301)	.649	5245 (1599)	10130 (3088)
	340 (103.6)	.356	4450 (1356)	2510 (765)	.412	1515 (462)	----	.626	----	----	---	----	----	---	----	----
	576 (175.6)	.214	----	----	---	----	----	---	----	----	.579[c]	8270[c] (2521)	13570[c] (4136)	---	----	----
3BLD,BD4	510 (155.5)	.183	6115 (1864)	5050 (1539)	---	----	----	.555	6470 (1972)	4190 (1277)	.644	7180 (2188)	6385 (1946)	.708	7350 (2240)	7120 (2170)
	340 (103.6)	.278	2960 (902)	3985 (1215)	.490	3800 (1158)	4420 (1347)	.712[a]	----	5430[a] (1655)	---	----	----	---	----	----
	576 (175.6)	---	----	----	---	----	----	---	----	----	---	----	----	---	----	----

VARIOUS DATA POINTS OBTAINED AT $V_F =$ [a] = 55; [b] = 75; [c] = 80; and [d] = 95 Ft/sec

* DATA POINT -- EARLIER SERIES OF WIND TUNNEL TESTS

DETECTION DISTANCES BASED ON LOW AMBIENT NOISE (FIG. 4)
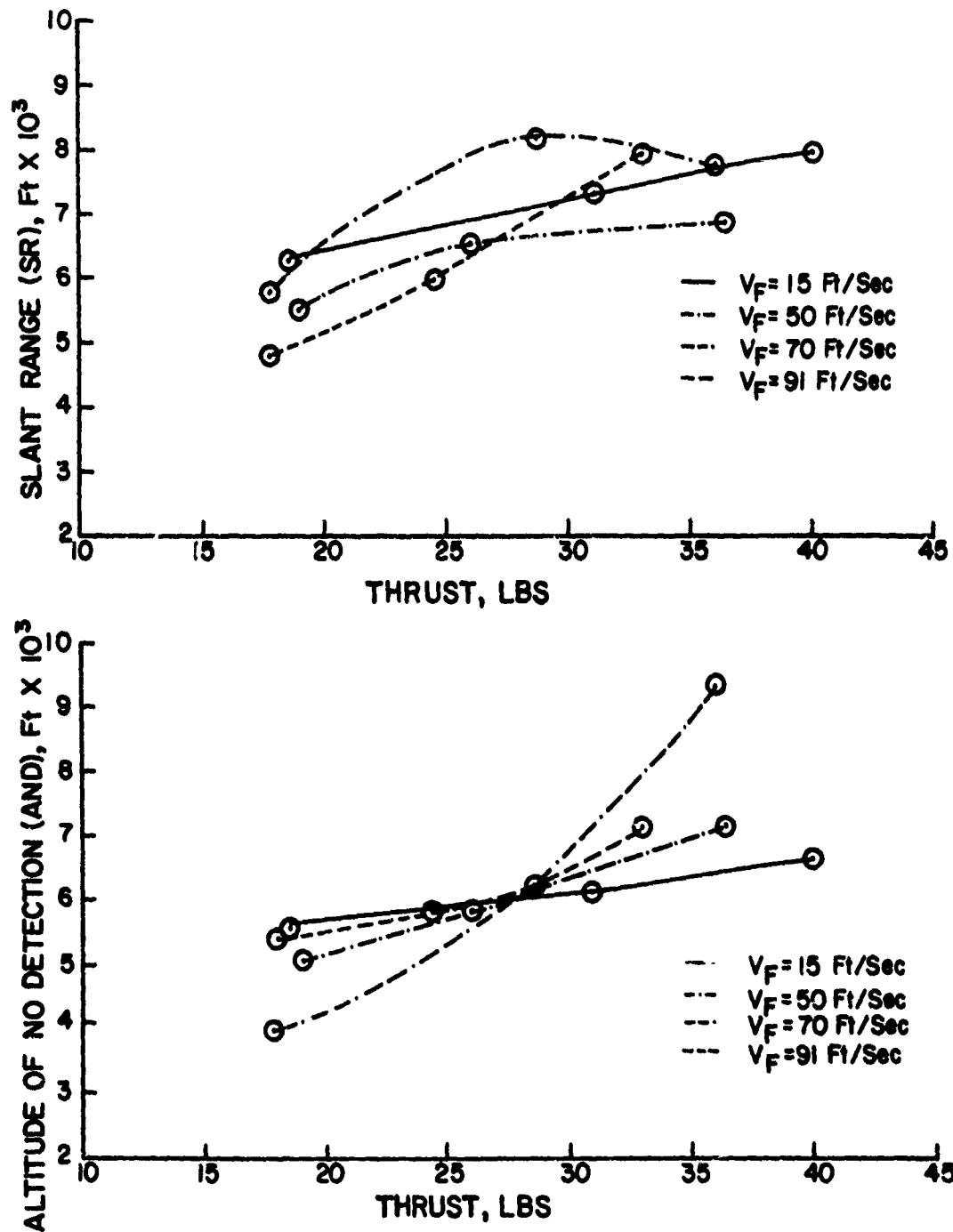
Figure 54. Effect of Thrust on the Detection Distances of a
            Three-Bladed BD3 Propeller.

148

range anywhere from 25% for a forward velocity of 50 ft/sec
(15.24 m/sec) to about 60% for a forward velocity of
91 ft/sec (27.74 m/sec). Table 14 lists the predicted
slant ranges (along with propulsive efficiencies) of three-
and four-bladed BD3 propellers for different values of
thrust at four different forward velocities. The data in
Table 14 shows that the effect of thrust on a four-bladed
propeller is much less than that on a three-bladed propel-
ler. As far as altitude of no detection is concerned, the
effect of increasing thrust on a three-bladed BD3 propeller
is much larger at a forward velocity of 70 ft/sec (21.34 m/
sec) than that at other forward velocities (see Fig. 54b).
Table 15 shows that for a four-bladed BD3 propeller, the
effect of thrust on the altitude of no detection is smaller
than that for the three-bladed propeller at some of the
forward velocities considered. In general, an increase in
the thrust developed by the propeller at a given tip speed
increases its detectability though the amount of increase
depends on such parameters as forward velocity and blade
number.

Effect of Upstream Turbulence

The effect of upstream turbulence on the detectability of
RPV propellers was obtained by comparing the detection dis-
tances of the tractor and pusher propeller configurations.
The acoustic data from the earlier series of tunnel tests
was used in the computations of these detection distances.
Table 16 lists the detection distances along with propulsive
efficiencies of some of the tractor, ducted, and pusher pro-
peller configurations tested at the design values of tip
speed and thrust. It can be seen from Table 16 that the
pusher propeller configurations generally have higher de-
tection distances (slant ranges as well as altitudes of no
detection) than their tractor counterparts, though the degree
of increase seems to depend on the type of propeller and
whether the propeller is ducted or not. The addition of an
upstream wing (turbulence generator) for pusher propeller
configurations did not significantly increase the detection
distances of these propellers. Since the detection distances
listed in Table 16 are obtained from the acoustic data of
propellers tested in the earlier series of tunnel tests, a
comparison of these detection distances with those of the
latter series of tunnel tests may be misleading since the
acoustic data from the two series of tests does not appear
to be consistent.

149

TABLE 14

VARIATION OF SLANT RANGE (SR) AND PROPULSIVE EFFICIENCY (η)
WITH THRUST OF BD3 PROPELLERS TESTED AT THE DESIGN TIP SPEED

PROP. CONFIG.	V_F 15 to 20 Ft/Sec			50 Ft/Sec			70 Ft/Sec			91 Ft/Sec		
	THRUST, Lb (n')	η	SR, Ft (m)	THRUST, Lb (n')	η	SR, Ft (m)	THRUST, Lb (n')	η	SR, Ft (m)	THRUST, Lb (n')	η	SR, Ft (m)
3BLD, BD3	18.5 (82.3)	.236	6315 (1925)	19.0 (84.5)	.564	5545 (1690)	17.8 (79.2)	.697	5820 (1774)	17.8 (79.2)	.773	4800 (1463)
	31.0 (137.9)	.253	7400 (2256)	26.0 (115.6)	.509	6600 (2012)	28.7 (127.7)	.624	8255 (2516)	24.5 (109.0)	.716	6070 (1850)
	40.0 (177.9)	.198	8010 (2441)	36.4 (161.9)	.445	6975 (2126)	36.0 (160.1)	.581	7830 (2387)	33.0 (146.8)	.745	8000 (2438)
4BLD, BD3	19.0 (84.5)	.199	5480 (1670)	18.4 (81.8)	.515	6690 (2039)	18.7 (83.2)	.595	7365 (2945)	17.5 (77.8)	.649	5245 (1599)
	25.0 (111.2)	.226	6315 (1925)	27.5 (122.3)	.539	6900 (2103)	29.0 (129.0)	.602	6895 (2102)	26.5 (117.9)	.647	5975 (1821)
	39.0 (173.5)	.228	6090 (1856)	35.5 (157.9)	.470	7450 (2271)	38.0 (169.0)	.572	7670 (2338)	36.5 (162.4)	.671	7080 (2158)

n' = Newtons

DETECTION DISTANCES BASED ON LOW AMBIENT NOISE (FIG. 4)

TABLE 15

VARIATION OF ALTITUDE OF NO DETECTION (AND) AND PROPULSIVE EFFICIENCY (η)

WITH THRUST OF BD3 PROPELLERS TESTED AT THE DESIGN TIP SPEED

PROP. CONFIG.	V_F 15 to 20 Ft/Sec			50 Ft/Sec			70 Ft/Sec			91 Ft/Sec		
	THRUST, Lb (η')	η	AND, Ft(m)	THRUST, Lb (η')	η	AND, Ft(m)	THRUST, Lb (η')	η	AND, Ft(m)	THRUST, Lb (η')	η	AND, Ft(m)
3BLD, BD3	18.5 (82.3)	.236	5620 (1713)	19.0 (84.5)	.564	5025 (1532)	17.8 (79.2)	.697	3970 (1210)	17.8 (79.2)	.773	5415 (1650)
	31.0 (137.9)	.253	6145 (1873)	26.0 (115.6)	.509	5825 (1775)	28.7 (127.7)	.624	6250 (1905)	24.5 (109.0)	.716	5820 (1774)
	40.0 (177.9)	.198	6695 (2041)	36.4 (161.9)	.445	7160 (2182)	36.0 (160.1)	.581	9350 (2850)	33.0 (146.8)	.745	7160 (2182)
4BLD, BD3	19.0 (84.5)	.199	10130 (3088)	18.4 (81.8)	.515	10830 (3301)	18.7 (83.2)	.595	10830 (3301)	17.5 (77.8)	.649	10130 (3088)
	25.0 (111.2)	.226	10830 (3301)	27.5 (122.3)	.539	11160 (3402)	29.0 (129)	.602	12170 (3709)	26.5 (117.9)	.647	12170 (3709)
	39.0 (173.5)	.228	12170 (3709)	35.5 (157.9)	.470	13090 (3990)	38.0 (169)	.572	13890 (4234)	36.5 (162.4)	.671	13890 (4234)

η' = Newtons

DETECTION DISTANCES BASED ON LOW AMBIENT NOISE (FIG. 4)

TABLE 16

EFFECT OF UPSTREAM TURBULENCE ON THE DETECTION DISTANCES OF A FEW PROPELLERS TESTED AT THE DESIGN VALUES OF THRUST AND TIP SPEED

PROPELLER CONFIGURATION	V_F = 91 Ft/Sec		
	EFFICIENCY	SLANT RANGE, Ft (m)	ALTITUDE OF NO DETECTION, Ft (m)
4BLD, BD1, Tractor	.787	6740 (2054)	13890 (4234)
4BLD, BD1, Pusher	.707	7900 (2408)	16445 (5012)
4BLD, BD1, Pusher w/Upstream Wing	.725	8550 (2606)	16445 (5012)
4BLD, BD1, Ducted Tractor	.584	6255 (1907)	9460 (2883)
4BLD, BD1, Ducted Pusher	.619	9175 (2797)	14300 (4359)
2BLD, BD2, Tractor	.827	6530 (1990)	11720 (3572)
2BLD, BD2, Pusher	.791	7815 (2382)	15865 (4836)
2BLD, BD2, Pusher w/Upstream Wing	.800	7860 (2396)	15865 (4836)
2BLD, BD2, Ducted Tractor	.557	9055 (2760)	9355 (2851)
2BLD, BD2, Ducted Pusher	.581	9325 (2842)	15030 (4581)
4BLD, BD3, Spaced Tractor	.556	6620 (2018)	13100 (3993)

NOTE: All Data Points Listed Above are From Earlier Series of Wind Tunnel Tests.

DETECTION DISTANCES BASED ON LOW AMBIENT NOISE (FIG. 4)

Effect of Ducts

Two sets of ducts were used in the wind tunnel tests. In the earlier series of wind tunnel tests, the interior surfaces of the ducts were lined with acoustic foam while in the latter series of tests the ducts had a hard fiberglass skin interior surface. A very limited amount of testing was done with the ducts lined with the hard fiberglass skin. These tests were conducted on a three-bladed BD3 propeller (see Table 10). The computations have shown that for a thrust value of 32 lbs (142.4 newtons) and a forward velocity of 15 ft/sec (4.6 m/sec) the three-bladed BD3 propeller with the hard skin duct had a slant range of about 6310 ft (1923 m) compared to about 7400 ft (2256 m) for the nonducted configuration tested at the same conditions, while for a forward velocity of about 50 ft/sec (15.24 m/sec) and a thrust value of 19 lbs (84.5 newtons), the same ducted propeller configuration had a slant range of about 6200 ft (1890 m) compared to about 5545 ft (1690 m) for the nonducted configuration at the same conditions. It was also found that the altitude of no detection for the three-bladed BD3 propeller with the hard skin duct was about 6620 ft (2018 m) at a forward velocity of 15 ft/sec (4.6 m/sec) and a thrust of about 32 lbs (142.4 newtons) as well as at a forward velocity of 50 ft/sec (15.24 m/sec) and a thrust of 19 lbs (84.5 newtons) compared to values of 6145 ft (1873 m) and 5025 ft (1532 m) respectively for the nonducted configuration. These values suggest that with the limited amount of data available, definite trends could not be established as far as the effect of ducts on the detectability characteristics of small-scale RPV propellers is concerned. This is also confirmed by the detectability data of the propellers with foam lined ducts (see Table 16) in tractor as well as pusher modes.

Summary

Parameters such as forward velocity, tip speed and thrust have a significant effect on the slant ranges as well as altitudes of no detection for small-scale RPV propellers. Other propeller parameters such as blade activity factor, blade number and blade radius seem to have a minor yet recognizable effect on the detection distances of RPV propellers. Pusher propeller configurations generally were more detectable compared to their tractor counterparts while definite trends could not be established regarding the effect of the ducts.

GENERAL REMARKS

Propellers for RPVs are generally characterized by small
diameters [less than 3 ft (.914 m)] and low disk loadings
[5 to 10 lb/ft^2 (240 to 480 newtons/m^2)]. It would be
highly desirable to develop a design method to help select
high performance and low noise fixed-pitch propellers to be
used in RPVs. A design method similar to the one developed
for large-scale propellers could be developed for deter-
mining the most efficient small-scale RPV propellers. How-
ever, such a design method requires extensive experimental
performance data for RPV propellers which typically operate
at Reynolds numbers of the order of 5 x 10^5. The perform-
ance data obtained in this investigation is inadequate and
is not amenable to the development of design charts similar
to those developed for large-scale propellers. It is there-
fore necessary to obtain extensive performance data (cover-
ing a wide range of performance variables such as advance
ratio and blade angle) for existing propellers such as those
used in this study as well as those designed by Borst[16]. It
is also recognized that aural detectability of RPV propellers
plays an important role in the success of any RPV mission.
Therefore, it is necessary to obtain extensive acoustic data
for these RPV propellers along with the performance data.
The acoustic data can then be used to determine the detec-
tion distances using such programs as the slant range pro-
gram.[27] The validity of the application of the slant range
program may need to be determined by correlating the pre-
dicted detection distances with flight test data which is
not yet available. From the detection distance data base,
it may be possible to develop suitable empirical relations
which can then be used in conjunction with the performance
design charts to help select fixed-pitch RPV propellers with
low detectability and high efficiency.

This investigation has shown that, of the different tractor
propeller configurations tested at the design conditions,
the three-bladed propellers generally have lower detection
distances and higher efficiencies. It was also found that
the three-bladed BD1 propeller (an optimum performance pro-
peller) was the best, considering both detectability and
efficiency at most of the forward velocities considered,
though other propeller configurations had lower detection
distances and higher propulsive efficiencies at some of the
other forward velocities. It is indeed encouraging to note
that a propeller designed for optimum performance for a
cruise speed of 127 ft/sec (38.6 m/sec) had some of the
lowest detection distances at most of the forward veloci-
ties considered in the tests. However, this may not always
be the case.

154

It is possible that RPV flight conditions such as launch, cruise and dash may have conflicting detectability and performance requirements. It is believed that while such RPV flight conditions as launch and landing may be the most important for the design based on performance, the cruise flignt condition would be the most important from the point of view of detectability. It would, therefore, be necessary to conduct trade-off studies between detectability and performance before a propeller is chosen for a given RPV airframe and a given set of flight conditions.

CONCLUSIONS

On the basis of the results obtained in this investigation, it is concluded that the acoustic and detectability characteristics of small-scale RPV propellers are generally significantly different from those of the large-scale propellers. This may have been due to either the low disk loading or the low operating Reynolds numbers of the RPV propellers investigated. It was found that the forward velocity has a significant effect on the acoustic characteristics as well as the detection distances of most of the RPV propeller configurations tested. It was also found, as expected, that such parameters as tip speed and thrust have a very strong effect on the detection distances and the acoustic characteristics of RPV propellers. Ducted and pusher propeller configurations are generally more detectable and less efficient than their open and tractor counterparts, respectively. Most of the propellers tested have a strong directivity in their acoustic radiation patterns.

In addition to these general conclusions, the following specific conclusions were also reached based on the analysis of the measured data.

PERFORMANCE CHARACTERISTICS

(1)   As expected, propellers designed based on optimum performance (BD1 and BD2 propellers) are more efficient than those designed based on acoustic considerations (BD3 and BD4 propellers).

(2)   Based on the static and limited forward flight data available, for the same design conditions of tip speed and thrust, ducted propellers are less efficient than their open counterparts and the expected thrust augmentation of the ducted configurations is not realized. This is possibly due to the occurrence of a possible separated flow near the duct leading edge and a nonuniform tip clearance around the azimuth.

(3)   All of the propellers tested are more efficient at the design conditions of tip speed and thrust than at the off-design tip speed and thrust conditions.

(4)   Definite trends regarding the effect of blade number and blade radius on the performance of small-scale propellers cannot be established due to the small changes in performance encountered among propellers with different blade numbers and radii.

ACOUSTIC CHARACTERISTICS

(1) For most of the propeller configurations tested, an increase in forward velocity (especially at low velocities) results in a significant drop in the SPLs at higher harmonics (beyond 4th or 5th) of the blade passage frequency in the forward direction as well as in and about the plane of the propeller. For instance, an increase of forward velocity from 15 ft/sec (4.6 m/sec) to 50 ft/sec (15.24 m/sec) results in a drop of about 10 to 20 dB in the higher harmonic SPLs which is believed to be mainly due to a more uniform inflow and less wake interaction at higher forward velocities.

(2) Directivity patterns of the propellers tested are not significantly affected by the forward velocity.

(3) The harmonic SPLs in the forward direction of pusher propellers are substantially higher (6 to 10 dB) than those of their tractor counterparts at a forward velocity of 91 ft/sec (27.74 m/sec), whereas the harmonic SPLs in the plane of the propellers for pushers are not significantly different from those of the tractors. The addition of an upstream wing (blockage turbulence generator) in the inflow does not cause a significant increase in the harmonic levels.

(4) For the same tip speed and thrust values, ducted propeller configurations (either with hard skin or foam lined interior) generally have much higher harmonic levels and broad-band noise than their open counterparts in the forward direction as well as in the plane of the propeller.

(5) Generally such blade parameters as activity factor, twist, and taper ratio do not have a strong effect on the harmonic levels of RPV propellers in forward flight. However, unlike the acoustic trends reported in the literature for large-scale propellers, RPV propeller configurations with wider blade chords (higher activity factor) and lower twists have slightly higher SPLs at the lower harmonics of the blade passage frequency than those with narrower chords (lower activity factor) and higher twist.

(6) For a given tip speed, thrust, and a given blade design (activity factor, twist, and taper ratio), an increase in the propeller diameter is not beneficial as far as acoustic characteristics in forward flight are concerned.

157

(7) An increase in the blade number generally has an atten-
uating effect on the harmonic levels of the propellers
at higher forward velocities.

(8) As expected, tip speed has a very strong effect on the
SPLs. For instance, at a forward velocity of 70 ft/sec
(21.34 m/sec), an increase of 13% in the tip speed from
the design value results in an increase of 5 to 10 dB
(depending upon the harmonic number) in the harmonic
levels of a three-bladed BD3 propeller.

(9) For a given tip speed, an increase in thrust value
results in an increase of the SPLs, especially at the
lower harmonics, though the amount of increase appears
to depend on parameters such as blade number and for-
ward velocity.

DETECTABILITY CHARACTERISTICS

(1) Based on the detection distances predicted, most of the
RPV propeller configurations tested would be detected
at one of the first few harmonics of their blade pas-
sage frequency (mostly first or second harmonic).

(2) The effect of forward velocity on the detection dis-
tances (slant range and altitude of no detection)
appears to be dependent on propeller parameters such
as blade number, blade radius, and blade design
(activity factor, twist, etc.).

(3) For most of the propeller configurations tested, the
variation of the slant range with forward velocity
is in general different from that of the altitude of
no detection, though they may be similar over a small
range of forward velocities.

(4) Of the tractor propellers tested at the design values
of thrust and tip speed, propellers with wider blade
chords (higher activity factor) have higher detection
distances than those with narrower blade chords (lower
activity factor).

(5) For a given tip speed, thrust, and blade design, an
increase in diameter results in an increase of the
slant range as well as the altitude of no detection.

(6) Of the propellers tested at the design values of tip speed and thrust, three-bladed propellers are generally less detectable than either the two- or four-bladed propellers for most of the forward velocities considered.

(7) As expected, tip speed has a very strong effect on the detectability of propellers. For instance, in the case of BD3 propellers, a 13% increase in the tip speed from the design value results in an increase in slant range anywhere from 30 to 70%, depending upon the forward velocity. The increases are much sharper (100 to 300%) for altitudes of no detection.

(8) An increase in the thrust developed by a propeller for a given tip speed generally increases its detectability, though the amount of increase appears to depend on such parameters as forward velocity and blade number.

(9) Pusher propeller configurations generally have higher detection distances (slant range and altitude of no detection) than their tractor counterparts, and the addition of an upstream wing (which generates turbulence) does not significantly increase their detection distances.

(10) Ducted propellers tested generally have higher slant ranges and altitudes of no detection than their open counterparts, though the amount of data available is very limited.

RECOMMENDATIONS

On the basis of the results obtained during this research program, it is recommended that the following efforts be undertaken.

(1) Obtain the performance data of the small-scale RPV propellers in a manner suitable to develop design charts similar to those developed for large-scale propellers. This will involve the consideration of a wider range of performance variables such as advance ratio and blade angle.

(2) Investigate the available performance prediction methods as regards their applicability to the design of fixed-pitch small-scale RPV propellers.

(3) Obtain experimental acoustic data of the present RPV propellers at higher forward velocities corresponding to at least the cruise and dash flight conditions of the next-generation RPVs.

(4) Conduct a more extensive study of the effect of spacing and phasing on the acoustic and detectability characteristics of small-scale RPV propellers.

(5) Conduct a more detailed study of the effect of ducts (with hard skin interior) on the acoustic and detectability characteristics of small-scale RPV propellers at higher forward velocities.

(6) Apply the available acoustic prediction theories to the present RPV propellers and conduct a correlation study with the available experimental data. Using a suitable acoustic prediction theory, investigate some of the reasons behind the trends observed for small-scale RPV propellers.

(7) Investigate the applicability of the slant range prediction method used in the determination of slant ranges of small-scale RPV propellers. It would be highly desirable to correlate the predicted slant ranges with any flight test data that will be available in the future.

160

(8) Develop a more accurate method of taking into account the directivity of propellers in the determination of their detection distances.

(9) Obtain the detection distances of RPV propellers for a wider range of flight conditions. Develop suitable empirical relations from the detection distance data which can be used in conjunction with performance design charts to help select fixed-pitch RPV propellers with high efficiency and low detectability.

LIST OF REFERENCES

1. Gutin, L., On the Sound Field of a Rotating Propeller, NACA TM 1195, 1948.

2. Hubbard, Harvey H., and Regier, Arthur A., Free-Space Oscillating Pressures Near the Tips of Rotating Propellers, NACA TR 996, 1950.

3. Garrick, I. E., and Watkins, C. E., A Theoretical Study of the Effect of Forward Speed on the Free-Space Sound-Pressure Field Around Propellers, Report 1198, NACA, 1954.

4. Ollerhead, J. B., and Lowson, M. V., Problems of Helicopter Noise Estimation and Reduction, Paper No. 69-195, AIAA, Feb. 17-19, 1969.

5. Arnoldi, R. A., Near-Field Computations of Propeller Blade Thickness Noise, Report R-0896-2, UAC Research Department, East Hartford, CT, Aug. 1956.

6. Yudin, E. Y., On the Vortex Sound from Rotating Rods, RM 1136, NACA, 1947.

7. Barry, Frank W., and Magliozzi, Bernard, Noise Detectability Prediction Method for Low Tip Speed Propellers, AFAPL-TR-71-37, Wright-Patterson AFB, OH, June 1971.

8. Brown, David, and Ollerhead, J. B., Propeller Noise at Low Tip Speeds, AFAPL-TR-71-55, Wright-Patterson AFB, OH, Sep. 1971.

9. Regier, A. A., and Hubbard, Harvey H., Factors Affecting the Design of Quiet Propellers, NACA RM No. L7405, Sep. 1947.

10. Magliozzi, B., V/STOL Rotary Propulsion Systems Noise Prediction and Reduction, Vol. 1, Report No. FAA-RD-76-49-1, US Dept of Transportation, Washington, D.C., May 1976.

11. Magliozzi, B., and Ganger, T. G., Advanced V/STOL Propeller Technology -- Far-Field Noise Investigation, AFFDL-TR-71-88, Vol. XIII, Wright-Patterson AFB, OH, Mar. 1972.

12. Magliozzi, B., The Influence of Forward Flight on Propeller Noise, NASA CR-145105, Feb. 1977.

13. Hubbard, Harvey H., *Sound Measurements for Five Shrouded Propellers at Static Conditions*, NACA TN No. 2024, Apr. 1950.

14. Longhouse, Richard E., *Application of External Aerodynamic Diffusion to Reduce Shrouded Propeller Noise*, Acoustical Society of America: Fall Meeting, Miami, FL, Nov. 28-Dec 1, 1972.

15. Rosen, George, and Rohrback, Carl, *The Quiet Propeller -- A New Potential*, Hamilton Standard, AIAA Paper No. 69-1038.

16. Borst, Henry V., et al., *Aerodynamic Design and Analysis of Propellers for Mini-Remotely Piloted Air Vehicles, Vol. I Open Propellers*, USAAMRDL TR-77-45A, Applied Technology Lab., US Army Research and Technology Labs. (AVRADCOM), Fort Eustis, VA., Jan. 1978, AD A050593.

17. Hoehne, Vernon O., and Luce, Ross G., *A Research Program to Define the Relationship Between Small-Scale Propeller Performance and Noise*, Final Report, Battelle Memorial Institute, Columbus, OH, Mar. 1969.

18. Trillio, R. L., *An Empirical Study of Hovercraft Propeller Noise*, Hovercraft and Hydrofoil, Dec.-Jan. 1965, pp. 12-34.

19. Shimovetz, R. M., and Smith, D. L., *Mini RPV Engine Noise Reduction*, AFFDL-TR-76-28, Wright-Patterson AFR, OH, Mar. 1976.

20. Grosche, F. R., and Stiewitt, H., *Investigation of Rotor Noise Source Mechanisms with Forward Speed Simulation*, Presented at AIAA 4th Aeroacoustics Conference, Atlanta, GA, Oct. 1977.

21. Betz, A., *Screw Propellers with Minimum Energy Loss*, Technical Translation 736, National Research Council of Canada, Ottawa, Ontario, Canada, 1958. Original work was published in 1919.

22. Theodorsen, T., *Theory of Propellers*, McGraw-Hill Book Company, Inc., New York, NY, 1948.

23. Jacobs, Eastman N., and Abbott, Ira H., Airfoil Section Data Obtained in the NACA Variable Density Tunnel as Affected by Support Interference and Other Corrections, NACA Report No. 669, 1939.

24. Jacobs, Eastman N., and Albert, Sherman, Airfoil Section Characteristics as Affected by Variations of the Reynolds Number, NACA Report No. 586, 1937.

25. Kaskel, A. L., Ordway, D. E., Hough, G. R., and Ritter, A., A Detailed Numerical Evaluation of Shroud Performance for Finite-Bladed Ducted Propellers, Therm, Inc., TAR TR-639, Dec. 1963.

26. Johnson, H. K., Development of an Improved Design Tool for Predicting and Simulating Helicopter Rotor Noise, RASA Report 74-02, USAAMRDL TR-74-37, Eustis Directorate, US Army Air Mobility R&D Laboratory, Ft Eustis, VA, June 1974, AD 785579.

27. Abrahamson, Louis A., Correlation of Actual and Analytical Helicopter Aural Detection Criteria, USAAMRDL TR-74-102A, Eustis Directorate, US Army Air Mobility R&D Laboratory, Ft Eustis, VA, Jan. 1975, ADB002067L.

28. Gessow, Alfred and Meyers, Garry C. Jr., Aerodynamics of the Helicopter, Frederick Ungar Pub. Co., 1967, pp. 68.

29. Ollerhead, J. B., Helicopter Aural Detectability, USAAMRDL TR-71-33, Eustis Directorate, US Army Air Mobility R&D Laboratory, Ft Eustis, VA., July 1971, AD730788.

30. The Boeing Company, Vertol Div., Analysis of the Effects of Aural-Detection Range on Helicopter Operations, USAAMRDL TR-73-80, Eustis Directorate, US Army Air Mobility R&D Laboratory, Ft. Eustis, Va., Mar. 1974, CONF.

31. Gangwani, S. T., The Effect of Main Rotor Blade Phasing and Spacing on Performance, Blade Loads and Acoustics, RASA Report 3169-14, NASA CR-2737, 1976.

32. Fidell, Sanford, Pearsons, Karl S., and Bennett, Ricarda L., Predicting Aural Detectability of Aircraft in Noise Backgrounds, AFFDL-TR-72-17, Wright-Patterson AFB, OH, July 1972.

33. White, Richard P. Jr., The Status of Rotor Noise Technology, One Man's Opinion, Presented at the Specialists Meeting, Helicopter Acoustics, NASA Langley, Hampton, VA., May 22-24, 1978.

LIST OF SYMBOLS

A·F	Activity factor
AND	Altitude of no detection, ft
BPF	Blade passage frequency, Hz
BW	Bandwidth, Hz
C	Blade chord, in
C'	Chord length of the duct, in
C_D	Drag coefficient of the airfoil section
$C_{L_{max}}$	Maximum lift coefficient of the airfoil section
C_S	Speed-power coefficient
D	Diameter of the propeller, in
FM	Figure of merit
H	Altitude of no detection, ft
K	Atmospheric absorption coefficient, dB/1000 ft
L_D	Detection level, dB
L_p	1/3 octave level of the acoustic signal, dB
N	rpm
n	Revolutions per second
P	Shaft horsepower
P'	Power absorbed by the shaft, ft-lbs/sec
Q	Torque absorbed by the shaft, ft-lbs
R_c	Radius to the duct chord surface, in
R, R_p	Radius of the propeller, in
R'	Distance the acoustic signal travels in the direction of θ in the atmosphere, ft
R_i	Radius of the inner surface of the duct or shroud in the plane of the propeller, in
r	Local blade radius, in
SPL	Sound pressure level, dB re 0.0002 μ bar

SR	Slant range, ft
T	Thrust, lb
t	Maximum thickness of the blade section, in
V_F	Forward velocity/tunnel velocity, ft/sec
w	Apparent wake velocity, ft/sec
$\bar{w}$	Apparent wake velocity parameter ($=w/V_F$)
x	Nondimensional local radius ($=r/R$)
X_p	Distance from the leading edge of the duct to the propeller plane, in
ΔZ	Axial spacing between two propeller planes, in
β, ϕ	Blade angle with respect to the disk plane, deg
θ	Azimuthal location of the microphone in a plane containing the thrust axis, deg
$\phi_{.75R}$	Blade angle at 3/4 radius of the blade, also referred to as collective pitch, deg
ρ	Density of air, slugs/ft^3
$\Delta\psi$	Angular phasing, the angle between two blades in the plane of the propeller, deg
η	Propulsive efficiency, %